Polytechnic University of Bari

Department of Mechanics, Mathematics and Management

Master's Degree in Mechanical Engineering

Final thesis in
Fluid-Structure Interaction and Multifield Problems

ADVANCED FINITE ELEMENTS FOR THE LARGE DISPLACEMENT (AND LARGE STRAINS) ANALYSIS OF MATERIALS AND STRUCTURES

Candidate
Piero Chiaia
Student ID: 583167

Supervisor
Maria Cinefra

Co-supervisor
Alfonso Pagani
Matteo Filippi

Acknowledgements

First of all, to my mother and father, always constant in supporting me and joyful to see me excel in my studies and in my life. To my family, always here for support.
To my grandmother, who also celebrates me from up there.
To my dearest friend, the oldest one and the newest one, every time at my side in this journey.

My sincere acknowledgment is devoted to prof. Maria Cinefra, who believed in me since the day of my examination, recognizing immediately my desire to work, offering me the wonderful opportunity to dedicate myself with passion to a new, stimulating research field. Thanks for encouraging and following me during this work with dedication and sincere affection.

I would like to express my gratitude for the possibility to work in contact with MUL2 research group in Polytechnic University of Turin, that has hosted me as if I were their student since beginning, making me feel part of the group since my first day in Turin.

I am deeply thankful to prof. Alfonso Pagani and prof. Matteo Filippi, that followed me in this difficult research work with constant daily support, motivation and knowledge, guaranteeing me one of the most beautiful work experience far from home.

De remi facemmo ali.

Abstract

In this thesis I discuss the implementation of advanced finite elements for large deflection and large strain analysis by Unified Formulation. The geometrically nonlinear analysis of beam, plates and solid structures is a fundamental topic in structural mechanics thanks to its applications in different engineering fields. In automotive or civil applications, small deformations are a fundamental requirement of the design process, like spur gears in mechanical engineering or beam structures in building design processes, otherwise structures do not work properly in their field of applications. Even so, models for high flexible and deformable components are recently spread due to renewed interests in biological applications, complex systems modeling and fluid-structure interaction problems. Also, in mechanical and aerospace engineering application, innovative materials allow to design structures capable of carrying high loads without failure after instabilities occur, becoming more and more used in aircraft components design. In the moderate/large displacements regime, however, instability caused by large displacements and rotations occurs. Accurate prediction of displacements and rotation, as well as stresses distribution in the medium/large displacement regime, is a challenging topic in solid mechanics and numerical analysis due to some already known mathematical limitations that, in the case of large-deflection analysis, are amplified by the presence of nonlinear terms in the governing equations.
The first part is devoted to the mathematical description of continuum mechanics governing equation for linear elastic and hyperelastic materials. Derivation of the large displacement formulation and stress tensors both in case of Hooke's law and strain energy functions is described. Strain and stress measures are here presented, introducing Cauchy "true" stress tensor and its expression in case of linear elastic materials and hyperleastic materials, Piola-Kirchoff 1 and Piola-Kirchoff 2 stress tensors. First-invariant hyperleasticity is here presented, deriving the constitutive law in terms of invariants of right Cauchy-Green tensor.
The second part is devoted to the description of numerical methods involved in nonlinear analysis: refined fully-nonlinear finite elements for beam, plate and solid structures under Unified Formulation are analysed. Carrera Unified Formulation is adopted in the implementation of finite elements: the primary unknown variables are discretized by kinematic models and arbitrary expansion cross-section function or thickness function coupled with the classical Finite Element Approximation. The nonlinear governing equation is exploited by means of principle of virtual displacements, taking into account the full Green-Lagrange tensor for finite deformations and expressed in terms of stiffness ma-

trices: the explicit forms of the secant and tangent stiffness matrices of unified beam, plate and generic 3D solid elements are presented in terms of fundamental nuclei.In the case of hyperelastic beam and solid model, also strain energy function expression are presented, and derivation of the tangent stiffness matrix and internal forces vector by means of Piola-Kirchoff 2 stress tensor is carried out, as well as the expression of the tangent elasticity tensor components required by the incremental scheme. The numerical solution of the nonlinear structural problem is obtained by means of linearized Newton-Raphson scheme combined by a path-following method based on the arc-length method, an adaptive parametrization incremental-iterative scheme that postulates simultaneous variations of primary displacements variables with load variations.
The last part is devoted to the discussion and validation of numerical results obtained by the present implementation: large deflection and post-buckling analysis of beam and plates structures obtained by 1D and 2D models are presented, and used as reference results to validate the one obtained adopting 3D nonlinear finite elements, implemented afterwards. Popular benchmark problems in geometrically non-linear solid mechanics are also analyzed to establish the capabilities of present implementation of fully-nonlinear solid elements in case of post-buckling analysis of beams, plates and curved structures, obtaining accurate results.
The present work is the first step in understanding complex structural problem also involving geometrical non-linearities. However, in this context, several aspects require further research efforts. Possible future works include large strain analysis, accounting of material non-linearities, hyperelasticity, fracture mechanics, nonlinear vibrations, fluid-structure interaction applications.

Contents

List of Figures

Chapter 1

Continuum Mechanics

1.1 Strain and stress analysis

1.1.1 Continuum bodies, displacements and deformations

Let Ω be a closed volume with regular surface of the three-dimensional euclidean space: this region has a continuous distribution of matter in space and time, namely is a *continuum* body, and it can be described by macroscopic quantities. Consider a continuum body Ω_0 and a particle P which is embedded in the body. As the continuum body moves in space, following its evolution in time, it occupies a continuous sequence of regions of the euclideian space: the regions occupied by the body at a certain time t are the *configurations* of the body. Starting from the reference configuration Ω_0, the configuration of the body at the generic instant t is called the *current configuration*.

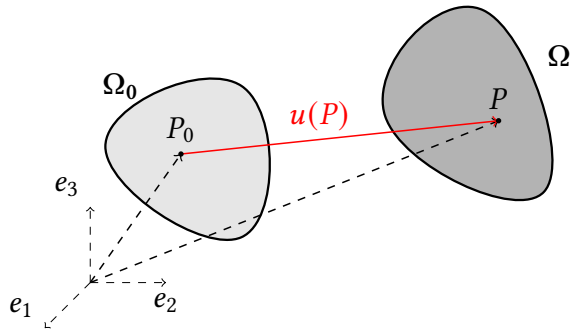

Figure 1.1.1: Refecence and actual configuration of a deformable body.

Introducing the classical orthonormal reference frame $\{e_1, e_2, e_3\}$, the position of a material point of a continuum body can be defined in terms of component:

$$\mathbf{P_0} = x_0\mathbf{e_1} + y_0\mathbf{e_2} + z_0\mathbf{e_3} \tag{1.1.1}$$

A *deformation* is a continous function that associates the position of the material point in the actual configuration to the related position in the reference, configuration:

$$\mathbf{f}(\mathbf{P_0}) = x\mathbf{e_1} + y\mathbf{e_2} + z\mathbf{e_3} = f_1(x_0, y_0, z_0)\mathbf{e_1} + f_2(x_0, y_0, z_0)\mathbf{e_2} + f_3(x_0, y_0, z_0)\mathbf{e_3} \tag{1.1.2}$$

The deformation function needs to fullfil physical plausibility conditions, namely $\mathbf{f}$ is injective and C^1, and $\mathbf{f}$ preserves the local orientation, namely do not allow compenetration of matter. In mathematical terms, these conditions are satified if $det\mathbf{F} \neq 0$, where $\mathbf{F}$ is the deformation gradient defined as:

$$\mathbf{F} = \nabla\mathbf{f} = \begin{bmatrix} \frac{\partial f_1}{\partial x} & \frac{\partial f_1}{\partial y} & \frac{\partial f_1}{\partial z} \\ \frac{\partial f_2}{\partial x} & \frac{\partial f_2}{\partial y} & \frac{\partial f_2}{\partial z} \\ \frac{\partial f_3}{\partial x} & \frac{\partial f_3}{\partial y} & \frac{\partial f_3}{\partial z} \end{bmatrix} \tag{1.1.3}$$

If $\mathbf{P_0}$ is a material point in the reference configuration, and $\mathbf{P}$ is the associated point in the actual configuration, let's define the displacement of the point as:

$$\mathbf{u}(\mathbf{P}) = \mathbf{P} - \mathbf{P_0} = u\mathbf{e_1} + v\mathbf{y_2} + w\mathbf{e_3} \tag{1.1.4}$$

As done for the deformation function, the displacement gradient $\mathbf{H}$ is defined as:

$$\mathbf{H} = \nabla\mathbf{u} = \begin{bmatrix} \frac{\partial u}{\partial x} & \frac{\partial u}{\partial y} & \frac{\partial u}{\partial z} \\ \frac{\partial v}{\partial x} & \frac{\partial v}{\partial y} & \frac{\partial v}{\partial z} \\ \frac{\partial w}{\partial x} & \frac{\partial w}{\partial y} & \frac{\partial w}{\partial z} \end{bmatrix} \tag{1.1.5}$$

Considering the definition of displacement function, denoting with $\mathbf{i}(\mathbf{P})$ is the identity vector transformation, and $\mathbf{I}$ the 3x3 identity matrix, *fundamental kinematics relation* in a continuum body is carried out:

$$\mathbf{u}(\mathbf{P}) = \mathbf{P} - \mathbf{P_0} = \mathbf{f}(\mathbf{P_0}) - \mathbf{i}(\mathbf{P_0}) \tag{1.1.6}$$

$$\mathbf{H} = \nabla\mathbf{u}(\mathbf{P}) = \nabla\mathbf{f}(\mathbf{P_0}) - \nabla\mathbf{i}(\mathbf{P_0}) = \mathbf{F} - \mathbf{I} \tag{1.1.7}$$

During the deformation, the most representantive quantity is the deformation gradient $\mathbf{F}$: by the definition, it maps points from the reference configuration to the actual one. Consider now a unit versor N associated on an infinitesimal material surface element dS: differently then before, the deformation do not map it to an unitary versor associated to an infinitesimal spacial surface element in the current configuration ds, namely during the deformation there is *change in volume* of the infinitesimal surface element.
One can prove that, after the deformation, the volume of the generic infinitesimal volume is given by:

$$dv = (\det\mathbf{F})\, dV = J\, dV \tag{1.1.8}$$

where $J = \det\mathbf{F}$ is the determinant of the deformation gradient, also called *volume ratio.*
Let's consider two unit versors, n and N on an arbitrary material line $d\mathbf{X}$ mapped to $d\mathbf{x}$ due to the deformation. The infinitesimal volumes in the reference and current configuration will be:

$$dv = dx_1 dx_2 dx_3 = d\mathbf{s} \cdot d\mathbf{x} = \mathbf{n}ds \cdot d\mathbf{x} \tag{1.1.9}$$

$$dV = dX_1 dX_2 dX_3 = d\mathbf{S} \cdot d\mathbf{X} = \mathbf{N} dS \cdot d\mathbf{X} \tag{1.1.10}$$

so, by considering the definition of volume ratio:

$$dv = J\, dV \quad \rightarrow \quad \mathbf{n} ds \cdot d\mathbf{x} = J\, \mathbf{N} dS \cdot d\mathbf{X} \quad \rightarrow \quad d\mathbf{s} \cdot d\mathbf{x} = J\, d\mathbf{S} \cdot d\mathbf{X} \tag{1.1.11}$$

Considering now the deformation gradient map and matrix identities, one can obtain:

$$d\mathbf{s} \cdot \mathbf{F} \cdot d\mathbf{X} = J\, d\mathbf{S} \cdot d\mathbf{X} \tag{1.1.12}$$

$$(\mathbf{F}^T \cdot d\mathbf{s}) d\mathbf{X} \cdot = J\, d\mathbf{S} \cdot d\mathbf{X} \tag{1.1.13}$$

$$(\mathbf{F}^T \cdot d\mathbf{s} - J\, d\mathbf{S}) \cdot d\mathbf{X} = 0 \tag{1.1.14}$$

finally, since the final equation holds for any arbitrary $d\mathbf{X}$, one obtain the *Nanson's formula*:

$$\mathbf{F}^T \cdot d\mathbf{s} - J\, d\mathbf{S} = 0 \tag{1.1.15}$$

1.1.2 Material strain tensors

Starting from above definitions, it is possible to study now what happens to two neighborhood points in the reference configuration during the evolution of the continuum body. Let $\mathbf{P}$ and $\mathbf{Q}$ two neighborhood points in Ω, $\mathbf{P}'$ and $\mathbf{Q}'$ the associated points in the actual configuration, as shown in the figure below:

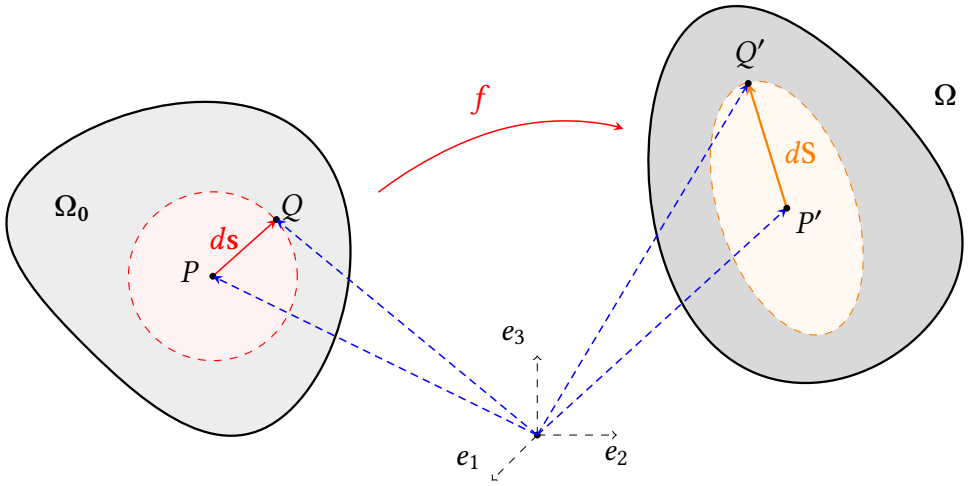

Figure 1.1.2: Finite deformation of a continuum body.

In differential terms, since the two point are considered very near, it is possible to linearize the change in lenght of the vector $(\mathbf{Q}' - \mathbf{P}')$ in terms of deformation gradient:

$$d\mathbf{S} = \mathbf{Q}' - \mathbf{P}' = \mathbf{F}\,(\mathbf{Q} - \mathbf{P}) = \mathbf{F}d\mathbf{s} \tag{1.1.16}$$

$$d\mathbf{s} = \mathbf{F}^{-1}d\mathbf{S} \tag{1.1.17}$$

thus, the modulus of these vectors are:

$$\|d\mathbf{S}\|^2 = d\mathbf{S}\cdot d\mathbf{S} = d\mathbf{S}^T d\mathbf{S} = (\mathbf{F}d\mathbf{s})^T(\mathbf{F}d\mathbf{s}) = d\mathbf{s}^T(\mathbf{F}^T\mathbf{F})d\mathbf{s} \tag{1.1.18}$$

$$\|d\mathbf{s}\|^2 = d\mathbf{s}\cdot d\mathbf{s} = d\mathbf{s}^T d\mathbf{s} = d\mathbf{s}^T(\mathbf{I})d\mathbf{s} \tag{1.1.19}$$

therefore, the variation of the distance between two near points from the reference configuration to the actual one is:

$$\epsilon^2 = \|d\mathbf{S}\|^2 - \|d\mathbf{s}\|^2 = d\mathbf{s}^T(\mathbf{F}^T\mathbf{F})d\mathbf{s} - d\mathbf{s}^T(\mathbf{I})d\mathbf{s} = d\mathbf{s}^T(\mathbf{F}^T\mathbf{F} - \mathbf{I})d\mathbf{s} \tag{1.1.20}$$

where the terms in brackets is related to the Green-Lagrange tensor for finite deformations, defined as the tensor:

$$\mathbf{E} = \frac{1}{2}\left(\mathbf{F}^T\mathbf{F} - \mathbf{I}\right) \tag{1.1.21}$$

Starting again from the fundamental kinematics relation eq.(1.1.7), the Green-Lagrange strain tensor can be rexpressed introducing the right Cauchy-Green strain tensor as follow:

$$\begin{aligned} \mathbf{C} = \mathbf{F}^T\mathbf{F} &= (\mathbf{H}+\mathbf{I})^T(\mathbf{H}+\mathbf{I}) \\ &= \mathbf{H}^T\mathbf{H}+\mathbf{H}^T\mathbf{I}+\mathbf{I}^T\mathbf{H}+\mathbf{I}^T\mathbf{I} \\ &= \mathbf{H}^T\mathbf{H}+\mathbf{H}^T+\mathbf{H}^T+\mathbf{I} \end{aligned} \tag{1.1.22}$$

$$\begin{aligned} \mathbf{E} &= \frac{1}{2}\left(\mathbf{F}^T\mathbf{F}-\mathbf{I}\right) \\ &= \frac{1}{2}\left(\mathbf{H}^T\mathbf{H}+\mathbf{H}^T+\mathbf{H}^T+\mathbf{I}-\mathbf{I}\right) \\ &= \frac{1}{2}\left(\mathbf{H}^T\mathbf{H}+\mathbf{H}^T+\mathbf{H}\right) \end{aligned} \tag{1.1.23}$$

In continuum mechanics, the analysis of strains corresponds to the computation of deformation gradient: in the general case, by the Polar Decomposition Theorem, it can be written as the matrix product of a pure strech tensor and a pure rotation tensor, namely $\mathbf{F}$ admits an unique polar decomposition in such a way $\mathbf{F} = \mathbf{RU}$.
The tensor $\mathbf{U}$ is the (right) material stretch tensor defined as:

$$\mathbf{U}^2 = \mathbf{UU} = \mathbf{C} \tag{1.1.24}$$

and it represents a measure of local stretching/contraction along the eigenvectors, namely principal directions, instead $\mathbf{R}$ is the unique rotation matrix defined in such a way $\mathbf{R}^T\mathbf{R} = \mathbf{I}$. The physical interpretation of the tensor $\mathbf{U}$ can be found in the definition of strech vector and its variation during the deformation: starting again from the initial spacial configuration of the body and considering two neighborhood points defining the direction $\mathbf{a_0}$ at distance $d\epsilon$, the stretch vector $\lambda_{\mathbf{a_0}}$ is defined as follows:

$$\lambda_{\mathbf{a_0}} = \mathbf{F}\mathbf{a_0} \tag{1.1.25}$$

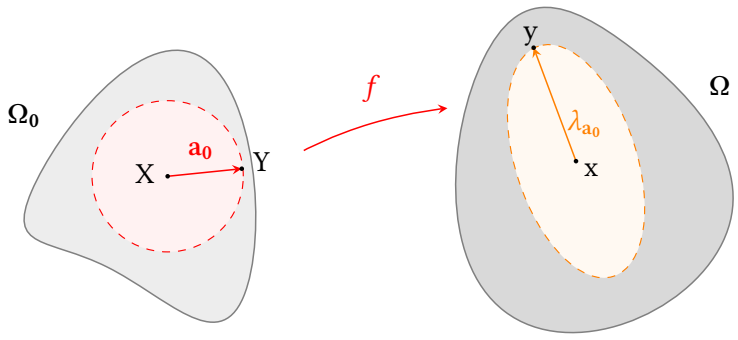

Figure 1.1.3: Stretch during deformation of a continuum body.

Considering the two same point in the actual current configuration, the vector the modulus of the distance can be computed by the previously adopted linearization:

$$y - x = \mathbf{F}\,(Y - X) = \mathbf{F} d\epsilon \mathbf{a_0} = \lambda_{\mathbf{a}_0} d\epsilon \tag{1.1.26}$$

$$|y - x| = \sqrt{(y - x) \cdot (y - x)} = d\epsilon \sqrt{\lambda_{\mathbf{a}_0} \cdot \lambda_{\mathbf{a}_0}} = \lambda d\epsilon \tag{1.1.27}$$

$$\lambda^2 = \lambda_{\mathbf{a}_0} \cdot \lambda_{\mathbf{a}_0} = \mathbf{F a_0} \cdot \mathbf{F a_0} = \mathbf{a_0}^T \mathbf{F^T F a_0} \tag{1.1.28}$$

where $\mathbf{F^T F}$ is the already defined right Cauchy-Green strain tensor: it is a measure of stretches between two neighborhood points during the deformation. One can note that $\mathbf{C}$ is a symmetric and positive-definite tensor. In addition, starting from this definition, using the Polar Decomposition Theorem:

$$\lambda = \mathbf{F a_0} = \mathbf{R U a_0} \rightarrow$$

$$\begin{aligned} \lambda^2 &= (\mathbf{R U a_0}) \cdot (\mathbf{R U a_0}) = \mathbf{a_0 U}^T \mathbf{R}^T \mathbf{R U a_0} = \\ &= \mathbf{a_0 U}^T \mathbf{U a_0} = (\mathbf{U a_0}) \cdot (\mathbf{U a_0}) = |\mathbf{U a_0}|^2 \end{aligned}$$

In other words, the right stretch tensor, and so Cauchy-Green strain tensor does not provide any information about the local change in orientation of two neighborhood points in the material configuration after the deformation.
Finally, it has to be noted that the Green-Lagrange strain tensor is a symmetric tensor and its components are:

$$\mathbf{E} = \begin{bmatrix} \epsilon_{xx} & \gamma_{xy} & \gamma_{xz} \\ \gamma_{xy} & \epsilon_{yy} & \gamma_{yz} \\ \gamma_{xz} & \gamma_{yz} & \epsilon_{zz} \end{bmatrix} \tag{1.1.29}$$

The components of $\mathbf{E}$, following the displacement gradient tensor definition eq.(1.1.5) and substituting into eq.(1.1.24), are then:

$$\epsilon_{xx} = \frac{\partial u}{\partial x} + \frac{1}{2}\left[\left(\frac{\partial u}{\partial x}\right)^2 + \left(\frac{\partial v}{\partial x}\right)^2 + \left(\frac{\partial w}{\partial x}\right)^2 \right] \tag{1.1.30}$$

$$\epsilon_{yy} = \frac{\partial v}{\partial x} + \frac{1}{2}\left[\left(\frac{\partial u}{\partial y}\right)^2 + \left(\frac{\partial v}{\partial y}\right)^2 + \left(\frac{\partial w}{\partial y}\right)^2 \right] \tag{1.1.31}$$

$$\epsilon_{zz} = \frac{\partial u}{\partial z} + \frac{1}{2}\left[\left(\frac{\partial u}{\partial z}\right)^2 + \left(\frac{\partial v}{\partial z}\right)^2 + \left(\frac{\partial w}{\partial z}\right)^2 \right] \tag{1.1.32}$$

$$\gamma_{xy} = \frac{1}{2}\left(\frac{\partial u}{\partial y} + \frac{\partial v}{\partial x}\right) + \frac{1}{2}\left[\frac{\partial u}{\partial x}\frac{\partial u}{\partial y} + \frac{\partial v}{\partial x}\frac{\partial v}{\partial y} + \frac{\partial w}{\partial x}\frac{\partial w}{\partial y} \right] \tag{1.1.33}$$

$$\gamma_{xz} = \frac{1}{2}\left(\frac{\partial u}{\partial z} + \frac{\partial w}{\partial x}\right) + \frac{1}{2}\left[\frac{\partial u}{\partial x}\frac{\partial u}{\partial z} + \frac{\partial v}{\partial x}\frac{\partial v}{\partial z} + \frac{\partial w}{\partial x}\frac{\partial w}{\partial z} \right] \tag{1.1.34}$$

$$\gamma_{xz} = \frac{1}{2}\left(\frac{\partial v}{\partial z} + \frac{\partial w}{\partial y}\right) + \frac{1}{2}\left[\frac{\partial u}{\partial y}\frac{\partial u}{\partial z} + \frac{\partial v}{\partial y}\frac{\partial v}{\partial z} + \frac{\partial w}{\partial y}\frac{\partial w}{\partial z} \right] \tag{1.1.35}$$

1.1.3 Equilibrium conditions and stress tensor

Consider a continuum body Ω subjected to surface and volume forces and geometrical constraints. Fixing a generic material point inside the body $\mathbf{P} \in \Omega$ let's consider a plane Π, passing through this point, and let $\mathbf{n}$ be its normal vector: this plane cuts the body and identifies two sub-bodies, Ω^+ and Ω^-.

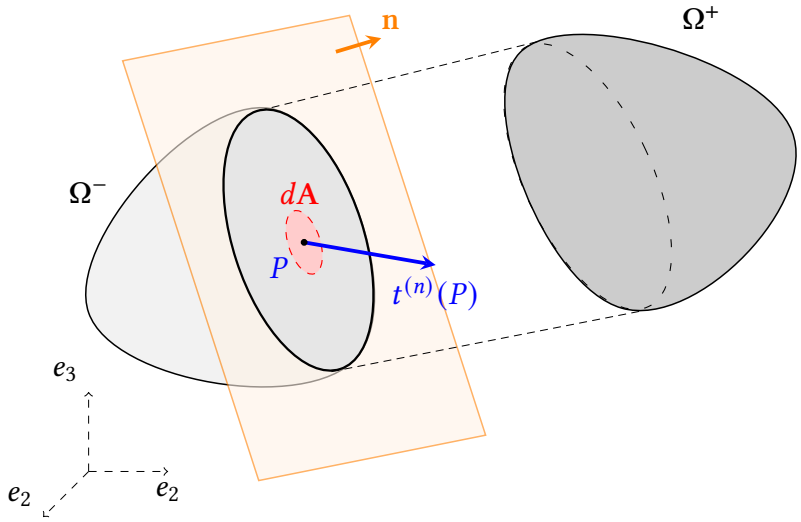

Figure 1.1.4: Cutting plane, tension vector in actual configuration

Euler-Cauchy deformable body assumption, also known as *Cauchy's section principle*: in an infinitesimal neighborhood dA of $\mathbf{P}$ (in the cutting plane) the action of a sub-body on the other one is a surface forces field defined over dA. If $d\mathbf{R}$ is the resultant vector of this vector force field, Cauchy's section principle means that $d\mathbf{R}$ admits finite limit when the infinitesimal neighborhood of $\mathbf{P}$ namely dA approaches zero:

$$\mathbf{t}^{(n)}(\mathbf{P}) = \lim_{dA \to 0} \frac{R^{(\mathbf{n})}}{dA} \tag{1.1.36}$$

This finite limit is called *tension*, in the point $\mathbf{P}$ related to the plane of normal vector $\mathbf{n}$. Under the Cauchy's section principle assumption, the tension vector is then function both of the material point and the cutting plane, but, fixing the material point, the tension vector changes only if the normal vector of the cutting plane changes.
Global equilibrium conditions for a deformable body are given by the *Cauchy's Theorem* for continuum body: if Ω is a deformable body, the internal forces and external forces field is known and the body is in equilibrium under the Euler-Cauchy assumption, then:

1. Existance of the stress tensor, namely *Cauchy's "true" stress tensor*:

$$\exists\, \boldsymbol{\sigma} \ni \mathbf{t}^{(n)}(\mathbf{P}) = \boldsymbol{\sigma}(\mathbf{P})\mathbf{n} \qquad \forall \mathbb{P}, \mathbf{n} \in \Omega \tag{1.1.37}$$

2. Translational equilibrium of the body: if $\mathbf{b}$ is the vector of volume forces, then

$$\nabla \cdot \boldsymbol{\sigma} + \mathbf{b} = 0 \tag{1.1.38}$$

3. Rotational equilibium: the stress tensor is symmetric

$$\boldsymbol{\sigma}(\mathbf{P}) = \boldsymbol{\sigma}^T(\mathbf{P}) \qquad \forall \mathbb{P} \in \Omega \tag{1.1.39}$$

Let $\{e_1, e_2, e_3\}$ be the orthonormal cartesian reference frame: the components of the stress tensor can be characterized by considering the three planes passing through the material point **P** and parallel to the coordinate planes: fixing as normal vector of the cutting plane the three normal vector of the cartesian basis, *normal stress components* and *tangential stress components* can be identified:

$$\begin{aligned}
\sigma_{xx} &= \mathbf{t}_1 \cdot \mathbf{e_1} = (\mathbf{T}\ \mathbf{e_1}) \cdot \mathbf{e_1} & \tau_{xy} &= \mathbf{t}_1 \cdot \mathbf{e}_2 = (\mathbf{T}\ \mathbf{e_1}) \cdot \mathbf{e}_2 & \tau_{xz} &= \mathbf{t}_1 \cdot \mathbf{e}_3 = (\mathbf{T}\ \mathbf{e_1}) \cdot \mathbf{e}_3 \\
\tau_{yx} &= \mathbf{t}_2 \cdot \mathbf{e_1} = (\mathbf{T}\ \mathbf{e}_2) \cdot \mathbf{e_1} & \sigma_{yy} &= \mathbf{t}_2 \cdot \mathbf{e}_2 = (\mathbf{T}\ \mathbf{e}_2) \cdot \mathbf{e}_2 & \tau_{yz} &= \mathbf{t}_2 \cdot \mathbf{e}_3 = (\mathbf{T}\ \mathbf{e}_2) \cdot \mathbf{e}_3 \\
\tau_{zx} &= \mathbf{t}_3 \cdot \mathbf{e_1} = (\mathbf{T}\ \mathbf{e}_3) \cdot \mathbf{e_1} & \tau_{zy} &= \mathbf{t}_3 \cdot \mathbf{e}_2 = (\mathbf{T}\ \mathbf{e}_3) \cdot \mathbf{e}_2 & \sigma_{zz} &= \mathbf{t}_3 \cdot \mathbf{e}_3 = (\mathbf{T}\ \mathbf{e}_3) \cdot \mathbf{e}_3
\end{aligned}$$

1.1.4 Piola-Kirchoff stress tensors

Starting from the definition, for every surface elements considered on the cutting plane of normal vector $\boldsymbol{n}$ the resultant *tension vector* can be defined starting either from reference or material configuration:

$$\begin{cases} \text{Actual:} & R^{(n)} = \mathbf{t}(\mathbf{x}, \mathbf{n})ds = \boldsymbol{\sigma}(\mathbf{x})\ \mathbf{n}\ ds = \boldsymbol{\sigma}(\mathbf{x})\ d\mathbf{s} \\ \text{Reference:} & R^{(N)} = \mathbf{T}(\mathbf{X}, \mathbf{n})dS = \mathbf{P}(\mathbf{X})\ \mathbf{N}\ dS = \mathbf{P}(\mathbf{X})\ d\mathbf{S} \end{cases} \tag{1.1.40}$$

Since the volume is in equilibrium:

$$\boldsymbol{\sigma}(\mathbf{x})\ d\mathbf{s} = \mathbf{P}(\mathbf{X})\ d\mathbf{S} \tag{1.1.41}$$

applying now Nanson's formula (1.1.15), $d\mathbf{s} = \mathbf{F}^{-T} J d\mathbf{S}$:

$$\boldsymbol{\sigma}(\mathbf{x})\ d\mathbf{s} = \boldsymbol{\sigma}(\mathbf{x})\ \mathbf{F}^{-T} J d\mathbf{S} = \mathbf{P}(\mathbf{X})\ d\mathbf{S} \tag{1.1.42}$$

The definition of PK1 (Piola-Kirchoff 1) stress tensor is obtained:

$$\mathbf{P}(\mathbf{X}) = J\boldsymbol{\sigma}(\mathbf{x})\mathbf{F}^{-T} \tag{1.1.43}$$

By energetic arguments and consideration, one can also define the work-conjugate of the Green-Lagrange strain tensor, the PK2 (Piola-Kirchoff 2) stress tensor, referred to the original configuration defined as:

$$\mathbf{S}(\mathbf{x}) = J\mathbf{F}^{-1}\boldsymbol{\sigma}(\mathbf{x})\mathbf{F}^{-T} = \mathbf{F}^{-1}\mathbf{P} \tag{1.1.44}$$

Starting from these definitions, *constitutive laws* are mathematical model that characterize the behavior of the material by relation between strain measures and stresses measures.

1.2 Principle of Virtual Displacements

Structural problem governing equations based on displacement formulation typically are derived from variational principles: these mathematical tools allow the formulations of many problems in the so-called *weak form*. Finite Element Method considered in the present work rely on the PVD (Principle of Virtual Displacement), a formulation of governing equation based on variational statement.

1.2.1 Governing equation in weak form

Let Ω be a continuum body: suppose that $\mathbf{u}$ is the displacement field and the body is in equilibrium under the Cauchy's conditions (1.1.38), with $\mathbf{b}$ is the vector of volume forces. On the body, both geometrical constraints and loads are applied, defining then initial and boundary value problem of the global equilibrium: one can consider a subdomain of the whole surface $\partial\Omega_\sigma$ on which only loads are applied, and $\partial\Omega_u$ on which geometrical constraints are applied, in such a way $\partial\Omega = \partial\Omega_\sigma \cup \partial\Omega_u$. In other words *Dirichlet* boundary conditions on the displacement field and *Neumann* boundary conditions on the loads are considered. In this formulation then, the governing equation are expressed as:

$$\begin{cases} \nabla \cdot \boldsymbol{\sigma} + \mathbf{b} = 0 \\ \mathbf{u} = \bar{\mathbf{u}} \qquad \text{on } \partial\Omega_u \\ \mathbf{t} = \sigma\mathbf{n} = \bar{\mathbf{t}} \quad \text{on } \partial\Omega_\sigma \end{cases} \tag{1.2.1}$$

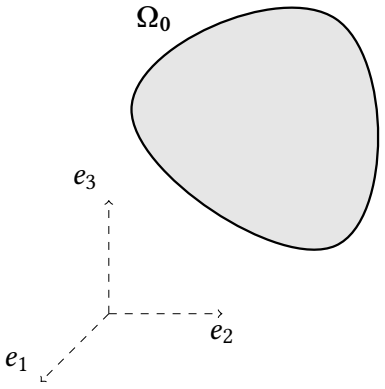

Figure 1.2.1: Initial and boundary value problem for structural governing equation

Analytical solutions of governing equations (1.2.1) are available only for very special and limited cases: the general solution can be obtained by approximated methods based on variational principles. Most variational principles are based on *calculus of variations*: let's consider a generic test function η and let's define the functional:

$$f(\mathbf{u}, \eta) = \int_\Omega (\nabla \cdot \boldsymbol{\sigma} + \mathbf{b}) \cdot \eta dV = 0 \tag{1.2.2}$$

Eq.(1.2.2) is the so call weak-form of equations of motion. The fundamental lemma of calculus of variations says that, since the test function is arbitrary, then $\nabla \cdot \boldsymbol{\sigma} + \mathbf{b}$ must be null

in the whole domain of integration, obtaining again Cauchy's equilibrium conditions: in other words, the solution of the strong form equilibrium equations is absolutely equivalent to the solution in weak form. Exploiting the scalar products, considering tensor calculus properties and Divergence's theorem, one can rewrite the weak form equation for the structural problem in a more convenient notation:

$$f(\mathbf{u}, \eta) = \int_{\Omega} (\boldsymbol{\sigma} : \nabla\eta + \mathbf{b} \cdot \eta) dV - \int_{\partial\Omega} \boldsymbol{\sigma}\eta \cdot \mathbf{n} dS = 0 \tag{1.2.3}$$

If the arbitrary test-function considered is the *virtual variation* of the displacement field, namely $\delta\mathbf{u}$, the *principle of Virtual Work* is obtained:

$$f(\mathbf{u}, \delta\mathbf{u}) = \int_{\Omega} (\boldsymbol{\sigma} : \delta\boldsymbol{\epsilon} + \mathbf{b} \cdot \delta\mathbf{u})\, dV - \int_{\partial\Omega} \bar{\boldsymbol{t}} \cdot \delta\mathbf{u}\, dS = 0 \tag{1.2.4}$$

This principle is one of the easiest variational principle: neglecting the contribution of the volume forces, the work contribution of the internal stresses ($\boldsymbol{\sigma} : \delta\boldsymbol{\epsilon}$ is equal to the work done by external loads along the virtual displacements $\bar{\boldsymbol{t}} \cdot \delta\mathbf{u}$. Defining the internal (mechanical) virtual work and external (mechanical) virtual work as:

$$\delta\mathbb{W}_{int} = \int_{\Omega} \boldsymbol{\sigma} : \delta\boldsymbol{\epsilon}\, dV \tag{1.2.5}$$

$$\delta\mathbb{W}_{ext} = \int_{\partial\Omega} \bar{\boldsymbol{t}} \cdot \delta\mathbf{u}\, dS - \int_{\Omega} \mathbf{b} \cdot \delta\mathbf{u}\, dV \tag{1.2.6}$$

PVD states that the virtual variation of the internal work is equal to the virtual variation of external work for any arbitrary virtual displacement.
In the framework of the present thesis, due to compact vector notation adopted both for displacements and strains, the internal work can be explicitly expressed as:

$$\begin{aligned} \delta\mathbb{W}_{int} &= \int_{\Omega} \delta\boldsymbol{\epsilon}^T \boldsymbol{\sigma}\, dV = \\ &= \int_{\Omega} (\sigma_{xx}\delta\epsilon_{xx} + \sigma_{yy}\delta\epsilon_{yy} + \sigma_{zz}\delta\epsilon_{zz} + \tau_{xz}\delta\epsilon_{xz} + \tau_{yz}\delta\epsilon_{yz} + +\tau_{xy}\delta\epsilon_{xy})\, dV \end{aligned} \tag{1.2.7}$$

Finally, the external work can be expressed as the sum of different contribution: volume forces $\mathbf{b}$, pressure forces p, distributed load on lines $\mathbf{q}$ and concentrated loads $\mathbf{P}$, obtaining

$$\begin{aligned} \delta\mathbb{W}_{ext} &= \int_{\partial\Omega} \bar{\boldsymbol{t}} \cdot \delta\mathbf{u}\, dS - \int_{\Omega} \mathbf{b} \cdot \delta\mathbf{u}\, dV = \\ &= \int_{\Omega} \delta\mathbf{u}^T \mathbf{g}\, dV + \int_{\partial\Omega} \delta\mathbf{u}^T \mathbf{p}\, dS + \int_{\partial\Omega_L} \delta\mathbf{u}^T \mathbf{q}\, dy + \delta\mathbf{u}^T \mathbf{P} \end{aligned} \tag{1.2.8}$$

This formulation is the starting point for the present implementation of 1D, 2D and 3D FEM-CUF finite elements: by imposing the polynomial expansion of the displacement field and by fixing the consititutive law for the Cauchy's stress tensor, governing equations in weak form will be written in matrix form.

Chapter 2

Constitutive laws

Consitutive laws are relations between the stress tensor and the strain tensor: in the general case, they are mathematical model for representing the actual behavior of materials and structures, describing the actual (or approximated) response of the material from a deformation point of view when loads and geometrical constraints are applied. In the specific case of structural mechanics, constitutive laws are mathematical relation describing connection between stresses or loads to strains.

2.1 Linear elastic materials

In the case of a *linear elastic material*, in a generic configuration of the body, the stress tensor $\boldsymbol{\sigma}$ is only function of instantaneous strain tensor previously defined as the Green-Lagrange strain tensor $\mathbf{E}$. In mathematical terms, a deformable body is linearly elastic if there exists an *elasticity tensor* $\mathbb{C}$ such that:

$$\boldsymbol{\sigma}(\mathbf{P}) = \mathbb{C}\mathbf{E} \qquad \sigma_{ij} = C_{ijkm}E_{km} \tag{2.1.1}$$

Where, in the expression in terms of components, Einstein notation is adopted: repeated indeces means sum over the indeces. The tensor $\mathbb{C}$ then is a fourth-order tensor, identified by 81 constant terms, that defines a linear transformation from the deformation space to the stress space, and it is able to characterize the behaviour of the material. By assigning the elasticity tensor of a material, is automatically assigned the behaviour of the body in terms of deformation and tension components.
Since both the strain tensor and the stress tensor are symmetric tensors, $\mathbb{C}$ need to satisfy particular simmetries, called *minor* and *major* symmetries. In the present work, mainly isotropic material are considered: in every material point of the body the constitutive properties of the material are the same in every direction of the space, namely the mechanical properties do not depend on the considered direction. The elasticity tensor of isotropic material fullfil both minor and major symmetries, therefore only two constants are required, namely:

$$\mathbb{C}_{ijkm} = \mathbb{C}_{jimk} = \mathbb{C}_{ijmk} = \mathbb{C}_{kmij} \tag{2.1.2}$$

$$\mathbb{C}_{ijkm} = G(\delta_{ij}\delta_{km} + \delta_{im}\delta_{jk}) + \lambda\delta_{ij}\delta_{km} \tag{2.1.3}$$

2.2 Isotropic hyperelastic materials

In the case of a *hyperelastic material*, the existance of a potential function Ψ is postulated: the material is described by a Helmholtz free-energy function defined per unit volume. When this free-energy function depends only on the deformation gradient, namely $\Psi = \Psi(\mathbf{F})$, this function is also called strain-energy or stored-energy function.
The physical relation between strains and stresses in the case of an hyperleastic material is given in terms of Piola-Kirchoff 1 stress tensor:

$$\mathbf{P} = \frac{\partial \Psi(\mathbf{F})}{\partial \mathbf{F}} \tag{2.2.1}$$

By thermodynamics argument, often $\mathbf{P}$ is said the thermodynamic force work conjugate to $\mathbf{F}$. It satisfy the normalization conditions, namely $\Psi(\mathbb{I}) = 0$ and in general is a non-negative function for each value of the deformation gradient (restricting the possible admissible deformation fields).
Recalling that, by Polar Decomposition Theorem, the deformation gradient can be expressed as a pure-rotational part and a pure stretch term, namely $\mathbf{F} = \mathbf{RU}$, by objectivity arguments one can find that the strain energy function is only depending on the stretching part of the deformation gradient, so $\Psi = \Psi(\mathbf{F}) = \Psi(\mathbf{U})$.
Finally, by imposing the chain rule of differentiation considering that the right Cauchy-Green strain tensor and the Green-Lagrange strain tensor are given by $\mathbf{C} = 2\mathbf{E} + \mathbf{I}$, one can finally find that $\Psi = \Psi(\mathbf{F}) = \Psi(\mathbf{U}) = \Psi(\mathbf{E})$.
Reduced form of constitutive equations can be obtained analyzing the time derivative of the strain-energy function. Since the right Cauchy-Green strain tensor is a symmetric tensor, the following relation holds:

$$\left(\frac{\partial \Psi(\mathbf{F})}{\partial \mathbf{F}}\right)^T = 2\left(\frac{\partial \Psi(\mathbf{C})}{\partial \mathbf{C}}\right)^T \mathbf{F}^T \tag{2.2.2}$$

From the already known definition of Piola-Kirchoff 1 stress tensor definition, remembering that the "true" Cauchy stress tensor is a symmetric tensor, one can obtain:

$$\sigma = J^{-1}\mathbf{P}\mathbf{F}^T = J^{-1}\mathbf{F}\mathbf{P}^T = J^{-1}\mathbf{F}\left(\frac{\partial \Psi(\mathbf{F})}{\partial \mathbf{F}}\right)^T = 2J^{-1}\mathbf{F}\left(\frac{\partial \Psi(\mathbf{C})}{\partial \mathbf{C}}\right)^T \mathbf{F}^T \tag{2.2.3}$$

Alternatively useful expression for the PK1 and PK2 stress tensor can be obtained:

$$\mathbf{P} = 2\mathbf{F}\frac{\partial \Psi(\mathbf{C})}{\partial \mathbf{C}} \tag{2.2.4}$$

$$\mathbf{S} = \mathbf{F}^{-1}\mathbf{P} = 2\mathbf{F}^{-1}\mathbf{F}\frac{\partial \Psi(\mathbf{C})}{\partial \mathbf{C}} = 2\frac{\partial \Psi(\mathbf{C})}{\partial \mathbf{C}} = \frac{\partial \Psi(\mathbf{E})}{\partial \mathbf{E}} \tag{2.2.5}$$

These expression represents the starting point for the derivation of the governing equation for an incompressible and compressible hypereleastic material, and they are independent on the model of strain-energy function adopted.

2.2.1 Constitutive equations in terms of invariants

In the case of isotropic hyperelastic material, invariance under rotation is fulfilled: governing equation can be expressed then in terms of invariant of tensor-variables by the representation theorem for invariants in the case of isotropic scalar functions. The definition of strain energy function in terms of invariants of right Cauch-Green tensor will be then:

$$\Psi(\mathbf{C}) = \Psi(\mathbf{C})(I_1(\mathbf{C}), I_2(\mathbf{C}), I_3(\mathbf{C})) \tag{2.2.6}$$

where $I_1,\ I_2, I_3$ are the invariants defined as:

$$I_1 = \mathrm{tr}(\mathbf{C}) \tag{2.2.7}$$

$$I_2 = \frac{1}{2}(I_1^2 - \mathrm{tr}(\mathbf{C}^2)) \tag{2.2.8}$$

$$I_3 = \det(\mathbf{C}) = \det(\mathbf{F}^T\mathbf{F}) = J^2 \tag{2.2.9}$$

In particular I_3 is square the volume ratio coefficient, a measure of the change in volume of an infinitesimal particle of the body during the deformation. If the material preserves the volume, namely it remains constant during the deformation, incompressibility constraint holds, $I_3 = J = 1$.
The derivative of the strain-energy function with respect of $\mathbf{C}$ can be computed by applying the chain rule:

$$\frac{\partial\Psi(\mathbf{C})}{\partial\mathbf{C}} = \frac{\partial\Psi(\mathbf{C})}{\partial I_1}\frac{\partial I_1}{\partial\mathbf{C}} + \frac{\partial\Psi(\mathbf{C})}{\partial I_2}\frac{\partial I_2}{\partial\mathbf{C}} + \frac{\partial\Psi(\mathbf{C})}{\partial I_3}\frac{\partial I_3}{\partial\mathbf{C}} \tag{2.2.10}$$

By tensor-algebra and tensor calculus, remembering the properties of double contraction, the general expression of derivatives of the invariant are obtained:

$$\frac{\partial I_1}{\partial\mathbf{C}} = \frac{\partial \mathrm{tr}\mathbf{C}}{\partial\mathbf{C}} = \frac{\partial(\mathbf{I} : \mathbf{C})}{\partial\mathbf{C}} = \mathbf{I} \tag{2.2.11}$$

$$\frac{\partial I_2}{\partial\mathbf{C}} = \frac{1}{2}\left(\mathrm{tr}\mathbf{C}\ \mathbf{I} - \frac{\partial \mathrm{tr}\mathbf{C}^2}{\partial\mathbf{C}}\right) = I_1\mathbf{I} - \mathbf{C} \tag{2.2.12}$$

$$\frac{\partial I_3}{\partial\mathbf{C}} = I_3\mathbf{C}^{-1} \tag{2.2.13}$$

Substituting these three above relations in (2.2.5), the most general expression of PK2 stress tensor in terms of invariant is found, and it characterize the behavior of isotropic hyperelastic materials in the finite strains scenario:

$$\mathbf{S} = 2\frac{\partial\Psi(\mathbf{C})}{\partial\mathbf{C}} = 2\left[\left(\frac{\partial\Psi}{\partial I_1} + I_1\frac{\partial\Psi}{\partial I_2}\right)\mathbf{I} - \frac{\partial\Psi}{\partial I_2}\mathbf{C} + I_3\frac{\partial\Psi}{\partial I_3}\mathbf{C}^{-1}\right] \tag{2.2.14}$$

2.2.2 Compressible hyperelastic materials constitutive equations

In literature, since there exists materials that behaves differently depending on the direction of loads applied, according to Flory [21] the deformation gradient is split into the so called *volumetric* and *isochoric* parts:

$$\mathbf{F} = (J^{\frac{1}{3}}\mathbf{I})\bar{\mathbf{F}} = \mathbf{F_{vol}}\bar{\mathbf{F}} \tag{2.2.15}$$

and, consistently with the strain measure already defined by the right Cauchy-Green tensor:

$$\mathbf{C} = (J^{\frac{2}{3}}\mathbf{I})\bar{\mathbf{C}} = \mathbf{C_{vol}}\bar{\mathbf{C}} \tag{2.2.16}$$

In the above relations, $\mathbf{F_{vol}}$, $\mathbf{C_{vol}}$ are associated to a *volume-chaning* behavior, instead $\bar{\mathbf{F}}$, $\bar{\mathbf{C}}$ to a *volume-preserving* behavior. In the principal reference frame of the eigenvector of each tensor, one can define then the so-called *modified principal stretches*.
In this framework then, the strain-energy function is assumed as a decoupled representation, in which the volumetric and isochoric part are distinct contributes:

$$\Psi(\mathbf{C}) = \Psi_{vol}(J) + \Psi_{iso}(\bar{\mathbf{C}}) = \Psi_{vol}(I_3) + \bar{\Psi}(\bar{I}_1, \bar{I}_2) \tag{2.2.17}$$

where $\bar{I}_1$, $\bar{I}_2$ are the invariants of the isochoric part of the right Cauchy-Green tensor $\bar{\mathbf{C}}$. In the present work, first-invariant hyperelasticity is considered: the strain-energy isochoric function depends only on $\bar{I}_1$, namely $\bar{\Psi} = \bar{\Psi}(\bar{I}_1)$.
Again, according to this decomposition, also the PK2 can be split in the sum of a purely volumetric part and a purely isochoric part:

$$\mathbf{S} = 2\frac{\partial \Psi(\mathbf{C})}{\partial \mathbf{C}} = \mathbf{S}_{vol} + \mathbf{S}_{iso} \tag{2.2.18}$$

where, in the above definition:

$$\mathbf{S}_{vol} = 2\frac{\partial \Psi_{vol}}{\partial \mathbf{C}} = J\ p\ \mathbf{C}^{-1} \tag{2.2.19}$$

$$\mathbf{S}_{vol} = 2\frac{\partial \bar{\Psi}}{\partial \mathbf{C}} = 2J^{-\frac{2}{3}}\ \frac{\partial \bar{\Psi}}{\partial \bar{I}_1}\left(\mathbf{I} - \frac{1}{3}\bar{I}_1\mathbf{C}^{-1}\right) \tag{2.2.20}$$

In this explicit form of governing equation, one important parameter appearing in the derivation is the *hydrostatic pressure* $p = \frac{\partial \Psi_{vol}}{\partial J}$.
As said before, this derivation holds independently on the specific strain energy function considered. In the present work, different hyperelastic models will be adopted, and the specific expression of strain-energy function considered can be found in App.C.

2.2.3 Material Jacobian tensor and incremental formulation

In the framework of total-Lagrangian formulation of nonlinear problems, typically incremental formulations are considered. According to Holzapfel [5], the constitutive equation (2.2.14) can be written by the total differential form considering and incremental formulation:

$$\Delta \mathbf{S} = C \frac{1}{2} \Delta \mathbf{C} \tag{2.2.21}$$

where C is the so-called *material Jacobian tensor*: in the linearized framwork of governing equation and in analogy with Hooke's law, it represents the tangent elasticity tensor, and is expressed as

$$C = 2\frac{\partial \mathbf{S}(\mathbf{C})}{\partial \mathbf{C}} = \frac{\partial \mathbf{S}(\mathbf{E})}{\partial \mathbf{E}} = 4\frac{\partial^2 \Psi}{\partial \mathbf{C} \partial \mathbf{C}} \tag{2.2.22}$$

According to [19], under the hypothesis of first-invariant hyperleasticity (namely, again, $\bar{\Psi} = \bar{\Psi}(\bar{I}_1)$), the material Jacobian tensor can be expressed, as already done for the PK2 stress tensor and strain energy function, as sum of a volumetric and isochoric part:

$$\boldsymbol{C} = \boldsymbol{C}_{vol} + \boldsymbol{C}_{iso} \tag{2.2.23}$$

$$\boldsymbol{C}_{vol} = J\frac{\partial \Psi_{vol}}{\partial J}(\mathbf{C}^{-1} \otimes \mathbf{C}^{-1} - 2\mathbb{I}_{\mathbf{C}^{-1}}) + J^2 \frac{\partial^2 \Psi_{vol}}{\partial J^2} \mathbf{C}^{-1} \otimes \mathbf{C}^{-1} \tag{2.2.24}$$

$$\boldsymbol{C}_{iso} = -\frac{4}{3} J^{-\frac{2}{3}} \frac{\partial \bar{\Psi}}{\partial \bar{I}_1} [\mathbf{I} \otimes \mathbf{C}^{-1} + \mathbf{C}^{-1} \otimes \mathbf{I} - I_1 (\mathbb{I}_{\mathbf{C}^{-1}} + \frac{1}{3} \mathbf{C}^{-1} \otimes \mathbf{C}^{-1})] + J^{-\frac{4}{3}} \bar{\mathbf{C}}_{\bar{\Psi}} \tag{2.2.25}$$

$$\bar{\mathbf{C}}_{\bar{\Psi}} = 4\frac{\partial^2 \bar{\Psi}}{\partial \bar{I}_1{}^2} [\mathbf{I} \otimes \mathbf{I} - \frac{1}{3} I_1 (\mathbf{I} \otimes \mathbf{C}^{-1} + \mathbf{C}^{-1} \otimes \mathbf{I}) + \frac{1}{9} I_1^2 \mathbf{C}^{-1} \otimes \mathbf{C}^{-1}] \tag{2.2.26}$$

where $\mathbb{I}_{\mathbf{C}^{-1}} = -\frac{\partial \mathbf{C}^{-1}}{\partial \mathbf{C}}$. A more detailed derivation can be found again in [5].

Chapter 3

Carrera Unified Formulation

This chapter is devoted to the description of the Finite Element Method and Carrera Unified Formulation, both adopted in the implementation of finite elements for geometrically nonlinear structural problems. After a brief introduction to adopted notation, derivation of nonlinear equation is carried out and methods of discretization are described.
Governing equations will be written in terms of nonlinear algebraic systems of equation considering each fundamental nuclei involved. The numerical schemes involved in algorithm for nonlinear problems will be presented, with particular focus on Crisfield modified formulation of arc-lenght method.

3.1 Governing equations in matrix form

3.1.1 Geometrical relations

Let $\mathbf{u}$ be the continuous displacement field of the body, function of the material point, expressed as coloumn vector:

$$\mathbf{u} = \mathbf{u}(x, y, z) = \{\ u(x, y, z),\ v(x, y, z),\ w(x, y, z)\ \}^T \tag{3.1.1}$$

Since both strain tensor and stress tensor are symmetric tensors, both will be expressed by Voigt's notation in vector form as follow:

$$\begin{aligned} \boldsymbol{\epsilon} &= \{\ \epsilon_{xx}, \epsilon_{yy}, \epsilon_{zz}, 2\gamma_{xz}, 2\gamma_{yz}, 2\gamma_{xy}\ \}^T = \\ &= \{\ \epsilon_{xx}, \epsilon_{yy}, \epsilon_{zz}, \epsilon_{xz}, \epsilon_{yz}, \epsilon_{xy}\ \}^T \end{aligned} \tag{3.1.2}$$

$$\boldsymbol{\sigma} = \{\ \sigma_{xx}, \sigma_{yy}, \sigma_{zz}, \sigma_{xz}, \sigma_{yz}, \sigma_{xy}\ \}^T \tag{3.1.3}$$

Starting from the general expression of the Green-Lagrange strain tensor eq.(1.1.24), the strain vector can be expressed as:

$$\boldsymbol{\epsilon} = (\mathbf{b_l} + \mathbf{b_{nl}})\ \mathbf{u} \tag{3.1.4}$$

where the matrices $\mathbf{b_l}$ and $\mathbf{b_{nl}}$ are the formal matrix of the linear derivatives operator and non-linear derivative operators defined as follow:

$$\mathbf{b_l} = \begin{bmatrix} \frac{\partial}{\partial x} & 0 & 0 \\ 0 & \frac{\partial}{\partial y} & 0 \\ 0 & 0 & \frac{\partial}{\partial z} \\ \frac{\partial}{\partial z} & 0 & \frac{\partial}{\partial x} \\ \frac{\partial}{\partial z} & \frac{\partial}{\partial y} & 0 \\ \frac{\partial}{\partial y} & \frac{\partial}{\partial x} & 0 \end{bmatrix} \qquad \mathbf{b_{nl}} = \begin{bmatrix} \frac{1}{2}\left(\frac{\partial}{\partial x}\right)^2 & \frac{1}{2}\left(\frac{\partial}{\partial x}\right)^2 & \frac{1}{2}\left(\frac{\partial}{\partial x}\right)^2 \\ \frac{1}{2}\left(\frac{\partial}{\partial y}\right)^2 & \frac{1}{2}\left(\frac{\partial}{\partial y}\right)^2 & \frac{1}{2}\left(\frac{\partial}{\partial y}\right)^2 \\ \frac{1}{2}\left(\frac{\partial}{\partial z}\right)^2 & \frac{1}{2}\left(\frac{\partial}{\partial z}\right)^2 & \frac{1}{2}\left(\frac{\partial}{\partial z}\right)^2 \\ \frac{\partial}{\partial x}\frac{\partial}{\partial z} & \frac{\partial}{\partial x}\frac{\partial}{\partial z} & \frac{\partial}{\partial x}\frac{\partial}{\partial z} \\ \frac{\partial}{\partial y}\frac{\partial}{\partial z} & \frac{\partial}{\partial y}\frac{\partial}{\partial z} & \frac{\partial}{\partial y}\frac{\partial}{\partial z} \\ \frac{\partial}{\partial x}\frac{\partial}{\partial y} & \frac{\partial}{\partial x}\frac{\partial}{\partial y} & \frac{\partial}{\partial x}\frac{\partial}{\partial y} \end{bmatrix}$$

3.1.2 Constitutive equation

In the present work, constitutive linear elastic material are considered. The constitutive equationin Voigt's notation can be rewritten as:

$$\boldsymbol{\sigma} = \mathbb{C}\boldsymbol{\epsilon} \tag{3.1.5}$$

where $\mathbb{C}$ is the symmetric elasticity tensor defined as:

$$\mathbb{C} = \begin{bmatrix} C_{11} & C_{12} & C_{13} & C_{14} & C_{15} & C_{16} \\ C_{12} & C_{22} & C_{23} & C_{24} & C_{25} & C_{26} \\ C_{13} & C_{23} & C_{33} & C_{34} & C_{35} & C_{36} \\ C_{14} & C_{24} & C_{34} & C_{44} & C_{45} & C_{46} \\ C_{15} & C_{25} & C_{35} & C_{45} & C_{55} & C_{56} \\ C_{16} & C_{26} & C_{36} & C_{46} & C_{56} & C_{66} \end{bmatrix} \tag{3.1.6}$$

In the present work, mainly isotropic material are considered: in this particular case, the elasticity tensor assume a simplyfied expression depending only on two constants:

$$\mathbb{C} = \begin{bmatrix} C_{11} & C_{12} & C_{12} & 0 & 0 & 0 \\ C_{12} & C_{11} & C_{12} & 0 & 0 & 0 \\ C_{12} & C_{12} & C_{11} & 0 & 0 & 0 \\ 0 & 0 & 0 & C_{44} & 0 & 0 \\ 0 & 0 & 0 & 0 & C_{44} & 0 \\ 0 & 0 & 0 & 0 & 0 & C_{44} \end{bmatrix} \tag{3.1.7}$$

In which every component is expressed in terms of Lamè parameters, Young modulus and Poisson coefficient:

$$C_{11} = 2G + \lambda; \quad C_{12} = \lambda; \quad C_{44} = G; \quad G = \frac{E}{2(1+\nu)}; \quad \lambda = \frac{\nu E}{(1+\nu)(1-2\nu)} \tag{3.1.8}$$

For sake of completeness, elasticity tensor for orthotropic material (for which there exists principal direction) is reported. The properties in the transversal direction of the fiber are different in respect of the main direction of the fiber: it is then necessary to define Young moduli and more coefficient for each direction. The elasticity tensor assume this form:

$$\mathbb{C} = \begin{bmatrix} C_{11} & C_{12} & C_{13} & 0 & 0 & 0 \\ C_{21} & C_{22} & C_{23} & 0 & 0 & 0 \\ C_{31} & C_{32} & C_{33} & 0 & 0 & 0 \\ 0 & 0 & 0 & C_{44} & 0 & 0 \\ 0 & 0 & 0 & 0 & C_{55} & 0 \\ 0 & 0 & 0 & 0 & 0 & C_{66} \end{bmatrix} \tag{3.1.9}$$

The generic element of the elasticity tensor will be function of (in general) all this coefficient just defined:

$$C_{ij} = C_{ij}(\ E_1,\ E_2,\ E_3,\ G_{23},\ G_{13},\ G_{12},\ \nu_{23},\ \nu_{13},\ \nu_{12}\ ) \tag{3.1.10}$$

The previous expression are referred to the material reference frame. Considering the expression of the same elasticity tensor in the global reference frame, it is necessary to apply a rotation as defined:

$$\mathbb{T} = \begin{bmatrix} \cos^2\theta & \sin^2\theta & 0 & 0 & 0 & -\sin 2\theta \\ \sin^2\theta & \cos^2\theta & 0 & 0 & 0 & \sin 2\theta \\ 0 & 0 & 1 & 0 & 0 & 0 \\ 0 & 0 & 0 & \cos\theta & \sin\theta & 0 \\ 0 & 0 & 0 & -\sin\theta & \cos\theta & 0 \\ \sin\theta\cos\theta & -\sin\theta\cos\theta & 0 & 0 & 0 & \cos 2\theta \end{bmatrix} \tag{3.1.11}$$

Applying this rotation, Hooke's law written in the global ref. frame becomes:

$$\boldsymbol{\sigma} = \mathbb{T}^T\mathbb{C}\mathbb{T}\epsilon = \mathbb{Q}\boldsymbol{\epsilon} \tag{3.1.12}$$

Where the compact global matrix is:

$$\mathbb{Q} = \begin{bmatrix} Q_{11} & Q_{12} & Q_{13} & 0 & 0 & Q_{16} \\ Q_{21} & Q_{22} & Q_{23} & 0 & 0 & Q_{26} \\ Q_{31} & Q_{32} & Q_{33} & 0 & 0 & Q_{36} \\ 0 & 0 & 0 & Q_{44} & Q_{45} & 0 \\ 0 & 0 & 0 & Q_{54} & Q_{55} & 0 \\ Q_{16} & Q_{26} & Q_{36} & 0 & 0 & Q_{66} \end{bmatrix} \tag{3.1.13}$$

The components of the matrix $[Q]$ are given by:

$$
\begin{aligned}
Q_{11} &= m^4 C_{11} + 2m^2 n^2 C_{12} + n^4 C_{22} + 4m^2 n^2 C_{66} \\
Q_{12} = Q_{21} &= m^2 n^2 C_{11} + m^4 C_{12} + n^4 C_{12} + n^2 n^2 C_{22} - 4m^2 n^2 C_{66} \\
Q_{13} = Q_{31} &= m^2 C_{13} + n^2 C_{23} \\
Q_{16} &= m^3 n C_{11} + m^3 n C_{12} + m n^3 C_{12} + m n^3 C_{22} - 2m^3 n C_{66} + 2m n^3 C_{66} \\
Q_{22} &= n^4 C_{11} + 2m^2 n^2 C_{12} + m^4 C_{22} + 4m^2 n^2 C_{66} \\
Q_{23} = Q_{32} &= n^2 C_{13} + m^2 C_{23} \\
Q_{26} &= m n^3 C_{11} + m^3 n C_{12} + m^3 n C_{22} + 2m^3 n C_{66} - 2m n^3 C_{66} \\
Q_{33} &= C_{33} \\
Q_{36} &= m n C_{13} + m n C_{23} \\
Q_{44} &= m^2 C_{44} + n^2 C_{55} \\
Q_{45} = Q_{54} &= -m n C_{44} + m n C_{55} \\
Q_{55} &= n^2 C_{44} + m^2 C_{55} \\
Q_{66} &= m^2 n^2 C_{11} + 2m^2 n^2 C_{12} + m^2 n^2 C_{22} + m^4 C_{66} - 2m^2 n^2 C_{66} + n^4 C_{66}
\end{aligned}
$$

where $m = \cos\theta$ and $n = \sin\theta$.
In the present work, mainly isotropic material are considered but, for future works, the full elasticity tensor without any material hypotesis superimpositions has been considered and implemented during the derivation of governing equation: in this way, the all the governing equation in weak form are completely independent from the material considered, and the derivation is straightforword.

3.2 Carrera Unified Formulation

According to Carrera Unified Formulation, the displacement field is expressed as an expansion of basic polynomial terms, increasing as necessary the order of expansion. The displacement field is then written as a combination of the nodal displacements of the finite element and it depends on the model considered: in 1D CUF models, thickness functions are used to approximate the displacement field along the cross-section of the beam, in 2D models thickness functions are used to approximate the displacement field along the thickness of the plate/shell.
The choice of cross-section/thickness expansion function is completely arbitrary but this choice characterize the model adopted: when Taylor polynomials are involved, structure is solved by considering an equivalent single layer for the whole cross-section (ESL models), instead when Lagrange polynomials are chosen a Layer-Wise description of the displacement field is allowed (LW models).

3.2.1 Beam 1D CUF-FEM finite element

In elongated structures namely beam structure, for which the characteristic length is far greater then the cross-section dimensions, 1D CUF models are adopted. In this model, the primary variables of the 3D displacement field are discretized by a classical FEM approximation along the axis, and used for the interpolation of the nodal cross-section displacement components.

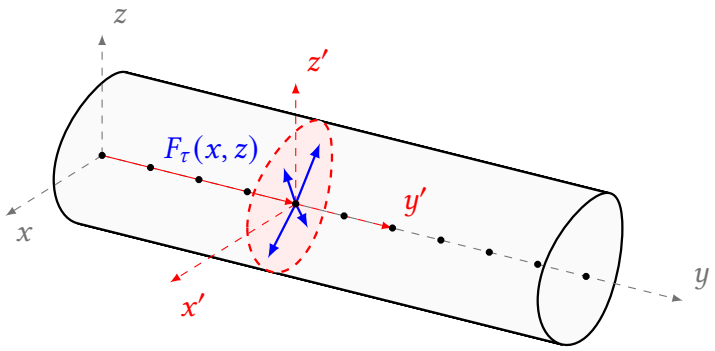

If y is the direction of the beam axis, and x', z' is the reference plane for the cross-section, according to Carrera Unified Formulation the displacement field is then:

$$\mathbf{u}(x,y,z) = F_\tau(x,z)\mathbf{u}_\tau(y) = F_\tau(x,z)N_i(y)\mathbf{q}_{\tau i} \qquad \tau = 1,2,..,K \tag{3.2.1}$$

where $F_\tau(x,z)$ are the cross-section expansion function, K is the order of expansion, $\mathbf{q}_{\tau i}$ are the nodal discrete displacements and $N_i(y)$ are the classical 1D shape functions involved in FEM used for the approximation along the beam axis. In the context of geometrically non linear elasticty, the geometrical relations can be rewritten as:

$$\boldsymbol{\epsilon} = (\mathbf{b_l} + \mathbf{b_{nl}})\ \mathbf{u} = (\mathbf{b_l} + \mathbf{b_{nl}})\ F_\tau(x,z)N_i(y)\mathbf{q}_{\tau i} = (\mathbf{B}_\mathbf{l}^{\tau i} + \mathbf{B}_\mathbf{nl}^{\tau i})\mathbf{q}_{\tau i} \tag{3.2.2}$$

where $\mathbf{B}_\mathbf{l}^{\tau i}$ and $\mathbf{B}_\mathbf{nl}^{\tau i}$ are the formal matrices of derivatives operators applied to shape functions and cross-section functions, that can be rewritten then as:

$$\mathbf{B}_\mathbf{l}^{\tau i} = \begin{bmatrix} F_{\tau,x}N_i & 0 & 0 \\ 0 & F_\tau N_{i,y} & 0 \\ 0 & 0 & F_{\tau,z}N_i \\ F_{\tau,z}N_i & 0 & F_{\tau,x}N_i \\ 0 & F_{\tau,z}N_i & F_\tau N_{i,y} \\ F_\tau N_{i,y} & F_{\tau,x}N_i & 0 \end{bmatrix} \tag{3.2.3}$$

$$\mathbf{B}_\mathbf{nl}^{\tau i} = \frac{1}{2}\begin{bmatrix} u_{x,x}F_{\tau,x}N_i & u_{y,x}F_{\tau,x}N_i & u_{z,x}F_{\tau,x}N_i \\ u_{x,y}F_\tau N_{i,y} & u_{y,y}F_\tau N_{i,y} & u_{z,y}F_\tau N_{i,y} \\ u_{x,z}F_{\tau,z}N_i & u_{y,z}F_{\tau,z}N_i & u_{z,z}F_{\tau,z}N_i \\ u_{x,x}F_{\tau,z}N_i + u_{x,z}F_{\tau,x}N_i & u_{y,x}F_{\tau,z}N_i + u_{y,z}F_{\tau,x}N_i & u_{z,x}F_{\tau,z}N_i + u_{z,z}F_{\tau,x}N_i \\ u_{x,y}F_{\tau,z}N_i + u_{x,z}F_\tau N_{i,y} & u_{y,y}F_{\tau,z}N_i + u_{y,z}F_\tau N_{i,y} & u_{z,y}F_{\tau,z}N_i + u_{z,z}F_\tau N_{i,y} \\ u_{x,x}F_\tau N_{i,y} + u_{x,y}F_{\tau,x}N_i & u_{y,x}F_\tau N_{i,y} + u_{y,y}F_{\tau,x}N_i & u_{z,x}F_\tau N_{i,y} + u_{z,y}F_{\tau,x}N_i \end{bmatrix} \tag{3.2.4}$$

3.2.2 Plate 2D CUF-FEM finite element

In structures where only the thickness is at least one order of dimension less then the other dimensions, 2D CUF models are adopted. In this model, the primary variables of the 3D displacement field are expressed adopting through-the-thickness expansion of finite nodes on the mid-surface of the plate, already discretized by a classical FEM approximation.
If z is the thickness direction, and x, y is the reference plane for the mid-surface of the plate, according to Carrera Unified Formulation the displacement field is written as:

$$\mathbf{u}(x,y,z) = F_\tau(z)\mathbf{u}_\tau(x,y) = F_\tau(x)N_i(x,y)\mathbf{q}_{\tau\mathbf{i}} \qquad \tau = 1,2,..,K \tag{3.2.5}$$

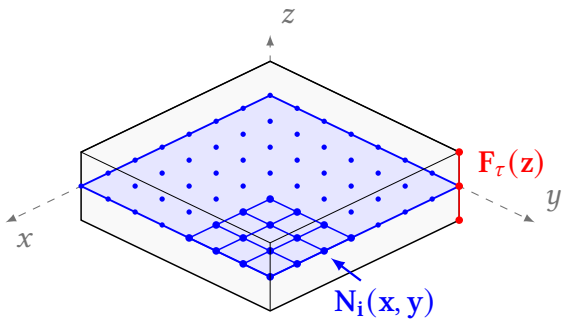

where $F_\tau(z)$ are the thickness expansion function, used for the approximation of the displacement field along the thickness, K is the order of expansion, $\mathbf{q}_{\tau i}$ are the nodal discrete displacements and $N_i(x,y)$ are the classical 2D shape functions involved in FEM used for the approximation of the displacement field along the mid-surface. In the context of geometrically non linear elasticity, the geometrical relations can be rewritten as:

$$\boldsymbol{\epsilon} = (\mathbf{b_l} + \mathbf{b_{nl}})\ \mathbf{u} = (\mathbf{b_l} + \mathbf{b_{nl}})\ F_\tau(x,z) N_i(y) \mathbf{q}_{\tau i} = (\mathbf{B}_\mathbf{l}^{\tau i} + \mathbf{B}_\mathbf{nl}^{\tau i}) \mathbf{q}_{\tau i} \tag{3.2.6}$$

where $\mathbf{B}_\mathbf{l}^{\tau i}$ and $\mathbf{B}_\mathbf{nl}^{\tau i}$ are the formal matrices of derivatives operators applied to shape functions and thickness function that can be rewritten then as:

$$\mathbf{B}_\mathbf{l}^{\tau i} = \begin{bmatrix} F_\tau N_{i,x} & 0 & 0 \\ 0 & F_\tau N_{i,y} & 0 \\ 0 & 0 & F_{\tau,z} N_i \\ F_{\tau,z} N_i & 0 & F_\tau N_{i,x} \\ 0 & F_{\tau,z} N_i & F_\tau N_{i,y} \\ F_\tau N_{i,y} & F_\tau N_{i,x} & 0 \end{bmatrix} \tag{3.2.7}$$

$$\mathbf{B}_\mathbf{nl}^{\tau i} = \frac{1}{2} \begin{bmatrix} u_{x,x} F_\tau N_{i,x} & u_{y,x} F_\tau N_{i,x} & u_{z,x} F_\tau N_{i,x} \\ u_{x,y} F_\tau N_{i,y} & u_{y,y} F_\tau N_{i,y} & u_{z,y} F_\tau N_{i,y} \\ u_{x,z} F_{\tau,z} N_i & u_{y,z} F_{\tau,z} N_i & u_{z,z} F_{\tau,z} N_i \\ u_{x,x} F_{\tau,z} N_i + u_{x,z} F_\tau N_{i,x} & u_{y,x} F_{\tau,z} N_i + u_{y,z} F_\tau N_{i,x} & u_{z,x} F_{\tau,z} N_i + u_{z,z} F_\tau N_{i,x} \\ u_{x,y} F_{\tau,z} N_i + u_{x,z} F_\tau N_{i,y} & u_{y,y} F_{\tau,z} N_i + u_{y,z} F_\tau N_{i,y} & u_{z,y} F_{\tau,z} N_i + u_{z,z} F_\tau N_{i,y} \\ u_{x,x} F_\tau N_{i,y} + u_{x,y} F_\tau N_{i,x} & u_{y,y} F_\tau N_{i,y} + u_{y,y} F_\tau N_{i,x} & u_{z,x} F_\tau N_{i,y} + u_{z,y} F_\tau N_{i,x} \end{bmatrix} \tag{3.2.8}$$

3.2.3 Isoparametric 3D finite element

In structures with complex geometries or without any prevalent dimension, 3D models are adopted. In this model, the primary variables of the 3D displacement field are expressed as an expansion of nodal displacement variables of the generic element, in which only shape FEM functions are involved because there is no other approximation along any direction: the displacement field is obtained only by FEM approximation of the considered domain.

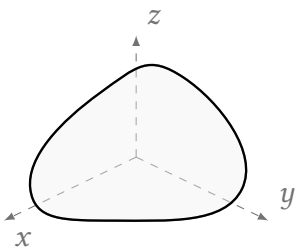

In the classical x, y, z reference frame, according to Finite Element Method, the displacement field is then:

$$\mathbf{u}(x,y,z) = N_i(x,y,z)\mathbf{q_i} \qquad i = 1, 2, .., N \tag{3.2.9}$$

where N is the order of the finite element, $\mathbf{q_i}$ are the nodal discrete displacements and $N_i(x,y,z)$ are the classical 3D shape functions involved in FEM used for the approximation of the displacement field over the whole domain. In the contex of geometrically non linear elasticty, the geometrical relations can be rewritten as:

$$\boldsymbol{\epsilon} = (\mathbf{b_l} + \mathbf{b_{nl}})\ \mathbf{u} = (\mathbf{b_l} + \mathbf{b_{nl}})\ N_i(x,y,z)\mathbf{q_i} = (\mathbf{B_l^i} + \mathbf{B_{nl}^i})\mathbf{q_i} \tag{3.2.10}$$

where $\mathbf{B_l^i}$ and $\mathbf{B_{nl}^i}$ are the formal matrices of derivatives operators applied to shape functions that can be rewritten then as:

$$\mathbf{B_l^i} = \begin{bmatrix} N_{i,x} & 0 & 0 \\ 0 & N_{i,y} & 0 \\ 0 & 0 & N_{i,z} \\ N_{i,z} & 0 & N_{i,x} \\ 0 & N_{i,z} & N_{i,y} \\ N_{i,y} & N_{i,x} & 0 \end{bmatrix} \tag{3.2.11}$$

$$\mathbf{B_{nl}} = \frac{1}{2}\begin{bmatrix} u_{x,x}N_{i,x} & u_{y,x}N_{i,x} & u_{z,x}N_{i,x} \\ u_{x,y}N_{i,y} & u_{y,y}N_{i,y} & u_{z,y}N_{i,y} \\ u_{x,z}N_{i,z} & u_{y,z}N_{i,z} & u_{z,z}N_{i,z} \\ u_{x,x}N_{i,z} + u_{x,z}N_{i,x} & u_{y,x}N_{i,z} + u_{y,z}N_{i,x} & u_{z,x}N_{i,z} + u_{z,z}N_{i,x} \\ u_{x,y}N_{i,z} + u_{x,z}N_{i,y} & u_{y,y}N_{i,z} + u_{y,z}N_{i,y} & u_{z,y}N_{i,z} + u_{z,z}N_{i,y} \\ u_{x,x}N_{i,y} + u_{x,y}N_{i,x} & u_{y,y}N_{i,y} + u_{y,y}N_{i,x} & u_{z,x}N_{i,y} + u_{z,y}N_{i,x} \end{bmatrix} \tag{3.2.12}$$

3.2.4 Lagrange Expansion Model

The Lagrange Expansion (LE) models adopts Lagrange polynomials to interpolate displacement variables: in the case of 1D/2D models, unknowns over the cross-section/thickness domain are interpolated, instead in the case of 3D models the displacement field is expressed as an expansion over all the unknown nodal displacements of the finite element. In the code, for 1D/2D element, different LE orders elements are implemented, namely Q4 (four node element), Q9 (nine node element) and Q16 (sixteen node element); in the case of 3D LE elements instead H8 (eight-node element), H20 (twenty-node element) and H27 (twentyseven-node element) are implemented.
In general, the expansion is defined in the natural reference frame: each polynomial is defined in the real interval $[-1;1]$: physical quantities depending on the Lagrange expansions need a change of variable where Jacobian is required.

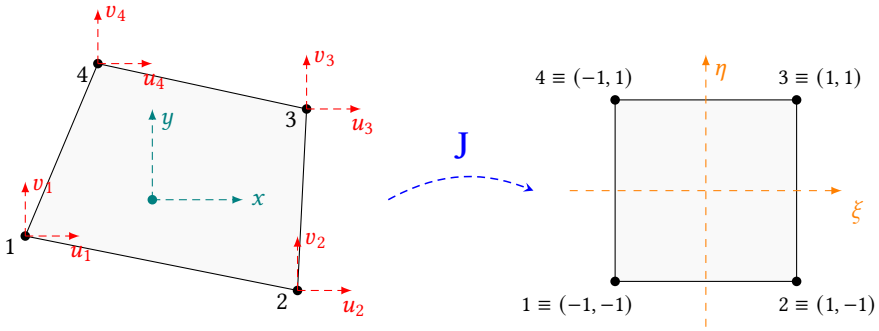

Figure 3.2.1: Lagrange Q4 linear plane element: from material to natural ref. frame

As an example, in the case of linear Q4 element as shown in fig.3.2.1, Lagrange polynomials in the natural reference frame are expressed as follows:

$$N_1(\xi,\eta) = \frac{1}{4}(1-\xi)(1-\eta) \qquad N_2(\xi,\eta) = \frac{1}{4}(1+\xi)(1-\eta)$$

$$N_3(\xi,\eta) = \frac{1}{4}(1+\xi)(1+\eta) \qquad N_1(\xi,\eta) = \frac{1}{4}(1-\xi)(1+\eta)$$

therefore, once the nodal displacements are computed, the displacement field of a Q4 domain in the physical reference frame is written as:

$$\begin{aligned} u_x &= N_1 u_{x_1} + N_2 u_{x_2} + N_3 u_{x_3} + N_4 u_{x_4} \\ u_y &= N_1 u_{y_1} + N_2 u_{y_2} + N_3 u_{y_3} + N_4 u_{y_4} \\ u_z &= N_1 u_{z_1} + N_2 u_{z_2} + N_3 u_{z_3} + N_4 u_{z_4} \end{aligned}$$

For example, in the case of linear H8 hexaedral element as shown in fig.3.2.2, Lagrange polynomials in the natural reference frame are expressed as follows:

$$N_1(\xi,\eta,\nu) = \frac{(1-\xi)(1-\eta)(1-\nu)}{8} \qquad N_2(\xi,\eta,\nu) = \frac{(1+\xi)(1-\eta)(1-\nu)}{8}$$

$$N_3(\xi,\eta,\nu) = \frac{(1+\xi)(1+\eta)(1-\nu)}{8} \qquad N_4(\xi,\eta,\nu) = \frac{(1-\xi)(1+\eta)(1-\nu)}{8}$$

$$N_5(\xi,\eta,\nu) = \frac{(1-\xi)(1-\eta)(1+\nu)}{8} \qquad N_6(\xi,\eta,\nu) = \frac{(1+\xi)(1-\eta)(1+\nu)}{8}$$

$$N_7(\xi,\eta,\nu) = \frac{(1+\xi)(1+\eta)(1+\nu)}{8} \qquad N_8(\xi,\eta,\nu) = \frac{(1-\xi)(1+\eta)(1+\nu)}{8}$$

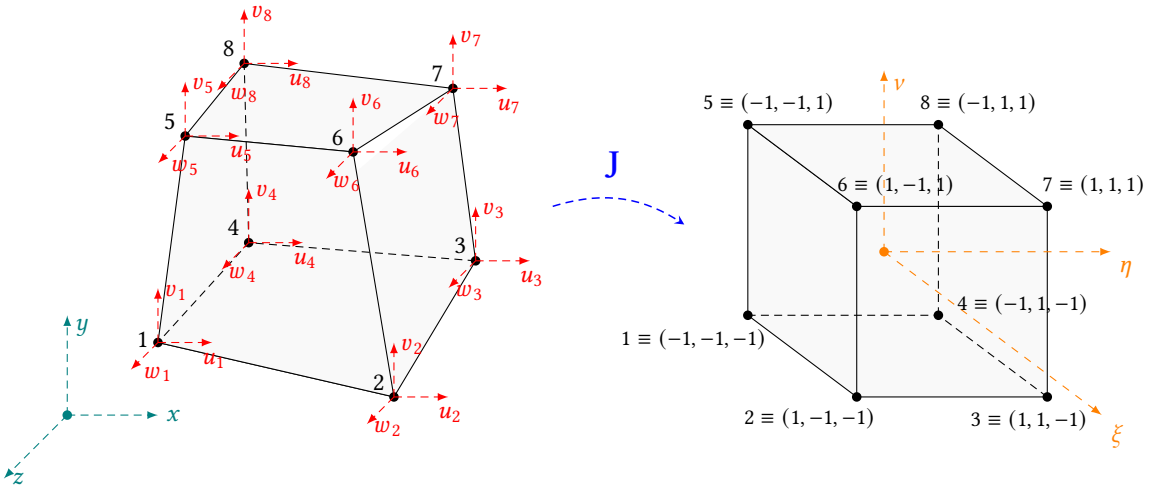

Figure 3.2.2: Lagrange H8 linear solid element: from material to natural ref. frame

therefore, once the nodal displacements are computed, the displacement field of a H27 domain in the physical reference frame is written as:

$$u_x = N_1 u_{x_1} + N_2 u_{x_2} + N_3 u_{x_3} + \ldots + N_9 u_{x_9}$$
$$u_y = N_1 u_{y_1} + N_2 u_{y_2} + N_3 u_{y_3} + \ldots + N_9 u_{y_9}$$
$$u_z = N_1 u_{z_1} + N_2 u_{z_2} + N_3 u_{z_3} + \ldots + N_9 u_{z_9}$$

3.2.5 Jacobian matrix

The computation of primary variables, derivatives of the thickness, cross-section or shape functions in the physical reference frame are in general required by the mathematical description of the Finite Element Method. In the present work, isoparametric finite elements adopted: computation can be performed in a convenient reference frame and express then results in terms of physical variabile by adopting the Jacobian.

Considering isoparametric elements, if nn is the number of nodes in the element, the geometrical variables can be computed by the nodal coordinates:

$$\begin{cases} x = \sum_{i=1}^{nn} N_i(\xi,\eta,\nu)\cdot x_i \\ y = \sum_{i=1}^{nn} N_i(\xi,\eta,\nu)\cdot y_i \\ z = \sum_{i=1}^{nn} N_i(\xi,\eta,\nu)\cdot z_i \end{cases} \tag{3.2.13}$$

as well as the computation of the derivatives, that becomes:

$$\begin{array}{lll} \dfrac{\partial x}{\partial \xi} = \sum_{i=1}^{nn} \dfrac{\partial N_i(\xi,\eta,\nu)}{\partial \xi}\cdot x_i & \dfrac{\partial x}{\partial \eta} = \sum_{i=1}^{nn} \dfrac{\partial N_i(\xi,\eta,\nu)}{\partial \eta}\cdot x_i & \dfrac{\partial x}{\partial \nu} = \sum_{i=1}^{nn} \dfrac{\partial N_i(\xi,\eta,\nu)}{\partial \nu}\cdot x_i \\ \dfrac{\partial y}{\partial \xi} = \sum_{i=1}^{nn} \dfrac{\partial N_i(\xi,\eta,\nu)}{\partial \xi}\cdot y_i & \dfrac{\partial y}{\partial \eta} = \sum_{i=1}^{nn} \dfrac{\partial N_i(\xi,\eta,\nu)}{\partial \eta}\cdot y_i & \dfrac{\partial y}{\partial \nu} = \sum_{i=1}^{nn} \dfrac{\partial N_i(\xi,\eta,\nu)}{\partial \nu}\cdot y_i \\ \dfrac{\partial z}{\partial \xi} = \sum_{i=1}^{nn} \dfrac{\partial N_i(\xi,\eta,\nu)}{\partial \xi}\cdot z_i & \dfrac{\partial z}{\partial \eta} = \sum_{i=1}^{nn} \dfrac{\partial N_i(\xi,\eta,\nu)}{\partial \eta}\cdot z_i & \dfrac{\partial z}{\partial \nu} = \sum_{i=1}^{nn} \dfrac{\partial N_i(\xi,\eta,\nu)}{\partial \nu}\cdot z_i \end{array}$$

So, in general, starting from the natural reference frame and considering the total-differential of each variabile, the Jacobian can be defined as:

$$\begin{Bmatrix} \dfrac{\partial}{\partial \xi} \\ \dfrac{\partial}{\partial \eta} \\ \dfrac{\partial}{\partial \nu} \end{Bmatrix} = \begin{bmatrix} \dfrac{\partial x}{\partial \xi} & \dfrac{\partial y}{\partial \xi} & \dfrac{\partial z}{\partial \xi} \\ \dfrac{\partial x}{\partial \eta} & \dfrac{\partial y}{\partial \eta} & \dfrac{\partial z}{\partial \eta} \\ \dfrac{\partial x}{\partial \nu} & \dfrac{\partial y}{\partial \nu} & \dfrac{\partial z}{\partial \nu} \end{bmatrix} \begin{Bmatrix} \dfrac{\partial}{\partial x} \\ \dfrac{\partial}{\partial y} \\ \dfrac{\partial}{\partial z} \end{Bmatrix} \tag{3.2.14}$$

and finally, all known the derivatives in the natural reference frame can be easily computed by the inverse Jacobian Matrix:

$$\begin{Bmatrix} \dfrac{\partial}{\partial \xi} \\ \dfrac{\partial}{\partial \eta} \\ \dfrac{\partial}{\partial \nu} \end{Bmatrix} = \begin{bmatrix} & J^{-1} & \end{bmatrix} \begin{Bmatrix} \dfrac{\partial}{\partial x} \\ \dfrac{\partial}{\partial y} \\ \dfrac{\partial}{\partial z} \end{Bmatrix} \tag{3.2.15}$$

Chapter 4

Nonlinear Unified Formulation

4.1 Linear elastic materials: stiffness matrices

The weak form governing equation of the nonlinear problem are carried out by means of Principle of Virtual Displacement. Supposing that the body volume gravity forces are negligible, PVD can be written as:

$$\delta \mathcal{L}_{int} = \delta \mathcal{L}_{ext} \tag{4.1.1}$$

where $\delta \mathcal{L}_{int}$ is the internal strain energy done by virtual displacement, $\delta \mathcal{L}_{ext}$ is the work of external loads done by virtual displacements and δ denotes the variation. The internal strain energy can be written as:

$$\delta \mathcal{L}_{int} = \int_{\Omega} \delta \boldsymbol{\epsilon}^T \boldsymbol{\sigma} dV \tag{4.1.2}$$

4.1.1 Derivation of secant stiffness matrix

Explicit expression of the secant stiffness matrix is now derived: for a more general description and derivation, general expansion for a 1D or 2D element is considered, taking into account also CUF. The expression of the secant matrix for the 3D element is similar, but there is no CUF approximation.
Starting from eq.(4.1.2), since the strain vector can be written in terms of generalized nodal displacements (unknown), as done in eq.(3.2.2) and (3.2.6):

$$\boldsymbol{\epsilon} = (\mathbf{B}_{\mathbf{l}}^{\tau \mathbf{i}} + \mathbf{B}_{\mathbf{nl}}^{\tau \mathbf{i}}) \mathbf{q}_{\tau \mathbf{i}}$$

the virtual variation of the strains can be derived in the same way by introducing the nodal virtual displacement (indeces s, j) as follows:

$$\delta \boldsymbol{\epsilon} = \delta((\mathbf{B}_{\mathbf{l}}^{\tau \mathbf{i}} + \mathbf{B}_{\mathbf{nl}}^{\tau \mathbf{i}}) \mathbf{q}_{\tau \mathbf{i}}) = (\mathbf{B}_{\mathbf{l}}^{\mathbf{sj}} + 2\mathbf{B}_{\mathbf{nl}}^{\mathbf{sj}}) \delta \mathbf{q}_{\mathbf{sj}} \tag{4.1.3}$$

Substituting eq.(4.1.3) and the constitutive law in matrix form (3.1.5) into the expression of the internal work eq.(4.1.2):

$$\begin{aligned}
\delta\mathcal{L}_{int} &= \int_\Omega \delta\mathbf{q_{sj}}^T(\mathbf{B_l^{sj}} + 2\mathbf{B_{nl}^{sj}})^T\mathbb{C}(\mathbf{B_l^{\tau i}} + \mathbf{B_{nl}^{\tau i}})\mathbf{q}_{\tau i}\ dV = \\
&= \delta\mathbf{q_{sj}}^T\left[\int_\Omega \mathbf{B_l^{sj}}^T\ \mathbb{C}\ \mathbf{B_l^{\tau i}} dV\right]\mathbf{q}_{\tau i} + \delta\mathbf{q_{sj}}^T\left[\int_\Omega \mathbf{B_l^{sj}}^T\ \mathbb{C}\ \mathbf{B_{nl}^{\tau i}} dV\right]\mathbf{q}_{\tau i} + \\
&\quad \delta\mathbf{q_{sj}}^T\left[\int_\Omega 2\mathbf{B_{nl}^{sj}}^T\ \mathbb{C}\ \mathbf{B_l^{\tau i}} dV\right]\mathbf{q}_{\tau i} + \delta\mathbf{q_{sj}}^T\left[\int_\Omega 2\mathbf{B_{nl}^{sj}}^T\ \mathbb{C}\ \mathbf{B_{nl}^{\tau i}} dV\right]\mathbf{q}_{\tau i} \qquad (4.1.4)
\end{aligned}$$

Introducing, starting from eq.4.1.4, some 3x3 matrices components:

$$\begin{cases}
\mathbf{K}_{ll}^{\tau sij} = \displaystyle\int_\Omega \mathbf{B_l^{sj}}^T\ \mathbb{C}\ \mathbf{B_l^{\tau i}} dV & \text{linear contribution} \\
\mathbf{K}_{lnl}^{\tau sij} = \displaystyle\int_\Omega \mathbf{B_l^{sj}}^T\ \mathbb{C}\ \mathbf{B_{nl}^{\tau i}} dV & \text{nonlinear contribution of I order} \\
\mathbf{K}_{nll}^{\tau sij} = \displaystyle\int_\Omega 2\mathbf{B_{nl}^{sj}}^T\ \mathbb{C}\ \mathbf{B_l^{\tau i}} dV & \text{nonlinear contribution of I order} \\
\mathbf{K}_{nlnl}^{\tau sij} = \displaystyle\int_\Omega 2\mathbf{B_{nl}^{sj}}^T\ \mathbb{C}\ \mathbf{B_{nl}^{\tau i}} dV & \text{nonlinear contribution of II order}
\end{cases} \qquad (4.1.5)$$

the virtual variation of the internal work can be rewritten as:

$$\begin{aligned}
\delta\mathcal{L}_{int} &= \int_\Omega \delta\mathbf{q_{sj}}^T(\mathbf{B_l^{sj}} + 2\mathbf{B_{nl}^{sj}})^T\mathbb{C}(\mathbf{B_l^{\tau i}} + \mathbf{B_{nl}^{\tau i}})\mathbf{q}_{\tau i}\ dV = \\
&= \delta\mathbf{q_{sj}}^T\mathbf{K}_{ll}^{\tau sij}\mathbf{q}_{\tau i} + \delta\mathbf{q_{sj}}^T\mathbf{K}_{lnl}^{\tau sij}\mathbf{q}_{\tau i} + \delta\mathbf{q_{sj}}^T\mathbf{K}_{nll}^{\tau sij}\mathbf{q}_{\tau i} + \delta\mathbf{q_{sj}}^T\mathbf{K}_{nlnl}^{\tau sij}\mathbf{q}_{\tau i} = \qquad (4.1.6) \\
&= \delta\mathbf{q_{sj}}^T\mathbf{K}_S^{\tau sij}\mathbf{q}_{\tau i} \qquad (4.1.7)
\end{aligned}$$

where the secant stiffness matrix is

$$\mathbf{K}_S^{\tau sij} = \mathbf{K}_{ll}^{\tau sij} + \mathbf{K}_{lnl}^{\tau sij} + \mathbf{K}_{nll}^{\tau sij} + \mathbf{K}_{nlnl}^{\tau sij} \qquad (4.1.8)$$

Matrices components $\mathbf{K}_{ll}^{\tau sij}$, $\mathbf{K}_{lnl}^{\tau sij}$, $\mathbf{K}_{nll}^{\tau sij}$ and $\mathbf{K}_{nlnl}^{\tau sij}$ are given in terms of fundamental nuclei: by imposing the cross-section (or thickness) functions and shape functions, expanding the summation over the indices τ, s and i, j, elemental stiffness matrix is obtained. It is important to note that, under CUF formulation, FN (fundamental nucleus) of secant stiffness matrix can be easily derived for any kinematics model and any cross-section polynomial function: for any arbitrary model, FN can be obtained just by exploiting the summation over the CUF indices. The complete expression of the secant stiffness matrix components are given in the appendix A, for 1D, 2D and 3D elements.

4.1.2 Derivation of tangent stiffness matrix

Explicit expression of the tangent stiffness matrix is now derived: for a more general description and derivation, general expansion for a 1D or 2D element is considered, taking into account also CUF. The expression of the secant matrix for the 3D element is similar, but there is no CUF approximation.
As done for the secan matrix, the strain vector can be written in terms of generalized nodal displacements (unknown), as done in eq.(3.2.2) and (3.2.6):

$$\boldsymbol{\epsilon} = (\mathbf{B}_{\mathbf{l}}^{\tau\mathbf{i}} + \mathbf{B}_{\mathbf{nl}}^{\tau\mathbf{i}})\mathbf{q}_{\tau\mathbf{i}}$$

the virtual variation of the strains can be derived in the same way by introducing the nodal virtual displacement (indeces s, j) as follows:

$$\delta\boldsymbol{\epsilon} = \delta((\mathbf{B}_{\mathbf{l}}^{\tau\mathbf{i}} + \mathbf{B}_{\mathbf{nl}}^{\tau\mathbf{i}})\mathbf{q}_{\tau\mathbf{i}}) = (\mathbf{B}_{\mathbf{l}}^{\mathbf{sj}} + 2\mathbf{B}_{\mathbf{nl}}^{\mathbf{sj}})\delta\mathbf{q}_{\mathbf{sj}}$$

The expression of fundamental nucleus of the tangent stiffness matrix is exploited by means of the linearization of the equilibrium equation: considering conservative loads, namely the virtual variation of the external work is null, only the virtual variation of the internal work has to be linearized. Starting from its, definition, distributing the virtual variation operator overe the product:

$$\delta(\delta\mathcal{L}_{int}) = \int_\Omega \delta(\delta\boldsymbol{\epsilon}^T\boldsymbol{\sigma})dV = \int_\Omega \delta\boldsymbol{\epsilon}^T\delta\boldsymbol{\sigma}dV + \int_\Omega \delta(\delta\boldsymbol{\epsilon}^T)\boldsymbol{\sigma}dV \tag{4.1.9}$$

The two terms at the right-hand side of eq.(4.1.9) side are now analysed separately.
The first term represents the linearization of constitutive equation. Assuming that the elasticity tensor is made by constant material coefficients (namely $\delta\mathbb{C} = 0$), from the definition of the virtual variation operator:

$$\delta\boldsymbol{\sigma} = \delta(\mathbb{C}\boldsymbol{\epsilon}) = \mathbb{C}\delta\boldsymbol{\epsilon} = \mathbb{C}(\mathbf{B}_{\mathbf{l}}^{\mathbf{sj}} + 2\mathbf{B}_{\mathbf{nl}}^{\mathbf{sj}})\delta\mathbf{q}_{\mathbf{sj}} \tag{4.1.10}$$

Since the indeces s, j are already assumed for the virtual variation of the strains, this virtual variation of stresses is exploited by means of indeces τ, i consistently with the notation. Thus, substituting into the first integral at the right-hand side of eq.(4.1.9):

$$\begin{aligned}
\int_\Omega \delta\boldsymbol{\epsilon}^T\delta\boldsymbol{\sigma}dV &= \int_\Omega \delta\mathbf{q}_{\mathbf{sj}}{}^T(\mathbf{B}_{\mathbf{l}}^{\mathbf{sj}} + 2\mathbf{B}_{\mathbf{nl}}^{\mathbf{sj}})^T\mathbb{C}(\mathbf{B}_{\mathbf{l}}^{\tau\mathbf{i}} + 2\mathbf{B}_{\mathbf{nl}}^{\tau\mathbf{i}})\delta\mathbf{q}_{\tau\mathbf{i}}\ dV = \\
&= \delta\mathbf{q}_{\mathbf{sj}}{}^T\left[\int_\Omega \mathbf{B}_{\mathbf{l}}^{\mathbf{sj}T}\ \mathbb{C}\ \mathbf{B}_{\mathbf{l}}^{\tau\mathbf{i}}dV\right]\delta\mathbf{q}_{\tau\mathbf{i}} + \delta\mathbf{q}_{\mathbf{sj}}{}^T\left[\int_\Omega \mathbf{B}_{\mathbf{l}}^{\mathbf{sj}T}\ \mathbb{C}\ 2\mathbf{B}_{\mathbf{nl}}^{\tau\mathbf{i}}dV\right]\delta\mathbf{q}_{\tau\mathbf{i}} + \\
&+ \delta\mathbf{q}_{\mathbf{sj}}{}^T\left[\int_\Omega 2\mathbf{B}_{\mathbf{nl}}^{\mathbf{sj}}{}^T\ \mathbb{C}\ \mathbf{B}_{\mathbf{l}}^{\tau\mathbf{i}}dV\right]\delta\mathbf{q}_{\tau\mathbf{i}} + \delta\mathbf{q}_{\mathbf{sj}}{}^T\left[\int_\Omega 2\mathbf{B}_{\mathbf{nl}}^{\mathbf{sj}}{}^T\ \mathbb{C}\ 2\mathbf{B}_{\mathbf{nl}}^{\tau\mathbf{i}}dV\right]\delta\mathbf{q}_{\tau\mathbf{i}}
\end{aligned}$$

Introducing, starting from eq.4.1.4, some 3x3 matrices components:

$$\begin{cases} \mathbf{K}^{\tau sij}_{ll,tan} = \int_\Omega \mathbf{B}_{\mathbf{l}}^{\mathbf{sj}^T} \mathbb{C}\, \mathbf{B}_{\mathbf{l}}^{\tau\mathbf{i}} dV = \mathbf{K}^{\tau sij}_{ll} \\ \mathbf{K}^{\tau sij}_{lnl,tan} = \int_\Omega \mathbf{B}_{\mathbf{l}}^{\mathbf{sj}^T} \mathbb{C}\, 2\mathbf{B}_{\mathbf{nl}}^{\tau\mathbf{i}} dV = 2\mathbf{K}^{\tau sij}_{lnl} \\ \mathbf{K}^{\tau sij}_{nll,tan} = \int_\Omega 2\mathbf{B}_{\mathbf{nl}}^{\mathbf{sj}^T} \mathbb{C}\, \mathbf{B}_{\mathbf{l}}^{\tau\mathbf{i}} dV = \mathbf{K}^{\tau sij}_{nll} \\ \mathbf{K}^{\tau sij}_{nlnl,tan} = \int_\Omega 2\mathbf{B}_{\mathbf{nl}}^{\mathbf{sj}^T} \mathbb{C}\, 2\mathbf{B}_{\mathbf{nl}}^{\tau\mathbf{i}} dV = 2\mathbf{K}^{\tau sij}_{nlnl} \end{cases}$$

the linearized constitutive equation can be rewritten as:

$$\begin{aligned} \int_\Omega \delta\boldsymbol{\epsilon}^T \delta\boldsymbol{\sigma} dV &= \int_\Omega \delta\mathbf{q}_{\mathbf{sj}}{}^T (\mathbf{B}_{\mathbf{l}}^{\mathbf{sj}} + 2\mathbf{B}_{\mathbf{nl}}^{\mathbf{sj}})^T \mathbb{C} (\mathbf{B}_{\mathbf{l}}^{\tau\mathbf{i}} + 2\mathbf{B}_{\mathbf{nl}}^{\tau\mathbf{i}}) \delta\mathbf{q}_{\tau\mathbf{i}}\ dV = \\ &= \delta\mathbf{q}_{\mathbf{sj}}{}^T \mathbf{K}^{\tau sij}_{ll,tan} \delta\mathbf{q}_{\tau\mathbf{i}} + \delta\mathbf{q}_{\mathbf{sj}}{}^T \mathbf{K}^{\tau sij}_{lnl,tan} \delta\mathbf{q}_{\tau\mathbf{i}} + \delta\mathbf{q}_{\mathbf{sj}}{}^T \mathbf{K}^{\tau sij}_{nll,tan} \delta\mathbf{q}_{\tau\mathbf{i}} + \delta\mathbf{q}_{\mathbf{sj}}{}^T \mathbf{K}^{\tau sij}_{nlnl,tan} \delta\mathbf{q}_{\tau\mathbf{i}} = \\ &= \delta\mathbf{q}_{\mathbf{sj}}{}^T \mathbf{K}^{\tau sij}_{ll} \delta\mathbf{q}_{\tau\mathbf{i}} + \delta\mathbf{q}_{\mathbf{sj}}{}^T (2\mathbf{K}^{\tau sij}_{lnl}) \delta\mathbf{q}_{\tau\mathbf{i}} + \delta\mathbf{q}_{\mathbf{sj}}{}^T \mathbf{K}^{\tau sij}_{nll} \delta\mathbf{q}_{\tau\mathbf{i}} + \delta\mathbf{q}_{\mathbf{sj}}{}^T (2\mathbf{K}^{\tau sij}_{nlnl}) \delta\mathbf{q}_{\tau\mathbf{i}} = \\ &= \delta\mathbf{q}_{\mathbf{sj}}{}^T \mathbf{K}^{\tau sij}_{ll} \delta\mathbf{q}_{\tau\mathbf{i}} + \delta\mathbf{q}_{\mathbf{sj}}{}^T \mathbf{K}^{\tau sij}_{T_1} \delta\mathbf{q}_{\tau\mathbf{i}} \end{aligned} \tag{4.1.11}$$

where $\mathbf{K}^{\tau sij}_{T_1} = 2\mathbf{K}^{\tau sij}_{lnl} + \mathbf{K}^{\tau sij}_{nll} + 2\mathbf{K}^{\tau sij}_{nlnl}$ is the non linear contribution to the tangent stiffness matrix coming from the linearization of the constitutive equation, $\mathbf{K}^{\tau sij}_{ll}$ is the same linear contribution of the secant stiffness matrix. It's important to note that in eq.(4.1.11), the fundamental nuclei $\mathbf{K}^{\tau sij}_{ll}$, $\mathbf{K}^{\tau sij}_{lnl}$, $\mathbf{K}^{\tau sij}_{nll}$ and $\mathbf{K}^{\tau sij}_{nlnl}$ are the same fundamental nuclei already defined for the secant stiffness matrix eq.(4.1.5).

The second term is the linearization of geometrical relations. From the definition of the virtual variation operator, the virtual variation of the virtual strains is written as:

$$\delta(\delta\boldsymbol{\epsilon}) = \begin{bmatrix} (\delta u_{x_{,x}})_v\ \delta u_{x_{,x}} + (\delta u_{y_{,x}})_v\ u_{x_{,y}} + (\delta u_{z_{,x}})_v\ \delta u_{z_{,x}} \\ (\delta u_{x_{,y}})_v\ \delta u_{x_{,y}} + (\delta u_{y_{,y}})_v\ u_{y_{,y}} + (\delta u_{z_{,y}})_v\ \delta u_{z_{,y}} \\ (\delta u_{x_{,z}})_v\ \delta u_{x_{,z}} + (\delta u_{y_{,z}})_v\ u_{y_{,z}} + (\delta u_{z_{,z}})_v\ \delta u_{z_{,z}} \\ [(\delta u_{x_{,x}})_v\ \delta u_{x_{,z}} + u_{x_{,x}}(\delta u_{x_{,z}})_v\ ] + [(\delta u_{y_{,x}})_v\ \delta u_{y_{,z}} + u_{y_{,x}}(\delta u_{y_{,z}})_v\ ] + [(\delta u_{z_{,x}})_v\ \delta u_{z_{,z}} + u_{z_{,x}}(\delta u_{z_{,z}})_v\ ] \\ [(\delta u_{x_{,y}})_v\ \delta u_{x_{,z}} + u_{x_{,y}}(\delta u_{x_{,z}})_v\ ] + [(\delta u_{y_{,y}})_v\ \delta u_{y_{,z}} + u_{y_{,y}}(\delta u_{y_{,z}})_v\ ] + [(\delta u_{z_{,y}})_v\ \delta u_{z_{,z}} + u_{z_{,y}}(\delta u_{z_{,z}})_v\ ] \\ [(\delta u_{x_{,x}})_v\ \delta u_{x_{,y}} + u_{x_{,x}}(\delta u_{x_{,y}})_v\ ] + [(\delta u_{y_{,x}})_v\ \delta u_{y_{,y}} + u_{y_{,x}}(\delta u_{y_{,y}})_v\ ] + [(\delta u_{z_{,x}})_v\ \delta u_{z_{,y}} + u_{z_{,x}}(\delta u_{z_{,y}})_v\ ] \end{bmatrix}$$

This vector can be rearranged by considering FEM and CUF approximation to the virtual variation variables (already defined as $\delta\mathbf{u} = F_s N_j \mathbf{q_{sj}}$) and linearized variables (already defined as $(\delta\mathbf{u})_v = F_\tau N_i \mathbf{q_{\tau i}}$) and written in matrix form. Defining the formal matrix $\mathbf{B}^*_{nl}$ of differential operators, then:

$$\delta(\delta\boldsymbol{\epsilon}) = \mathbf{B}^*_{nl} \begin{Bmatrix} \delta q_{x_{\tau i}} \delta q_{x_{sj}} \\ \delta q_{y_{\tau i}} \delta q_{y_{sj}} \\ \delta q_{z_{\tau i}} \delta q_{z_{sj}} \end{Bmatrix} \tag{4.1.12}$$

therefore, the second contribution related to linearized geometrical relations is:

$$\begin{aligned} \int_\Omega \delta(\delta\boldsymbol{\epsilon})^T \boldsymbol{\sigma} dV &= \int_\Omega \begin{Bmatrix} \delta q_{x_{\tau i}} \delta q_{x_{sj}} \\ \delta q_{y_{\tau i}} \delta q_{y_{sj}} \\ \delta q_{z_{\tau i}} \delta q_{z_{sj}} \end{Bmatrix}^T \mathbf{B}^{*T}_{nl} \boldsymbol{\sigma} dV \\ &= \int_\Omega \delta\mathbf{q}^T_{sj} \mathrm{diag}(\mathbf{B}^{*T}_{nl}\sigma)\ \delta\mathbf{q}_{\tau i} dV = \\ &= \delta\mathbf{q}^T_{sj} \mathbf{K}^{\tau sij}_\sigma \delta\mathbf{q}_{\tau i} \end{aligned} \tag{4.1.13}$$

where $\mathrm{diag}(\mathbf{B}^{*T}_{nl}\boldsymbol{\sigma})$ is a 3x3 diagonal matrix, defined in such a way on the main diagonal the components of the vector $\mathbf{B}^{*T}_{nl}\boldsymbol{\sigma}$ are present. This contribution, coming from linearization of nonlinear strains-displacement relation, defines the geometric stiffness matrix $\mathbf{K}^{\tau sij}_\sigma$.

Substituting finally the expression of the contribution coming from the linearization of the constitutive equation eq.(4.1.11) and the one coming from linearization of the geometrical relations eq.(4.1.13), the fundamental nucleus of the tangent stiffness matrix is defined as:

$$\begin{aligned}
\delta(\delta\mathcal{L}_{int}) &= \int_\Omega \delta\boldsymbol{\epsilon}^T \delta\boldsymbol{\sigma} dV + \int_\Omega \delta(\delta\boldsymbol{\epsilon}^T)\boldsymbol{\sigma} dV = \\
&= \delta\mathbf{q_{sj}}^T \mathbf{K}_{ll}^{\tau sij} \delta\mathbf{q}_{\tau\mathbf{i}} + \delta\mathbf{q_{sj}}^T \mathbf{K}_{T_1}^{\tau sij} \mathbf{q}_{\tau\mathbf{i}} + \delta\mathbf{q}_{sj}^T \mathbf{K}_{\sigma}^{\tau sij} \delta\mathbf{q}_{\tau i} = \\
&= \delta\mathbf{q_{sj}}^T \mathbf{K}_{T}^{\tau sij} \delta\mathbf{q}_{\tau\mathbf{i}} \qquad (4.1.14)
\end{aligned}$$

Some fundamental remark in this derivation of the linearized governing equation in matrix form refer to secant and tangent stiffness matrix symmetry condition: it is verified that the fundamental nucleus of the tangent stiffness matrix is symmetric, unlike the secant stiffness matrix that in general is non-symmetric. From a numerical point of view, the numerical solution of a linear system of equation in which the matrix of system coefficients is not symmetric can lead to numerical problem: a symmetric form of the secant stiffness matrix can be easily derived, rewriting the nonlinear governing equation in such a way to solve symmetric systems for which numerical solver are faster and more accurate.

4.2 Isotropic hyperelastic materials: stiffness matrix

Explicit expression of the tangent stiffness matrix for an hyperelastic CUF-FEM formulation is now derived: for a more general description and derivation, general expansion for a 1D or 2D element is considered, taking into account also CUF. The expression of the secant matrix is not provided due to consistent-linearized formulation of the problem that do not require the secant matrix, but only the tangent matrix.
As done before, the strain vector can be written in terms of generalized nodal displacements (unknown), as done in eq.(3.2.2) and (3.2.6). Assuming in this case $\mathbf{E}$ the strain vector coming from the full Green-Lagrange strain tensor and U_{sj} the nodal virtual displacements, one can write:

$$\boldsymbol{E} = (\mathbf{b_l} + \mathbf{b_{nl}})\ \mathbf{u} = (\mathbf{b_l} + \mathbf{b_{nl}})\ F_\tau(x,z)N_i(y)\mathbf{U}_{\tau\mathbf{i}} = (\mathbf{B}_\mathbf{l}^{\tau\mathbf{i}} + \mathbf{B}_\mathbf{nl}^{\tau\mathbf{i}})\mathbf{U}_{\tau\mathbf{i}} \tag{4.2.1}$$

$$\delta\boldsymbol{E} = \delta((\mathbf{B}_\mathbf{l}^{\tau\mathbf{i}} + \mathbf{B}_\mathbf{nl}^{\tau\mathbf{i}})\mathbf{U}_{\tau\mathbf{i}})\mathbf{U}_{\mathbf{sj}}) = (\mathbf{B}_\mathbf{l}^{\mathbf{sj}} + 2\mathbf{B}_\mathbf{nl}^{\mathbf{sj}})\delta\mathbf{U}_{\mathbf{sj}} \tag{4.2.2}$$

The expression of fundamental nucleus of the tangent stiffness matrix is exploited by means of the linearization of the equilibrium equation: considering conservative loads, namely the virtual variation of the external work is null, only the virtual variation of the internal work has to be linearized. Starting from its, definition, distributing the virtual variation operator over the product:

$$\delta(\delta\mathcal{L}_{int}) = \int_\Omega \delta(\delta\boldsymbol{E}^T\boldsymbol{S})dV = \int_\Omega \delta\boldsymbol{E}^T\delta\boldsymbol{S}dV + \int_\Omega \delta(\delta\boldsymbol{E}^T)\boldsymbol{S}dV \tag{4.2.3}$$

As done for the FN of the tangent stiffness matrix for a linear elastic materials, the two terms at the right-hand side of eq.(4.2.3) are now analyzed separately.
The first term is the linearization of constitutive equation. According to Holpfazel formulation adopted in first-invariant hyperelasticity already discussed:

$$\delta\mathbf{S} = \boldsymbol{C}\frac{1}{2}\delta\mathbf{C} = \boldsymbol{C}\delta\mathbf{E} = \boldsymbol{C}(\mathbf{B}_\mathbf{l}^{\mathbf{sj}} + 2\mathbf{B}_\mathbf{nl}^{\mathbf{sj}})\delta\mathbf{U}_{\mathbf{sj}} \tag{4.2.4}$$

where $\boldsymbol{C}$ is the tangent elasticity tensor already discussed before. Thus, the linearization of the constitutive weak-form equation can be written as:

$$\begin{aligned}
\int_\Omega \delta\boldsymbol{E}^T\delta\boldsymbol{S}dV &= \int_\Omega \delta\mathbf{U}_{\mathbf{sj}}{}^T(\mathbf{B}_\mathbf{l}^{\mathbf{sj}} + 2\mathbf{B}_\mathbf{nl}^{\mathbf{sj}})^T\boldsymbol{C}(\mathbf{B}_\mathbf{l}^{\tau\mathbf{i}} + 2\mathbf{B}_\mathbf{nl}^{\tau\mathbf{i}})\delta\mathbf{U}_{\tau\mathbf{i}}\ dV = \\
&= \delta\mathbf{U}_{\mathbf{sj}}{}^T\left[\int_\Omega \mathbf{B}_\mathbf{l}^{\mathbf{sj}T}\ \boldsymbol{C}\ \mathbf{B}_\mathbf{l}^{\tau\mathbf{i}}dV\right]\delta\mathbf{U}_{\tau\mathbf{i}} + \delta\mathbf{U}_{\mathbf{sj}}{}^T\left[\int_\Omega \mathbf{B}_\mathbf{l}^{\mathbf{sj}T}\ \boldsymbol{C}\ 2\mathbf{B}_\mathbf{nl}^{\tau\mathbf{i}}dV\right]\delta\mathbf{U}_{\tau\mathbf{i}} + \\
&+ \delta\mathbf{U}_{\mathbf{sj}}{}^T\left[\int_\Omega 2\mathbf{B}_\mathbf{nl}^{\mathbf{sj}T}\ \boldsymbol{C}\ \mathbf{B}_\mathbf{l}^{\tau\mathbf{i}}dV\right]\delta\mathbf{U}_{\tau\mathbf{i}} + \delta\mathbf{U}_{\mathbf{sj}}{}^T\left[\int_\Omega 2\mathbf{B}_\mathbf{nl}^{\mathbf{sj}T}\ \boldsymbol{C}\ 2\mathbf{B}_\mathbf{nl}^{\tau\mathbf{i}}dV\right]\delta\mathbf{U}_{\tau\mathbf{i}}
\end{aligned} \tag{4.2.5}$$

Introducing, starting from eq.4.2.5, some 3x3 matrices components:

$$\begin{cases} \mathbf{K}^{\tau sij}_{ll,tan} = \int_\Omega \mathbf{B_l^{sj}}^T \boldsymbol{C}\, \mathbf{B_l^{\tau i}} dV = \mathbf{K}^{\tau sij}_{ll} \\ \mathbf{K}^{\tau sij}_{lnl,tan} = \int_\Omega \mathbf{B_l^{sj}}^T \boldsymbol{C}\, 2\mathbf{B_{nl}^{\tau i}} dV = 2\mathbf{K}^{\tau sij}_{lnl} \\ \mathbf{K}^{\tau sij}_{nll,tan} = \int_\Omega 2\mathbf{B_{nl}^{sj}}^T \boldsymbol{C}\, \mathbf{B_l^{\tau i}} dV = \mathbf{K}^{\tau sij}_{nll} \\ \mathbf{K}^{\tau sij}_{nlnl,tan} = \int_\Omega 2\mathbf{B_{nl}^{sj}}^T \boldsymbol{C}\, 2\mathbf{B_{nl}^{\tau i}} dV = 2\mathbf{K}^{\tau sij}_{nlnl} \end{cases}$$

the linearized constitutive equation can be rewritten as:

$$\begin{aligned} \int_\Omega \delta \boldsymbol{E}^T \delta \boldsymbol{S} dV &= \int_\Omega \delta \mathbf{U_{sj}}^T (\mathbf{B_l^{sj}} + 2\mathbf{B_{nl}^{sj}})^T \boldsymbol{C} (\mathbf{B_l^{\tau i}} + 2\mathbf{B_{nl}^{\tau i}}) \delta \mathbf{U_{\tau i}}\ dV = \\ &= \delta \mathbf{U_{sj}}^T \mathbf{K}^{\tau sij}_{ll,tan} \delta \mathbf{U_{\tau i}} + \delta \mathbf{U_{sj}}^T \mathbf{K}^{\tau sij}_{lnl,tan} \delta \mathbf{U_{\tau i}} + \delta \mathbf{U_{sj}}^T \mathbf{K}^{\tau sij}_{nll,tan} \delta \mathbf{U_{\tau i}} + \delta \mathbf{U_{sj}}^T \mathbf{K}^{\tau sij}_{nlnl,tan} \delta \mathbf{U_{\tau i}} = \\ &= \delta \mathbf{U_{sj}}^T \mathbf{K}^{\tau sij}_{ll} \delta \mathbf{U_{\tau i}} + \delta \mathbf{U_{sj}}^T (2\mathbf{K}^{\tau sij}_{lnl}) \delta \mathbf{U_{\tau i}} + \delta \mathbf{U_{sj}}^T \mathbf{K}^{\tau sij}_{nll} \delta \mathbf{U_{\tau i}} + \delta \mathbf{U_{sj}}^T (2\mathbf{K}^{\tau sij}_{nlnl}) \delta \mathbf{U_{\tau i}} = \\ &= \delta \mathbf{U_{sj}}^T \mathbf{K}^{\tau sij}_{ll} \delta \mathbf{U_{\tau i}} + \delta \mathbf{U_{sj}}^T \mathbf{K}^{\tau sij}_{T_1} \delta \mathbf{U_{\tau i}} \end{aligned} \tag{4.2.6}$$

where $\mathbf{K}^{\tau sij}_{T_1} = 2\mathbf{K}^{\tau sij}_{lnl} + \mathbf{K}^{\tau sij}_{nll} + 2\mathbf{K}^{\tau sij}_{nlnl}$ is the non linear contribution to the tangent stiffness matrix coming from the linearization of the constitutive equation and $\mathbf{K}^{\tau sij}_{ll}$ is the same linear contribution of the secant stiffness matrix. It's important to note that in eq.(4.1.11), the fundamental nuclei $\mathbf{K}^{\tau sij}_{ll}$, $\mathbf{K}^{\tau sij}_{lnl}$, $\mathbf{K}^{\tau sij}_{nll}$ and $\mathbf{K}^{\tau sij}_{nlnl}$ are the same fundamental nuclei already defined for the tangent stiffness matrix for linear-elastic materials but the elasticity tensor is the tangent elasticity tensor coming from first-invariant hyperelastic formulation.
The second term is the linearization of geometrical relations: the derivation is the same described before, thus one can defining the formal matrix $\mathbf{B}^*_{nl}$ of differential operators and rewrite the virtual variation of the virtual strains as:

$$\delta(\delta \boldsymbol{E}) = \mathbf{B}^*_{nl} \begin{Bmatrix} \delta U_{x_{\tau i}} \delta U_{x_{sj}} \\ \delta U_{y_{\tau i}} \delta U_{y_{sj}} \\ \delta U_{z_{\tau i}} \delta U_{z_{sj}} \end{Bmatrix} \tag{4.2.7}$$

therefore, the second contribution related to linearized geometrical relations is:

$$\begin{aligned} \int_\Omega \delta(\delta \boldsymbol{E})^T \boldsymbol{S} dV &= \int_\Omega \begin{Bmatrix} \delta U_{x_{\tau i}} \delta U_{x_{sj}} \\ \delta U_{y_{\tau i}} \delta U_{y_{sj}} \\ \delta U_{z_{\tau i}} \delta U_{z_{sj}} \end{Bmatrix}^T \mathbf{B}^{*T}_{nl} \boldsymbol{S} dV \\ &= \int_\Omega \delta \mathbf{U}^T_{sj} \mathrm{diag}(\mathbf{B}^{*T}_{nl} S)\ \delta \mathbf{U}_{\tau i} dV = \\ &= \delta \mathbf{U}^T_{sj} \mathbf{K}^{\tau sij}_{\sigma} \delta \mathbf{U}_{\tau i} \end{aligned} \tag{4.2.8}$$

where $\text{diag}(\mathbf{B}_{nl}^{*T}\boldsymbol{S})$ is a 3x3 diagonal matrix, defined in such a way on the main diagonal the components of the vector $\mathbf{B}_{nl}^{*T}\boldsymbol{S}$ are present. This contribution, coming from linearization of nonlinear strains-displacement relation, defines the geometric stiffness matrix $\mathbf{K}_{\sigma}^{\tau sij}$. Substituting finally the expression of the contribution coming from the linearization of the constitutive equation eq.(4.1.11) and the one coming from linearization of the geometrical relations eq.(4.1.13), the fundamental nucleus of the tangent stiffness matrix is defined as:

$$\begin{aligned}
\delta(\delta\mathcal{L}_{int}) &= \int_{\Omega} \delta\boldsymbol{E}^T \delta\boldsymbol{S} dV + \int_{\Omega} \delta(\delta\boldsymbol{E}^T)\boldsymbol{S} dV = \\
&= \delta\mathbf{U_{sj}}^T \mathbf{K}_{ll}^{\tau sij} \delta\mathbf{U}_{\tau\mathbf{i}} + \delta\mathbf{U_{sj}}^T \mathbf{K}_{T_1}^{\tau sij} \mathbf{U}_{\tau\mathbf{i}} + \delta\mathbf{U}_{sj}^T \mathbf{K}_{\sigma}^{\tau sij} \delta\mathbf{U}_{\tau i} = \\
&= \delta\mathbf{U_{sj}}^T \mathbf{K}_{T}^{\tau sij} \delta\mathbf{U}_{\tau\mathbf{i}} \qquad (4.2.9)
\end{aligned}$$

4.3 Load vector and internal forces vector

Explicit expression of the external load vector, common either in case of linear elastic materials and hyperleastic material, is now derived: for a more general description and derivation, general expansion for a 1D or 2D element is considered, taking into account also CUF.
Starting from CUF definition, displacement field can be written in terms of generalized nodal displacements (unknown), as done in eq.(3.2.1):

$$\mathbf{u}(x,y,z) = F_\tau(x,z)\mathbf{u}_\tau(y) = F_\tau(x,z)N_i(y)\mathbf{q}_{\tau\mathbf{i}}$$

Same line of reasoning applies to virtual variation of the displacements, that can be derived in the same way by introducing the nodal virtual displacement (indeces s, j) as follows:

$$\delta\mathbf{u}(x,y,z) = F_s(x,z)\delta\mathbf{u}_\mathbf{s}(y) = F_s(x,z)N_i(y)\delta\mathbf{q}_{\mathbf{sj}}$$

The expression of fundamental nucleus of the external load vector is exploited by means of the definition of virtual variation of external works: if p is the vector of conservative loads:

$$\delta\mathcal{L}_{ext} = \int_\Omega \delta\boldsymbol{u}^T\boldsymbol{p}dV = \int_\Omega \delta\mathbf{q}_{\mathbf{sj}}{}^T F_s(x,z)N_i(y)\boldsymbol{p}dV = \delta\mathbf{q}_{\mathbf{sj}}{}^T\boldsymbol{p}_{sj} \tag{4.3.1}$$

In the case of hyperelastic material, due to the incremental formulation of the PK2 stress tensor, the secant matrix is not even defined. The virtual variation of the internal work then can be expressed by the 3x1 fundamental nucleus of the internal forces vector, obtained by its definition:

$$\delta\mathcal{L}_{int} = \int_\Omega \delta\boldsymbol{E}^T\boldsymbol{S}dV \tag{4.3.2}$$

where **E** is the full Green-Lagrange strain tensor and **S** is the PK2 stress tensor. As done during the derivation of the fundamental nucleus of the secant matrix, adopting the same definition of generalized strains expressed by nodal displacement unknowns, one can write:

$$\delta\boldsymbol{E} = \delta((\mathbf{B}_\mathbf{l}^{\tau\mathbf{i}} + \mathbf{B}_\mathbf{nl}^{\tau\mathbf{i}})\mathbf{U}_{\tau\mathbf{i}}) = (\mathbf{B}_\mathbf{l}^{\mathbf{sj}} + 2\mathbf{B}_\mathbf{nl}^{\mathbf{sj}})\delta\mathbf{U}_\mathbf{sj}$$

and substituting into the definition of internal work:

$$\delta\mathcal{L}_{int} = \int_\Omega \delta\boldsymbol{E}^T\boldsymbol{S}dV = \int_\Omega \delta\mathbf{U}_\mathbf{sj}{}^T(\mathbf{B}_\mathbf{l}^{\mathbf{sj}} + 2\mathbf{B}_\mathbf{nl}^{\mathbf{sj}})^T\boldsymbol{S}dV \tag{4.3.3}$$

one finally obtain the fundamental nucleus of the internal forces vector:

$$\mathbf{F}_{int}^{sj} = \int_\Omega (\mathbf{B}_\mathbf{l}^{\mathbf{sj}} + 2\mathbf{B}_\mathbf{nl}^{\mathbf{sj}})^T\boldsymbol{S}dV \tag{4.3.4}$$

4.4 Assembly of the global stiffness matrix

Once defined the fundamental nucleus for the single element of the discretized domain by the Principle of Virtual Displacements, in a Lagrange-exp. based model the total stiffness matrix is assembled considering the connectity between elements both of purely FEM nodes with the CUF expansion nodes, remembering that:

- Indices τ and s define the accuracy of the model, since they represents the order of expansion of CUF models, $\tau, s = 1,\ 2,\ \ldots\ M$;
- Indices i and j are defined starting from the number of nodes of the single finite element: $i, j = 1,\ 2,\ \ldots\ N_n$;

Each fundamental nucleus defined do not change considering different number of nodes of the element or different shape functions: formally, its general form is independent on the expansion model adopted. Starting from the definition, one can observe that fundamental nucleus of a stiffness matrix is a 3x3 matrix, obtained by the row-by-column product between formal matrices of differential operator and the elasticity tensor, thus:

$$\mathbf{K}^{\tau sij} = \int_\Omega \mathbf{B}^{\mathbf{sj}^T}\, \mathbb{C}\, \mathbf{B}^{\tau\mathbf{i}} dV = \int_\Omega \underbrace{\begin{bmatrix} & 3x6 & \end{bmatrix}}_{\mathbf{B}^{\mathbf{sj}^T}} \overbrace{\begin{bmatrix} & 6x6 & \end{bmatrix}}^{\mathbb{C}} \underbrace{\begin{bmatrix} & 6x3 & \end{bmatrix}}_{\mathbf{B}^{\tau\mathbf{i}}} dV = \begin{bmatrix} k_{xx}^{ij} & k_{xy}^{ij} & k_{xz}^{ij} \\ k_{xy}^{ij} & k_{yy}^{ij} & k_{yz}^{ij} \\ k_{xz}^{ij} & k_{yz}^{ij} & k_{zz}^{ij} \end{bmatrix} \tag{4.4.1}$$

Exploiting the summation over the indices i and j, one can obtain the matrix of the single element, instead summation over the indices τ and s are required for summation over CUF expansion for every single node of the element. Once obtained the fundamental nucleus for a single element, by considering the common nodes and the connectivity between elements, stiffness matrix is then assembled by classical FEM assembly procedures. A graphical representation of assembly procedure is provided in fig.4.4.1.

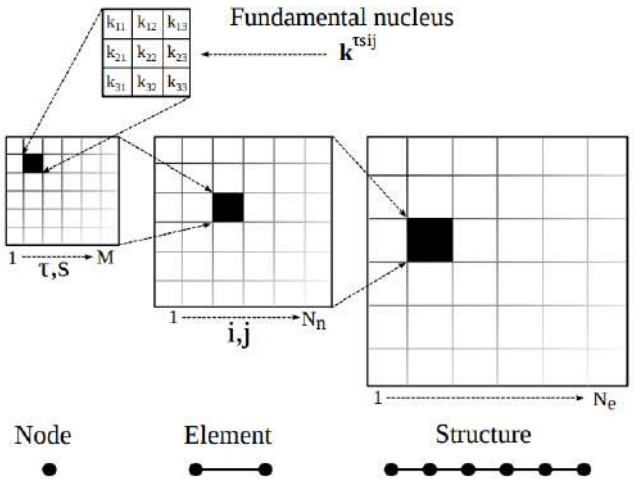

Figure 4.4.1: Assembly procedure with FEM-CUF elements

Chapter 5

Numerical schemes for nonlinear equations

5.1 Matrix form of the nonlinear governing equations

The elastic equilibrium problem is formulated, as described in ch.4.1, in its weak form: governing equation of the nonlinear problem are carried out by means of Principle of Virtual Displacement.

$$\delta \mathcal{L}_{int} = \delta \mathcal{L}_{ext} \tag{5.1.1}$$

where $\mathcal{L}_{int}$ is the internal strain energy, $\delta \mathcal{L}_{ext}$ is the work of external loads and δ denotes the variation. In this specific application of Finite Element Analysis to large deflection structural problems, the equilibrium condition is expressed as an nonlinear algebraic system of equations. Carrera Unified Formulation and theory of finite elements approximation here both implemented led to a unified governing equilibrium equation:

$$\mathbf{K}_S^{\tau s i j} \mathbf{q}_{\tau i} - \mathbf{p}_{\tau i} = 0 \tag{5.1.2}$$

where $\mathbf{K}_S^{\tau s i j}$ is the fundamental nucleus of the secant stiffness matrix and $\mathbf{p}_{\tau i}$ is the fundamental nucleus of the external nodal loading vector. After the assembly procedure described in ch.4.4, the global final system fo equations (at equilibrium) is:

$$\mathbf{K}_S(\mathbf{q})\ \mathbf{q} - \mathbf{p} = 0 \tag{5.1.3}$$

By its definition, the global coefficient matrix $\mathbf{K}_S$ is function of the nodal displacements $\mathbf{q}_{\tau i}$: the final assembled stiffness matrix depends on the unknown solution vector, so it can not be directly evaluated. Most common numerical procedures to solve these kind of systems are iterative. According to Reddy [4], the nonlinear system can be expressed as an equivalent minimization problem of the residual function defined as:

$$\phi_{\mathbf{res}} = \mathbf{K}_S(\mathbf{q})\ \mathbf{q} - \mathbf{p} \tag{5.1.4}$$

In eq.(5.1.4), $\phi_{\mathbf{res}}$ is also called the unbalanced nodal forces vector: at equilibrium, due to balance, the residual nodal forces are obviously null, $\phi_{\mathbf{res}} = 0$.

5.1.1 Newton-Raphson linearization of nonlinear equations

The expression (5.1.4) can be linearized around a known condition $(\mathbf{q}, \mathbf{p})$:

$$\phi_{\mathbf{res}}(\mathbf{q} + \delta\mathbf{q}, \mathbf{p} + \delta\mathbf{p}) = \phi_{\mathbf{res}}(\mathbf{q}, \mathbf{p}) + \frac{\partial \phi_{\mathbf{res}}}{\partial \mathbf{q}}\delta\mathbf{q} + \frac{\partial \phi_{\mathbf{res}}}{\partial \mathbf{p}}\delta\mathbf{p} = 0 \tag{5.1.5}$$

Assuming now the direction of load vector $\mathbf{p}$ remains constant during the analysis, so only the magnitude can change, the external nodal loading vector is expressed as a reference nodal loading vector $\mathbf{p}_{ref}$ in such a way $\mathbf{p} = \lambda\mathbf{p}_{ref}$. Virtual variation of the nodal loading vector is expressed then as virtual variation of the rate of change $\delta\mathbf{p} = \delta(\lambda\mathbf{p}_{ref}) = \delta\lambda\mathbf{p}_{ref}$. Under this assumption, it is possible to control how the external loading nodal vector increases or decreases by controlling the scalar load parameter λ. Observing that $\frac{\partial \phi_{\mathbf{res}}}{\partial \mathbf{q}} = \mathbf{K}_T$ is the tangent stiffness matrix and $\frac{\partial \phi_{\mathbf{res}}}{\partial \mathbf{p}} = -\mathbf{I}$, equation (5.1.5) can be rewritten as:

$$\mathbf{K}_T\delta\mathbf{q} = \delta\lambda\mathbf{p}_{ref} - \phi_{\mathbf{res}} \tag{5.1.6}$$

In (5.1.6), the unknowns are $\mathbf{q}$ and λ: since the load-scaling parameters is taken as unknown, an additional constraint equation is needed for closure condition:

$$\begin{cases} \mathbf{K}_T\delta\mathbf{q} = \delta\lambda\mathbf{p}_{ref} - \phi_{\mathbf{res}} \\ c(\delta\mathbf{q}, \delta\lambda) = 0 \end{cases} \tag{5.1.7}$$

The constraint equation (5.1.7)(2) characterizes the numerical procedure considered. In the next section, different numerical schemes are described, derived starting from the definition of constraint equation.

5.1.2 Linearization for hyperelastic materials

The expression (5.1.4) can be linearized around a known condition $(\mathbf{q}, \mathbf{p})$:

$$\phi_{\mathbf{res}}(\mathbf{U} + \delta\mathbf{U}, \mathbf{F}_{ext} + \delta\mathbf{F}_{ext}) = \phi_{\mathbf{res}}(\mathbf{U}, \mathbf{F}_{ext}) + \frac{\partial \phi_{\mathbf{res}}}{\partial \mathbf{U}}\delta\mathbf{U} + \frac{\partial \phi_{\mathbf{res}}}{\partial \mathbf{F}_{ext}}\delta\lambda\delta\mathbf{F}_{ext}^{rif} = 0 \tag{5.1.8}$$

where the virtual variation of the nodal loading vector is expressed as virtual variation of the rate of change $\mathbf{F}_{ext} = \delta(\lambda\mathbf{F}_{ext}^{ref}) = \delta\lambda\mathbf{F}_{ext}^{ref}$. Observing that $\frac{\partial \phi_{\mathbf{res}}}{\partial \mathbf{U}} = \mathbf{K}_T$ is the tangent stiffness matrix and $\frac{\partial \phi_{\mathbf{res}}}{\partial \mathbf{F}_{ext}} = -\mathbf{I}$, equation (5.1.5) can be rewritten as:

$$\mathbf{K}_T\delta\mathbf{q} = \delta\lambda\mathbf{F}_{ext}^{ref} - \phi_{\mathbf{res}} \tag{5.1.9}$$

The constraint equation and the numerical methods adopted in the computation of the numerical nonlinear solution are the same for linear-elastic material finite element formulation. A more detailed derivation can be found in [22].

5.1.3 Picard method

Picard method, known also as *successive substitution method*, is the simplest method for the solution of nonlinear system of equations: is a fixed-point iteration method that computes the solution for a specific external nodal forces vector (applied as boundary conditions), and specifically deals with eq.(5.1.3). The general algorithm is repeated until convergence is reached: during iterations, the approximated solution become close to the actual one. Starting from a fixed initial guess $\mathbf{q}^{(0)}$, a first approximation of the unknown vector can be found by considering:

$$\mathbf{q}^{(1)} = [\mathbf{K}_S(\mathbf{q}^{(0)})]^{-1} \cdot \mathbf{p} \tag{5.1.10}$$

with $\mathbf{q}^{(1)} \neq \mathbf{q}^{(0)}$. A second approximation can be obtained by using the last approximation to compute the updated secant stiffness matrix, obtaining so:

$$\mathbf{q}^{(2)} = [\mathbf{K}_S(\mathbf{q}^{(1)})]^{-1} \cdot \mathbf{p} \tag{5.1.11}$$

This procedure is repeated iteratively until convergences is reached: thus, convergence criterion has to be defined. In general, Picard iterations are repeated until the relative error norm between two successive iteration is less then the convergence tolerance, that can be arbitrary superimposed:

$$\begin{cases} \mathbf{q}^{(k)} = [\mathbf{K}_S(\mathbf{q}^{(k-1)})]^{-1} \cdot \mathbf{p} \\ \\ \sqrt{\dfrac{||\mathbf{q}^{(k)} - \mathbf{q}^{(k-1)}||^2}{||\mathbf{q}^{(k)}||^2}} < \epsilon \end{cases} \tag{5.1.12}$$

From a geometrical point of view, Picard method can be depicted as a general fixed-point iteration method, in which solution is reached slowly by successive iterations, as depicted in fig.5.1.1. Starting from the initial guess configuration $\mathbf{q}^{(0)}$, secant matrix $\mathbf{K}_S(\mathbf{q}^{(0)})$ is computed and by inversion the displacement vector associated to the external forces vector $\bar{F}$, $\mathbf{q}^{(1)}$ is then obtained. In the new displacement configuration, secant matrix $\mathbf{K}_S(\mathbf{q}^{(1)})$ is updated and used to obtain $\mathbf{q}^{(2)}$ associated to external forces vector $\bar{F}$. Following this procedure iteratively, the solution $\bar{\mathbf{q}}$ is reached.

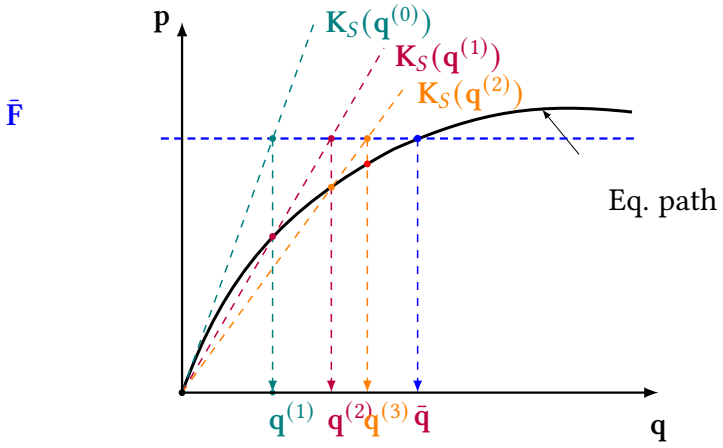

Figure 5.1.1: Picard method: geometrical interpretation

5.1.4 Load control method

Iterative solvers for nonlinear problems, in the general case, deal at the same time both with nodal displacements $\mathbf{q}$ unknowns and scalar load parameter λ unknown: most of them make use of incremental iterative approaches, obtaining the new convergent solution computing increments of the unknown displacements and an increment for the load parameter, that are in general mutually linked.
Newton *load control* method is an iterative method that postulates a fixed variation of the load at each iteration: in this method, at every increment, variation of λ is considered fixed up to a certain increment $\Delta\lambda$ and, by the unbalanced residual forces, the actual configuration that satisfies the equilibrium in this new load condition is calculated: this procedure is then an iterative one only with respect of displacement variations.
If the last convergent solution is $(\mathbf{q}^{(0)}, \lambda_0)$, postulating an increment as:

$$\lambda' = \lambda_0 + \Delta\lambda \tag{5.1.13}$$

the new updated load configuration, obtained by $\Delta\lambda$, immediately violates equilibrium condition. Thus, it is necessary to update the nodal displacement vector by a factor $\Delta\mathbf{q}$ in such a way:

$$\mathbf{q}' = \mathbf{q}^{(0)} + \Delta\mathbf{q} \tag{5.1.14}$$

the configuration $\mathbf{q}'$ satisfies equilibrium condition. Starting from the Taylor expansion around of the unbalanced residual forces eq.(5.1.5), imposing constraint condition on the load parameter variation, one can obtain:

$$\phi_{\mathbf{res}|\mathbf{q}^{(0)}} + \mathbf{K}_{T_{|\mathbf{q}^{(0)}}}\Delta\mathbf{q} - \Delta\lambda\mathbf{p}_{ref} = 0 \tag{5.1.15}$$

Since $(\mathbf{q}^{(0)}, \lambda_0)$ is an equilibrium condition, the unbalanced nodal forces computed at the equilibrium condition are identically null, the increment of the displacement vector can be easily computed:

$$\mathbf{K}_{T_{|\mathbf{q}^{(0)}}}\Delta\mathbf{q} - \Delta\lambda\mathbf{p}_{ref} = 0 \quad \rightarrow \quad \Delta\mathbf{q} = [\mathbf{K}_{T_{|\mathbf{q}^{(0)}}}]^{-1}(\Delta\lambda\mathbf{p}_{ref}) \tag{5.1.16}$$

However, even if the displacement correction $\Delta\mathbf{q}$ is defined in such a way eq.(5.1.15) is satisfied, the truncation at first-order of Taylor expansion prevents the immediate achievement of the new equilibrium condition at the configuration $(\mathbf{q}^{(0)} + \Delta\mathbf{q}, \lambda_0 + \Delta\lambda)$. Thus, by the unbalanced residual forces, another displacement correction $\delta\mathbf{q}$ has be evaluated, superimposing a variation only of the displacement variables in the Taylor series:

$$\phi_{\mathbf{res}}(\mathbf{q}^{(0)} + \Delta\mathbf{q} + \delta\mathbf{q}) = 0 \quad \rightarrow \quad \phi_{\mathbf{res}}(\mathbf{q}^{(0)} + \Delta\mathbf{q}) + \mathbf{K}_{T_{|\mathbf{q}^{(0)}+\Delta\mathbf{q}}}\delta\mathbf{q} = 0 \tag{5.1.17}$$

$$\delta\mathbf{q} = -[\mathbf{K}_{T_{|\mathbf{q}^{(0)}+\Delta\mathbf{q}}}]^{-1}\phi_{res}(\mathbf{q}^{(0)} + \Delta\mathbf{q}) \tag{5.1.18}$$

Subsequently, the new displacement correction is then obtained, so is new configuration $(\mathbf{q}^{(0)} + \Delta\mathbf{q} + \delta\mathbf{q}, \lambda_0 + \Delta\lambda)$: in general, this configuration leads to a smaller residual unbalanced forces. By updating iteratively the displacement variable, the equilibrium condition at incremented value of the external forces is finally computed. Again, convergence criterion on the unbalanced residual forces has to be satisfied.

From this final convergent configuration, a new increment of the load scaling parameter can be considered, starting again with the same procedure in order to find the new condition at a new load condition. From a geometrical point of view, the general iterations of Newton's load control method in the single step increment can be depicted as a general Newton's tangent method in nonlinear equations, as depicted in fig.5.1.2. Below, $\mathbf{q}^{(0)}$ is taken as the solution of the linear problem, and each $\mathbf{q}^{(i)}$ is the solution at the i-th iteration, that tends iteratively to $\bar{\mathbf{q}}$. At each iteration, the nodal displacement vector is used for the update of the tangent matrix that is used then to obtain the following nodal displacement vector associated to the external forces vector $\bar{F}$.

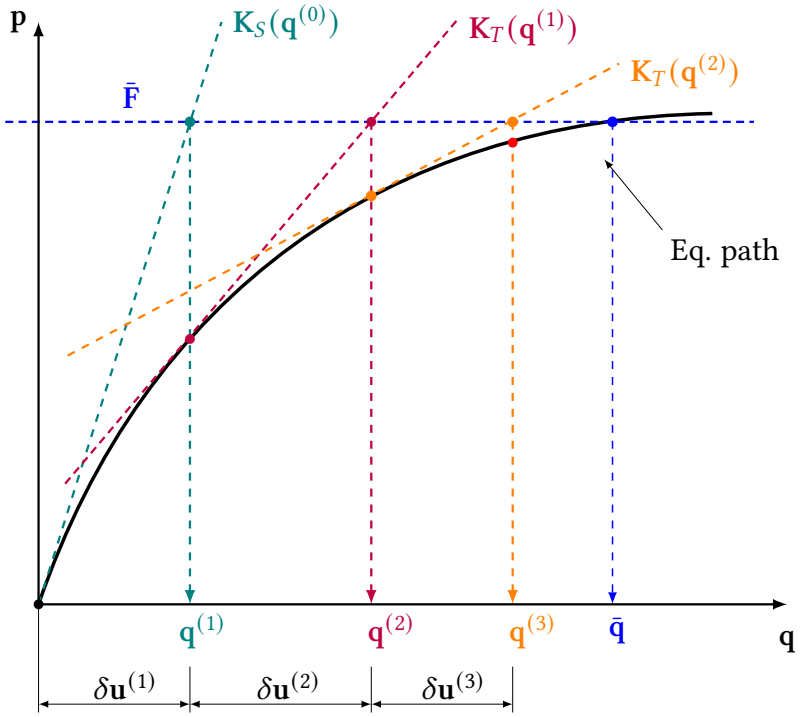

Figure 5.1.2: Load control method: geometrical interpretation

5.1.5 Arc-length modified Crisfield method

Arc-length method is a very efficient iterative numerical method for nonlinear problems, especially in the presence of one or more critical points. The nonlinear problem is solved as an equivalent optimization problem of the residual unbalanced forces, as described before:

$$\phi_{\mathbf{res}} = \mathbf{K}_S(\mathbf{q})\ \mathbf{q} - \mathbf{p} = 0 \quad \rightarrow \quad \mathbf{K}_S(\mathbf{q})\ \mathbf{q} = \mathbf{p} \tag{5.1.19}$$

In this method, in spite of load control method, simultaneous variations of displacement variables and scalar load parameter are that postulated, and eq.(5.1.19) is solved for both variables. As done for the load control method, if $(\mathbf{q}^{(0)}, \lambda)$ is the starting equilibrium condition, considering an increment $(\Delta\mathbf{q}, \Delta\lambda)$ one can write:

$$\phi_{\mathbf{res}}(\mathbf{q}^{(0)} + \Delta\mathbf{q}, \lambda_0 + \Delta\lambda) = \mathbf{K}_S(\mathbf{q}^{(0)})\ (\mathbf{q}^{(0)} + \Delta\mathbf{q}) - (\lambda_0 + \Delta\lambda)\mathbf{p} \tag{5.1.20}$$

If, in the updated configuration $(\mathbf{q}^{(0)} + \Delta\mathbf{q}, \lambda_0 + \Delta\lambda)$, the unbalanced residual forces vector $\phi_{\mathbf{res}}(\mathbf{q}^{(0)} + \Delta\mathbf{q}, \lambda_0 + \Delta\lambda) = 0$, then the updated point belong to the equilibrium path and solution can be updated. However, as observed previously, this condition is not guaranteed in general due to truncation of Taylor series up to the first order. Thus, another displacement and load factor correction $(\delta\mathbf{q}, \delta\lambda)$ is required in order to satisfy eq.(5.1.20). Hence,

$$\phi_{\mathbf{res}}(\mathbf{q}^{(0)}+\Delta\mathbf{q}+\delta\mathbf{q}, \lambda_0+\Delta\lambda+\delta\lambda) = \mathbf{K}_S(\mathbf{q}^{(0)}+\Delta\mathbf{q})\ (\mathbf{q}^{(0)}+\Delta\mathbf{q}+\delta\mathbf{q}) - (\lambda_0+\Delta\lambda+\delta\lambda)\mathbf{p} = 0 \tag{5.1.21}$$

Finally, as done for the load control method, considering a Taylor series of the unbalanced residual forces, the new system of equation will have form:

$$[\mathbf{K}_{T_{|\mathbf{q}^{(0)}+\Delta\mathbf{q}}}]\delta\mathbf{q} - \delta\lambda\mathbf{p} = -\phi_{res}(\mathbf{q}^{(0)} + \Delta\mathbf{q}) \tag{5.1.22}$$

This approach lead to an undetermined system of equations since there is one more unconstrained degree-of-freedom, λ: system of equation eq.(5.1.22) is not sufficient for both displacement correction and load correction unknowns. This problem is overcome considering an additional constraint equation, typically referred as "arc-length equation", whose general expression is:

$$(\Delta\mathbf{q} + \delta\mathbf{q})^T(\Delta\mathbf{q} + \delta\mathbf{q}) + \psi^2(\Delta\lambda + \delta\lambda)^T(\mathbf{p}^T \cdot \mathbf{p}) = \Delta l^2 \tag{5.1.23}$$

in which ψ and Δl are user-defined parameter. Particularly, Δl has the same meaning of $\Delta\lambda$ in load control method, it is a measure of "how far" the next equilibrium point is.

Combining eq.(5.1.22) and eq.(5.1.23), governing equation for the correction parameters can be rewritten in a more compact way:

$$\begin{bmatrix} [\mathbf{K}_{T_{|\mathbf{q}^{(0)}+\Delta\mathbf{q}}}] & -\mathbf{p} \\ 2\Delta\mathbf{q}^T & 2\psi^2\Delta\lambda(\mathbf{p}^T \cdot \mathbf{p}) \end{bmatrix} \cdot \begin{bmatrix} \delta\mathbf{q} \\ \delta\lambda \end{bmatrix} = \begin{bmatrix} -\phi_{res}(\mathbf{q}^{(0)} + \Delta\mathbf{q}) \\ -(\Delta\mathbf{q}^T \cdot \Delta\mathbf{q} + \psi^2\delta\lambda^2(\mathbf{p}^T \cdot \mathbf{p}) - \Delta l^2) \end{bmatrix} \tag{5.1.24}$$

Eq.(5.1.24) is solved for the updating correction value displacements and load factor $(\delta\mathbf{q}, \delta\lambda)$.
The procedure here described is iteratively repeated until correction factors obtained by eq.(5.1.24) fulfill eq.(5.1.21): in this case, iterations are repeated until convergence is reached up to a certain tolerance factor on the unbalanced residual nodal vector, that can be superimposed a priori before the computation.
However, the present implementation of geometrically nonlinear finite elements makes use of Crisfield'a approach for arc-length method. Starting from eq.(5.1.22), the displacement correction can be rearranged as:

$$\delta\mathbf{q} \;=\; -[\mathbf{K}_{T_{|\mathbf{q}^{(0)}+\Delta\mathbf{q}}}]^{-1}\phi_{res}(\mathbf{q}^{(0)}+\Delta\mathbf{q}) + [\mathbf{K}_{T_{|\mathbf{q}^{(0)}+\delta\lambda\Delta\mathbf{q}}}]^{-1}\mathbf{p} \;=\; \delta\bar{\mathbf{q}} + \delta\lambda\delta\mathbf{q_t} \tag{5.1.25}$$

$$\begin{cases} \delta\bar{\mathbf{q}} = -[\mathbf{K}_{T_{|\mathbf{q}^{(0)}+\Delta\mathbf{q}}}]^{-1}\phi_{res}(\mathbf{q}^{(0)}+\Delta\mathbf{q}) \\ \delta\mathbf{q_t} = [\mathbf{K}_{T_{|\mathbf{q}^{(0)}+\delta\lambda\Delta\mathbf{q}}}]^{-1}\mathbf{p} \end{cases} \tag{5.1.26}$$

Note that the expressions of auxiliary variables $\delta\bar{\mathbf{q}}$ and $\delta\mathbf{q_t}$ in eq.(5.1.26) are known since they require only known quantities. Substituting this decomposition of $\delta\mathbf{q}$ into the arc-length constraint equation eq.(5.1.23), a quadratic equation for $\delta\lambda$ is obtained:

$$\begin{cases} \alpha_1\delta\lambda^2 + \alpha_2\delta\lambda + \alpha_3 = 0 \\ \alpha_1 = \delta\mathbf{q}^T\mathbf{q} + \psi^2(\mathbf{p}^T\mathbf{p}) \\ \alpha_2 = 2(\Delta\mathbf{q} + \delta\bar{\mathbf{q}})^T\delta\mathbf{q_t} + 2\psi^2\Delta\lambda(\mathbf{p}^T\mathbf{p}) \\ \alpha_3 = (\Delta\mathbf{q} + \delta\bar{\mathbf{q}})^T(\Delta\mathbf{q} + \delta\bar{\mathbf{q}}) + \psi^2\Delta\lambda^2(\mathbf{p}^T\mathbf{p}) - \Delta l^2 \end{cases} \tag{5.1.27}$$

Once $\delta\lambda$ is obtained from this simple equation, in which all the coefficients are known, it can be directly substituted into eq.(5.1.25) to compute the displacement correction, completing the iteration procedure. This whole algorithm is iteratively repeated until convergence is reached (criteria con unbalanced residual forces), so finally displacement and load are updated to the new equilibrium convergent point of the equilibrium path.

On of the most important application of modified Crisfield arc-length procedure is the case of $\psi = 1$ that is also called *spherical arc-length procedure*, since the arc-length equation eq.(5.1.23) takes the form of an hyper-sphere constraint equation. From a geometrical point of view, Crisfield formulation of arc-length method can be interpreted as a successive updated of the solution by a circular constraint equation.

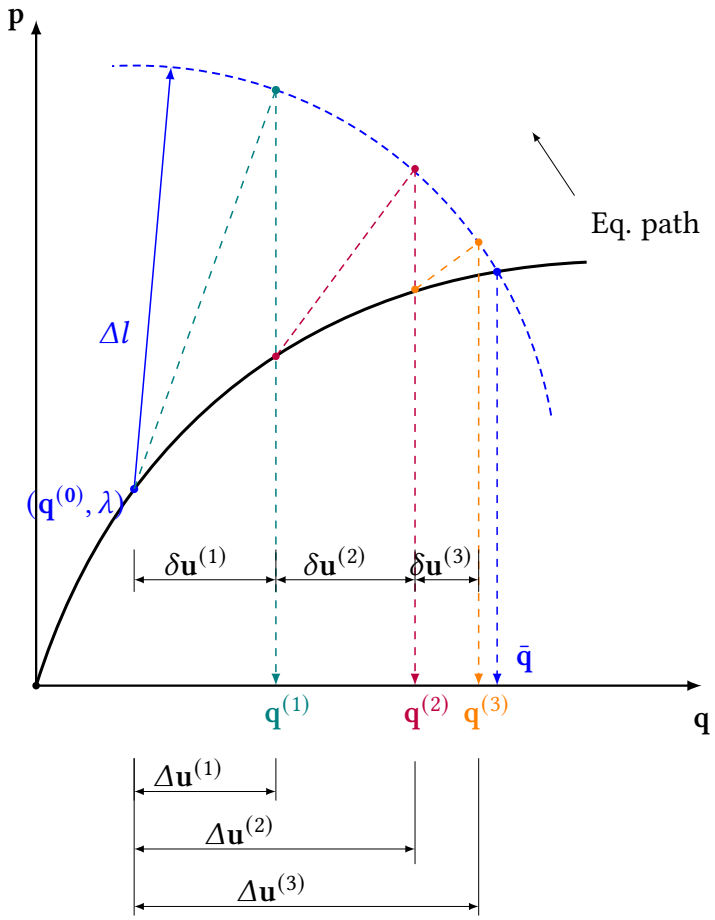

Figure 5.1.3: Crisfield arc-length method: geometrical interpretation

5.2 Description of the MUL^2 code

All the simulations have been carried out by means of the MUL^2 code built by MUL^2 research group in Polytechnic University of Turin: Carrera Unified Formulation and Node Dependent Kinematics are implemented for purely structural and multifield problem in the linear elastic domain, geometrically nonlinear elastic domain and constitutive inelastic problems. It is entirely written in Fortran language.
The code is made up by a collection of libraries and modules that contains all the procedures and routines related to a specific analysis. All the numerical procedures implemented in the code refers to structural variables, that allow the implementation of NDK (Node Dependent Kinematics) and general algorithms independently on the nature of finite element considered. One of the most powerful aspect of the NDK is the simulations of structures with discretization made up by different elements: it is possible to combine 1D, 2D and 3D elements by superimposing the connectivity between FEM indeces and CUF indeces.

In the pre-processor step, inputs related to the geometry, discretization adopted and material properties are processed and NDK is inizialized. In the procedure step, finite element procedures implemented are executed: computation and assembly of stiffness matrices fundamental nuclei are performed, then PARDISO solver is used to obtain the solution of sparse linear system of equations. Integrals required by the fundamental nuclei are computed by means of Gauss-Legendre quadrature implemented in the code: in specific Fortran modulus, displacements derivatives and shape functions are evaluated at specified Gauss integration points and used for the computation of fundamental nuclei.
Distinct numerical schemes considering different problems are implemented in specific and independent subroutines, which call external routines for the computation of stiffness matrices: this programming choice allow the computation of same matrices in different procedures.
After obtaining the solution, post-processing step prints out results in term of displacements, strain and stresses in the requested points, as well as Paraview 3D post-processing of the deformed configurations.

The most important part of this thesis work was dedicated to the implementation of the 3D nonlinear finite element using Carrera Unified Formulation and Node Dependent Kinematics in the already available interface.
Fundamental nuclei of secant and tangent stiffness matrices for 3D geometrically nonlinear elements were derived by means of Mathematica Notebook and were implemented in the related routines. In addition, computation of displacements derivatives, strains and stresses for 3D finite elements were required and implemented, as well as adaption of the already available code in which specific select-cases for 3D element variables computation were added.
In the implementation, the computation of fundamental nuclei were implemented in two different ways: the first one, secant and tangent stiffness matrices are computed component by component, and then memorized in the single 3x3 nucleus; instead, in the second one, formal matrices of derivatives $\mathbf{B}_l^{ri}$, and $\mathbf{B}_{nl}^{ri}$, $(\mathbf{B}_l^{sj})^T$ and $(\mathbf{B}_{nl}^{sj})^T$ are implemented and the following raw-by-coloumn product is left to Fortran commands, so each fundamental nucleus is derived by imposing manually the matrix product B^TCB. During the compu-

tation and analysis of considered case, the second way results in faster calculation with respect of the first way, since the matrix operation are made by the the processor and it is not necessary to implement hundreds of manual operations. Solution of nonlinear systems of equations require in general the computation of residuals: in the specific case of constitutive linear elastic materials, they can be calculated adopting the secant matrix, but computation of residual internal forces by integration of internal strain energy has been also implemented for further applications and future works, since including also material non-linearities, the secant matrix is no more representative of the residues.

After the implementation of solid FEM elements for linear-elastic materials, the same procedure have been imported and adapted in the available code for isotropic hyperelastic materials: once the code is validated from a procedural point of view by linear-elastic material study cases, it has been adopted for the computation of isotropic hyperelastic stiffness matrices and internal forces vector. As said before, the programming choice adopted in the already available interfaces allowed a rapidly implementation same procedures in different parts of the codes. Referring then to hyperleastic materials, computation of derivatives and integral required by the fundamental nuclei have been implemented, but routines for the computation of PK1 and PK2 and tangent elasticity tensor have been used with their nominal definition since they are independent on the model chosen.

Chapter 6

Numerical results

This chapter is devoted to the analysis of the numerical results of different study cases, involving 1D, 2D and 3D refined non-linear finite elements according to Carrera Unified Formulation and Finite Element analysis described before. Aim of this chapter is to validate the present formulation of 3D non-linear finite elements by comparing the actual numerical results with study cases takes from literature, demonstrating the capabilities of the present formulation of 3D elements. All the numerical simulations were carried out by using the MUL^2 in-house code.

6.1 Refined fully-nonlinear 1D beam elements

6.1.1 Large deflections of cantilever square cross-section beam

First, large deflections of 1D solid cross section are analyzed. In the first case, a cantilever, square cross-section beam subjected to a vertical concentrated load in considered. The beam is made in aluminum, the mechanical properties are given in terms of elastic modulus $E = 75$ GPa and Poisson's ratio $\nu = 0.3$. For convergence reasons, 20 B4 elements are used along the beam axis, and one Q9 quadratic element is considered in the description of the cross-section discretization, as described in Pagani *et al.*[10]

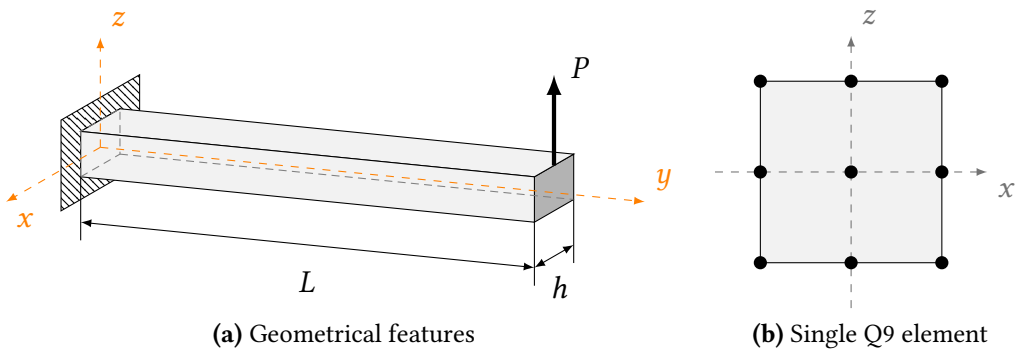

(a) Geometrical features **(b)** Single Q9 element

Figure 6.1.1: Cantilever beam: geometrical properties and cross-section discretization

The effects of lenght to cross-section side ratio are analyzed: given the lenght $L = 1$m of the beam, two cases are analyzed: $L/h = 10$ and $L/h = 100$.
Fig.6.1.2 shows the equilibrium curves of the beam subjected to a verical loading, instead fig.6.1.3 shows the distribution of the non-dimensional axial stress component $\sigma_{yy}\frac{2I}{PLh}$ for different loading conditions.

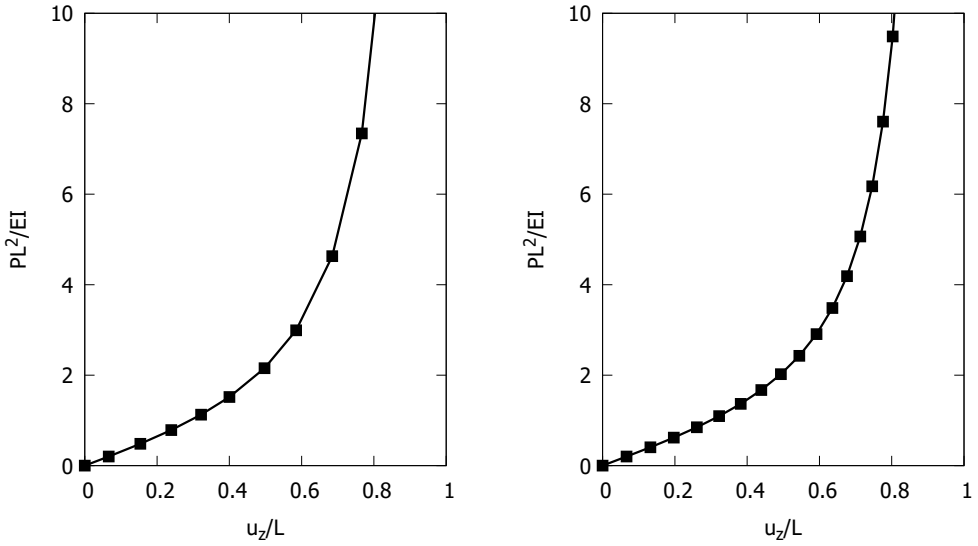

(a) $L/h = 10$ **(b)** $L/h = 100$

Figure 6.1.2: Cantilever square cross-section beam: equilibrium curves obtained by refined 1D CUF elements

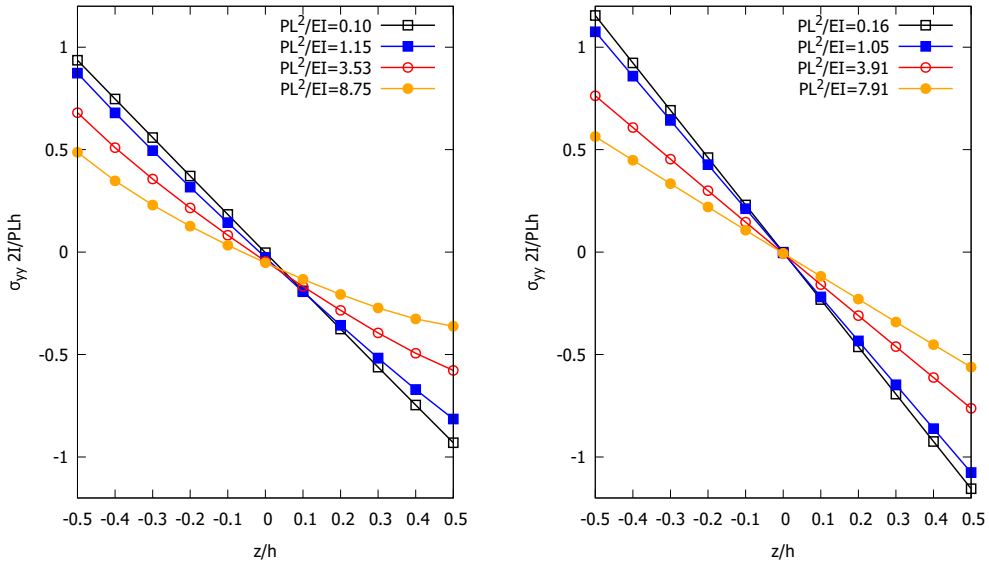

(a) $L/h = 10$ **(b)** $L/h = 100$

Figure 6.1.3: Cantilever square cross-section beam: through-the-thickness distribution of non-dimensional
axial stress $\sigma_{yy}\frac{2I}{PLh}$ obtained by refined 1D CUF elements

6.1.2 Post-buckling of cantilever square cross-section beam

Let's consider again the cantilever square cross-section beam beam, case $L/h = 100$, subjected now to an eccentric concentrated compression load P directed along the axis of the beam, with a defect load $d = 0.002\pi^2 EI/4L^2$ to drive instability.
Fig.6.1.5 shows the post-buckling equilibrium curves of the cantilever square-cross section beam, depending on the compression load P, scaled with respect of the critical Eulerian's instability load:

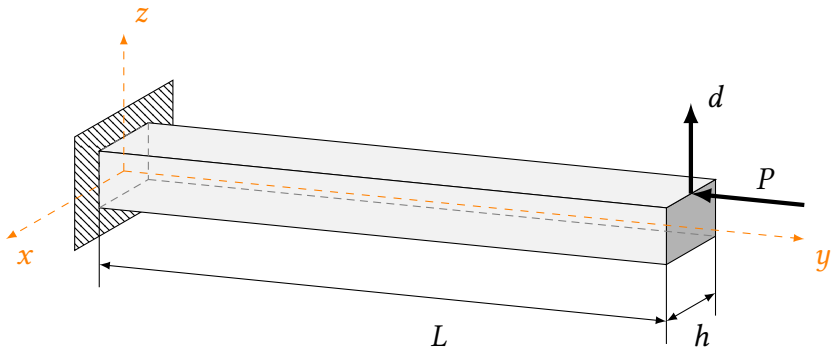

Figure 6.1.4: Square cross-section beam: geometrical features and load conditions for post-buckling analysis

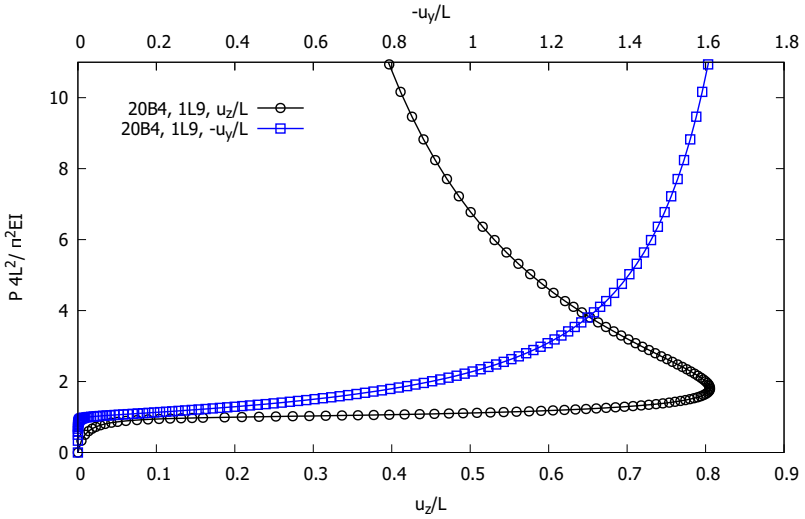

Figure 6.1.5: Cantiliver square cross-section beam: post-buckling equilibrium curves obtained by refined 1D CUF elements

6.1.3 Large deflections of thin-walled unsymmetric C-section beam

Large deflection analysis in the case of a cantilever, unsymmetrical cross-section beam subjected to large deflection due to a vertical load is now carried out. The beam is made in aluminum, the mechanical properties are given in terms of elastic modulus $E = 75$ GPa and Poisson's ratio $\nu = 0.3$. The dimensions of the cross-section are $h_1 = 48mm$, $h_2 = 88mm$, $t = 8mm$ and $w = 100mm$. For convergence reasons, 20 B4 elements are used along the beam axis, and seven Q9 quadratic element are emplyoed in the discretization of the cross-section, as depicted in fig.6.1.7(b), as described in Pagani *et al. et al.*[10]

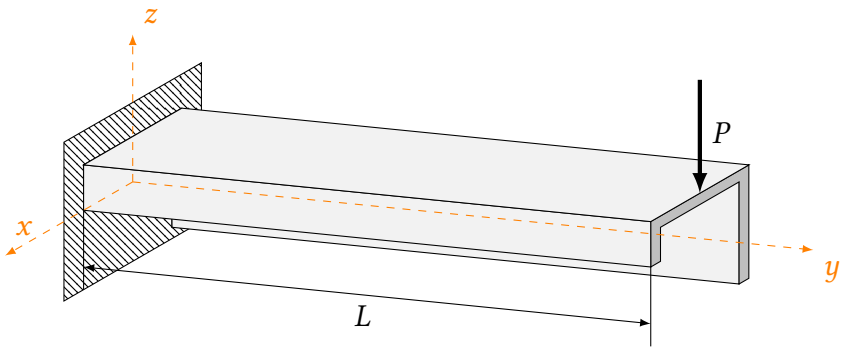

Figure 6.1.6: Unsymmetric C-section beam: geometrical features and load conditions

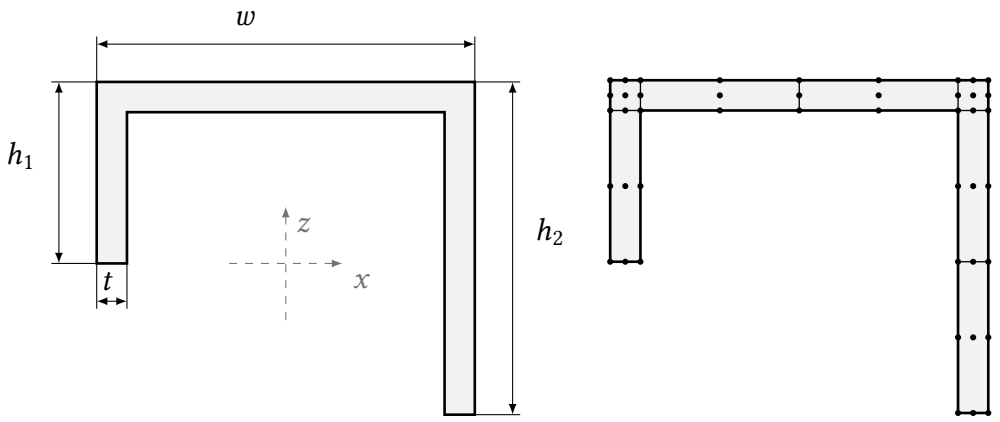

(a) Cross-section geom. features

(b) Discretization with 7 Q9 elements

Figure 6.1.7: Unsymmetric C-section beam: cross section geometrical properties and adopted discretization

Fig.6.1.8 shows the equilibrium curves of the beam in the ranges of small/moderate displacements and large displacements, evaluated at the point $A = (46, 1000, 40)\ mm$ on the free end of the beam:

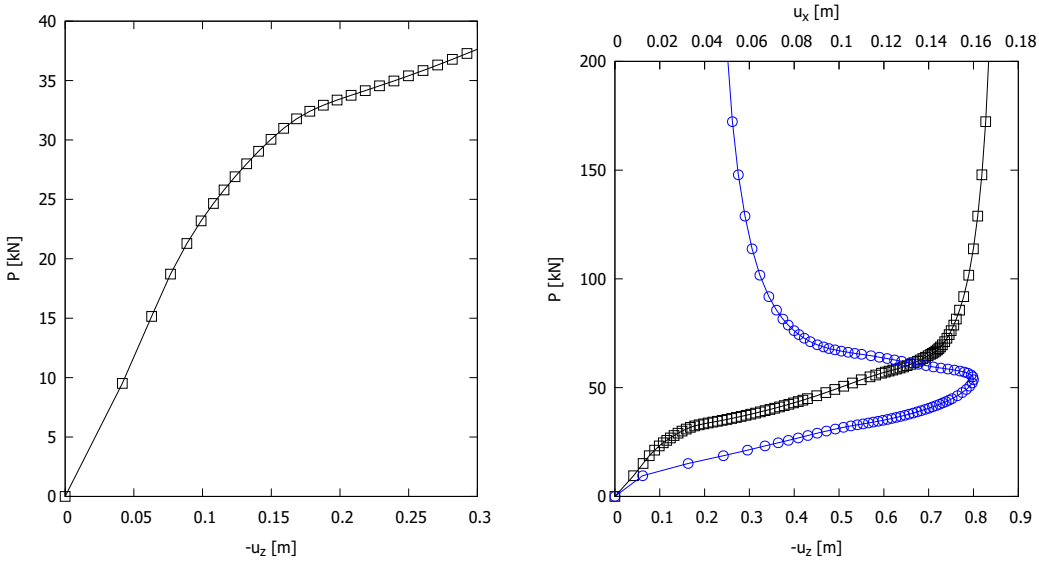

(a) $L/h = 10$ **(b)** $L/h = 100$

Figure 6.1.8: Unsymmetric C-section beam: displacement component at point A on the tip cross-section of the beam depending on the load. Behaviour in the range of small/moderate and large displacements

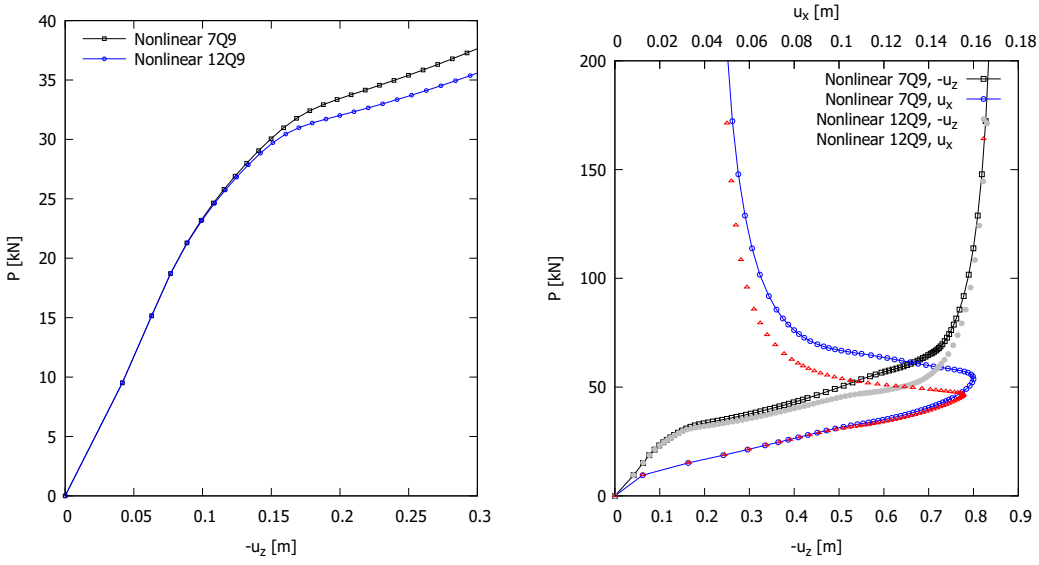

(a) $L/h = 10$ **(b)** $L/h = 100$

Figure 6.1.9: Unsymmetric C-section beam: displacement component at point A on the tip cross-section of the beam depending on the load. Behaviour in the range of small/moderate and large displacements

6.2 Refined fully-nonlinear 2D plate elements

6.2.1 Large deflections of square plates

Large deflection of 2D thin and thick squared plates are now analyzed. An homogeneous isotropic square plate subjected to large deflection due to a vertical uniform pressure applied in the z direction is considered. The mechanical properties of the plate are given in terms of elastic modulus $E = 75$ GPa and Poisson's ratio $\nu = 0.3$. The sides of the plate are $a = b = 1.2m$ and two thickness-to-side ratio h/a are considered to analyze the behavior of relatively thin plates and relatively thick plates. For convergence reasons, 10 Q9 elements for each direction of the mid surface are employed in the discretization, and one B3 quadratic element is considered in the thickness direction.

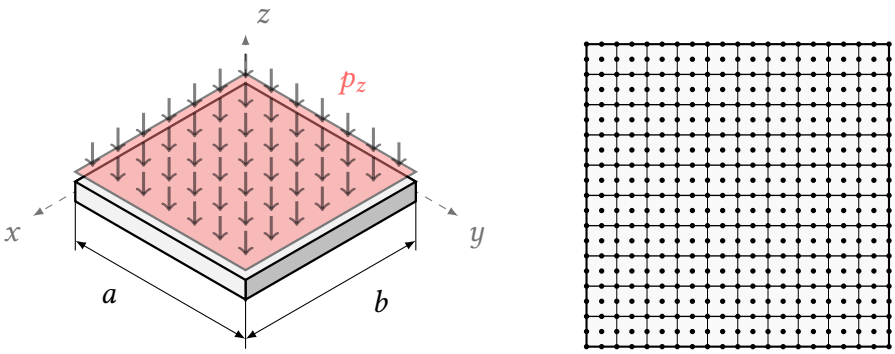

(a) Square plate geom. features **(b)** Mesh: 10x10 Q9 elem.

Figure 6.2.1: Square plate: geometrical properties and adopted discretization

Different geometrical support constraints conditions are considered for the same loading case:

1. "CCCC", all edges clamped, namely $u = v = w = 0$ at $x = 0$, $x = a$, $y = 0$ and $y = a$;
2. "SSSS", all edges simply supported, namely $u = v = w = 0$ at $z = 0,\ x = 0, a$ and $z = 0,\ y = 0, a$;
3. "CSCS", alternated edge conditions, clamped-(simply supported)-clamped-(simply supported), namely $u = v = w = 0$ at $z = 0,\ x = 0, a$, $y = 0$ and $y = a$;

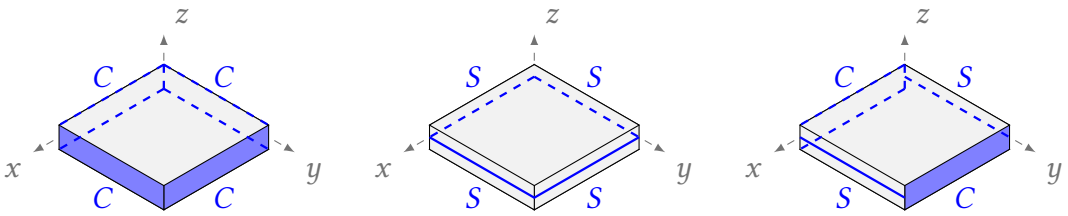

(a) CCCC **(b)** SSSS **(c)** CSCS

Figure 6.2.2: Different edge support conditions: (a) CCCC, (b) SSSS, (c) CSCS

The large deflection equilibirium curves for the square plate subjected to a vertical uniform pressure load is shown in fig.6.2.3:

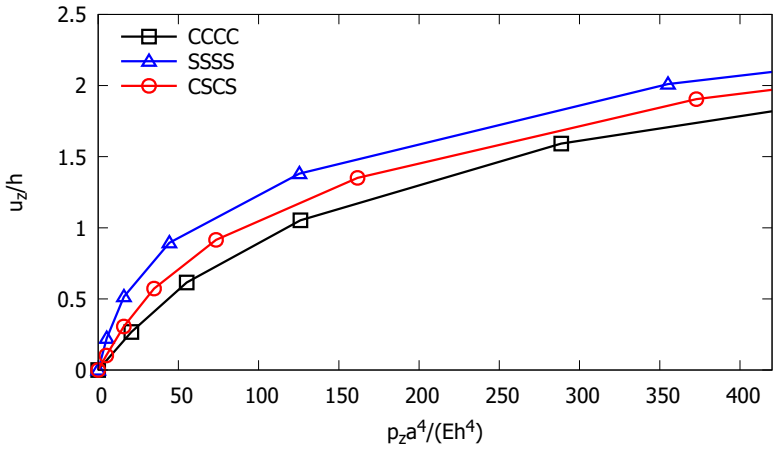

(a) Thin plate: $h/a = 0.02$

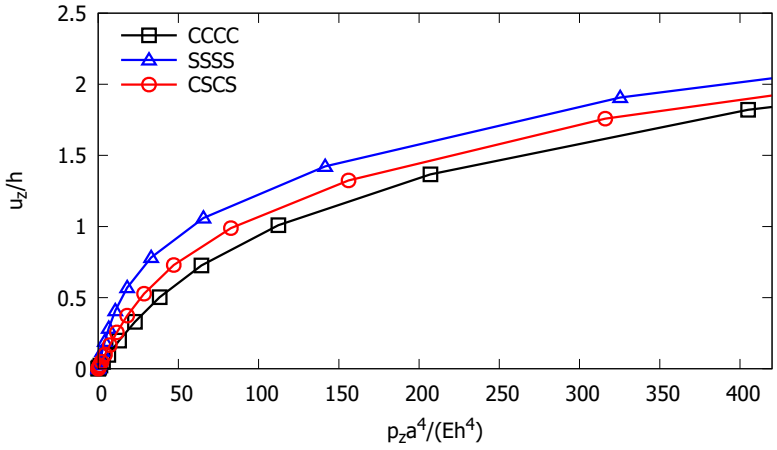

(b) Thick plate: $h/a = 0.1$

Figure 6.2.3: Square plate:equilibrium curves of the plate subjected to transvers pressure for each boundary condition considered

6.3 Fully-nonlinear 3D elements

6.3.1 Cantilever square cross-section beam: convergence analysis

First, large deflections of a square cross-section beam are analyzed: again, the same cantilever beam subjected to large deflection due to a vertical load, made of the same material, in considered. In this study case, a convergence analysis adopting solid finite elements is carried out, considering the effects of length to cross-section side ratio: given the length $L = 1$m of the beam, the same two cases are analyzed: $L/h = 10$ and $L/h = 100$. In this case, reference solution is known by previous analysis and taken by Pagani *et al.*[10]: for the fixed value of P such that $PL^2/EI = 3$, $u_z^{ref}/L = 0.603$. The numerical scheeme adopted in this case is the Picard method: only the secant matrix is adopted.

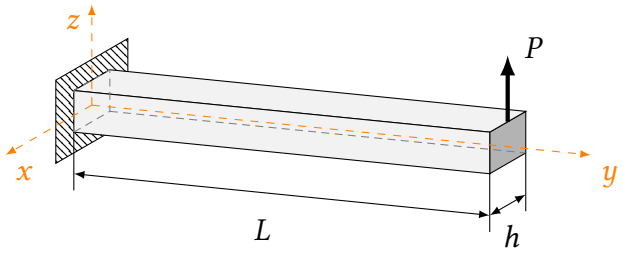

Figure 6.3.1: Cantilever square cross-section beam: geometrical features and load conditions

		Linear model (H8)		**Parabolic model (H27)**	
	N. elem.	DOFs	$\mathbf{u_z/L}$	DOFs	$\mathbf{u_z/L}$
L/h = 10	10	*132*	0.4494	*567*	0.5638
	15	*192*	0.4875	*837*	0.5654
	20	*252*	0.5043	*1107*	0.5638
	25	*312*	0.5254	*1377*	0.5663
L/h = 100	40	*492*	0.2606	*2187*	0.6002
	50	*612*	0.3267	*2727*	0.6006
	60	*732*	0.3768	*3267*	0.6008
	80	*972*	0.4392	*4347*	0.6010

Table 6.1: Cantilever square cross-section beam: convergence analysis results

As shown in table 6.1, any linear model is not suitable for the large displacement analysis of this study case: locking phenomenon prevents the computation of a correct solution adopting a linear model, therefore at least a parabolic model is needed. In the case of parabolic model, for the case $L/h = 10$, convergent results are near the analytic reference solution but are not accurate as in the case of $L/h = 100$ beam in which, adopting every discretization, reference value is correctly obtained. This very simple study case is able to prove the limitation of linear solid elements in the case of large deflection analysis: therefore, starting from this point, adopted discretization will be the one with 20 H27 in the case of $L/h = 10$ beam, and 60 H27 in the case of $L/h = 100$.

6.3.2 Cantilever square cross-section beam: 3D model results

First, large deflections of a square cross-section beam are analyzed: again, the same cantilever beam subjected to large deflection due to a vertical load, made of the same material, in considered. The effects of lenght to cross-section side ratio is analyzed: given the lenght $L = 1$m of the beam, the same two cases are analyzed: $L/h = 10$ and $L/h = 100$, by considering the two previously obtained convergent meshes, made of 60H27 for $L/h = 100$ case and 20H27 for $L/h = 10$ case.
Fig.6.3.2 shows the equilibrium curves of the beam subjected to a vertical loading comparing the solution obtained by 1D beam elements with the present implementation of 3D fully nonlinear elements.
Fig.6.3.4 and fig.6.3.3 shows the distribution of the non-dimensional axial stress component σ_{yy} both in the case of $L/h = 10$ and $L/h = 100$: the solution obtained by the present implementation of 3D fully nonlinear elements is compared with the one obtained by 1D beam elements.

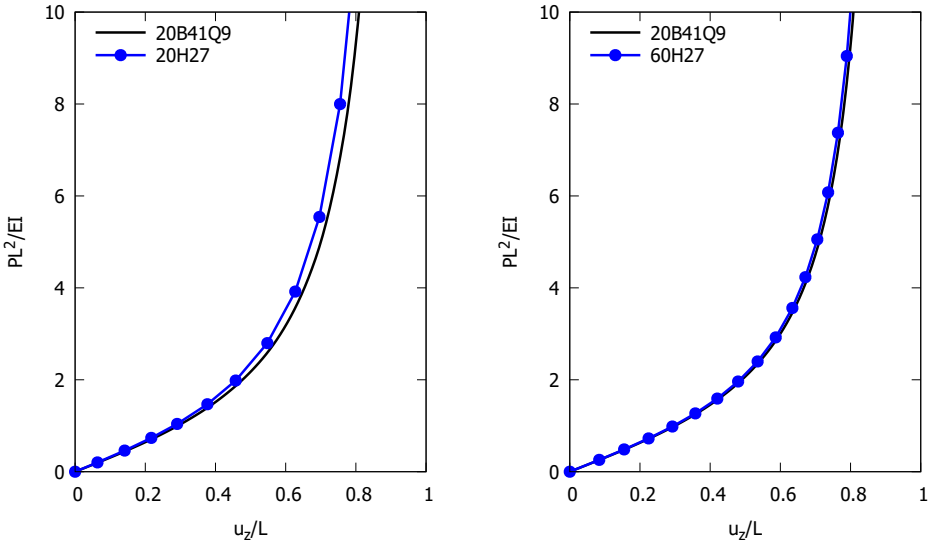

(a) $L/h = 10$ **(b)** $L/h = 100$

Figure 6.3.2: Cantiliver beam equilibrium curve: 1D and 3D model results

As already proven in the previous study case, for the $L/h = 10$ cantilever beam, solution obtained by the solid elements discretization is a bit far from the one obtained by refined fully non-linear 1D CUF elements: this can be justified by the behavior of deep beams in the range of large displacements, due to geometry of the structures. Also, this behavior is also observed in the description of non-dimensional σ_{yy} along the thickness of the beam: in order to cope with these errors, much more efforts in the discretization of the structure are required, adopting for example more elements in the discretization along the thickness. At the contrary, for the $L/h = 100$ cantilever beam, results are accurate.

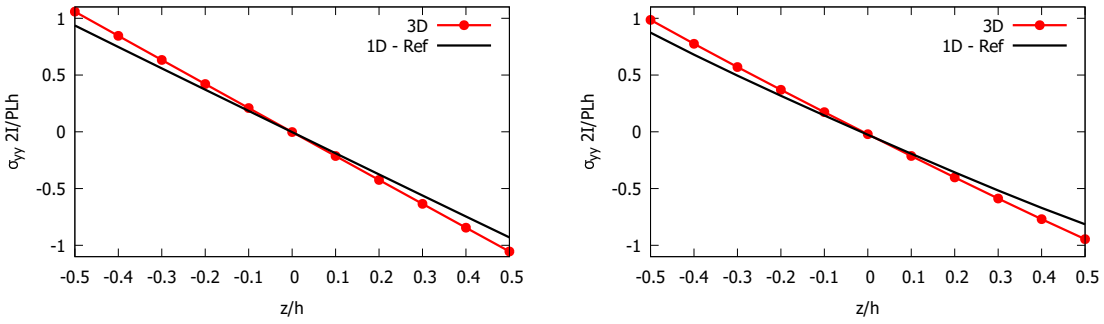

(a) $PL^2/EI = 0.10$ **(b)** $PL^2/EI = 1.15$

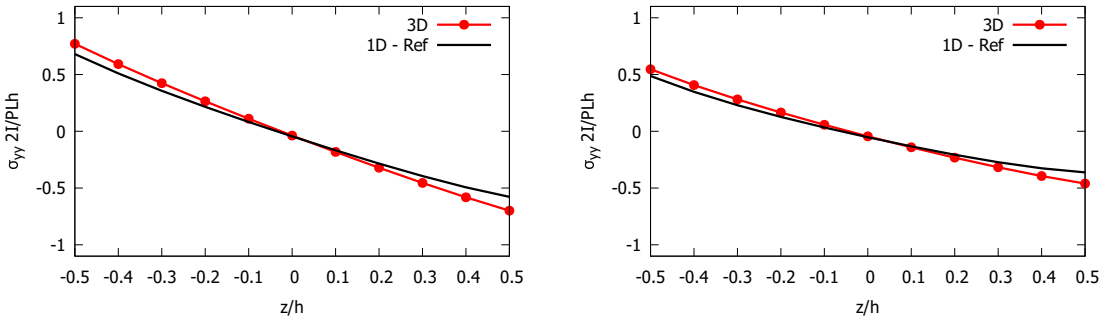

(c) $PL^2/EI = 3.53$ **(d)** $PL^2/EI = 8.75$

Figure 6.3.3: Cantiliver beam, case $L/h = 10$, non-dimensional σ_{yy} plot: 1D and 3D model results

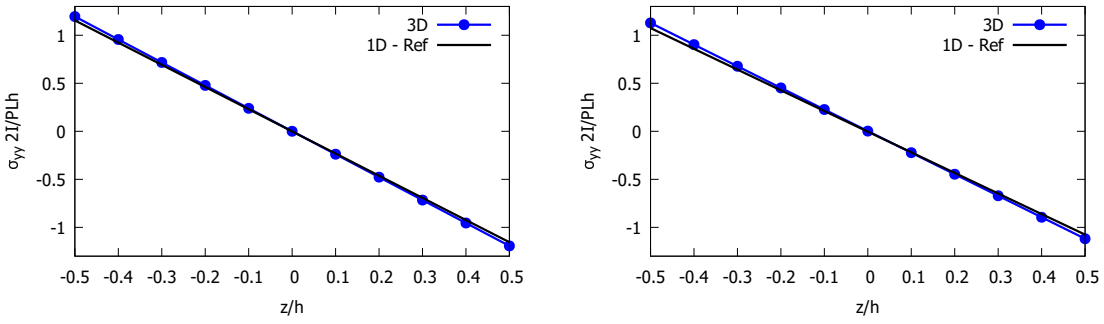

(a) $PL^2/EI = 0.16$ **(b)** $PL^2/EI = 1.15$

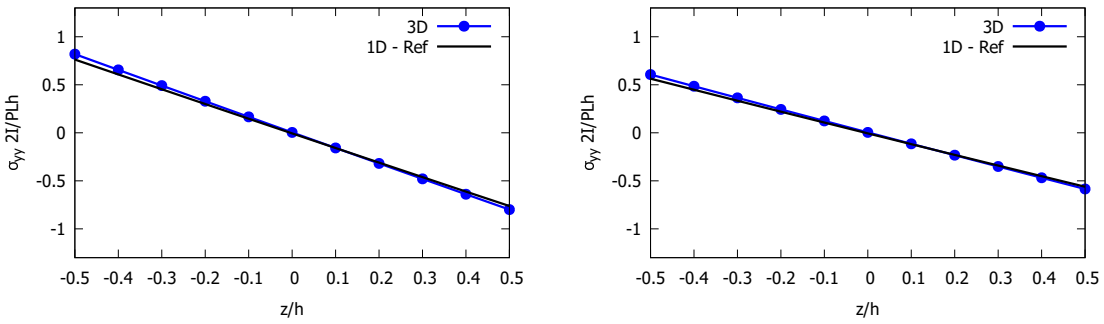

(c) $PL^2/EI = 3.91$ **(d)** $PL^2/EI = 7.91$

Figure 6.3.4: Cantiliver beam, case $L/h = 100$, non-dimensional σ_{yy} plot: 1D and 3D model results

Afterwards, post-buckling analysis of the same cantilever beam is carried out. Consider the same cantilever beam, case $L/h = 100$, subjected now to an eccentric compression load P and a vertical load $d = 0.002\pi^2 EI/4L^2$: solution is obtained in this case using solid elements instead of 1D beam elements, adopting the convergent mesh with 60H27 discretization.
Fig.6.3.6 shows the post-buckling equilibrium curves of the cantilever square-cross section beam, depending on the compression load P, scaled with respect of the critical Eulerian's instability load: the solution obtained by the present implementation of 3D fully nonlinear elements is compared with the one obtained by 1D beam elements.

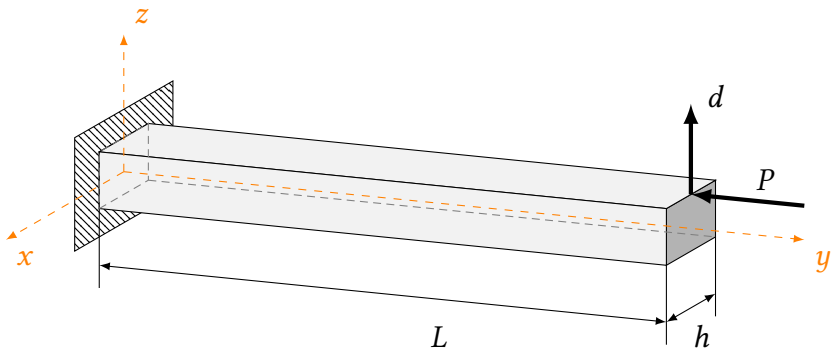

Figure 6.3.5: Cantiliver beam, post-buckling analysis: geom. features and load conditions

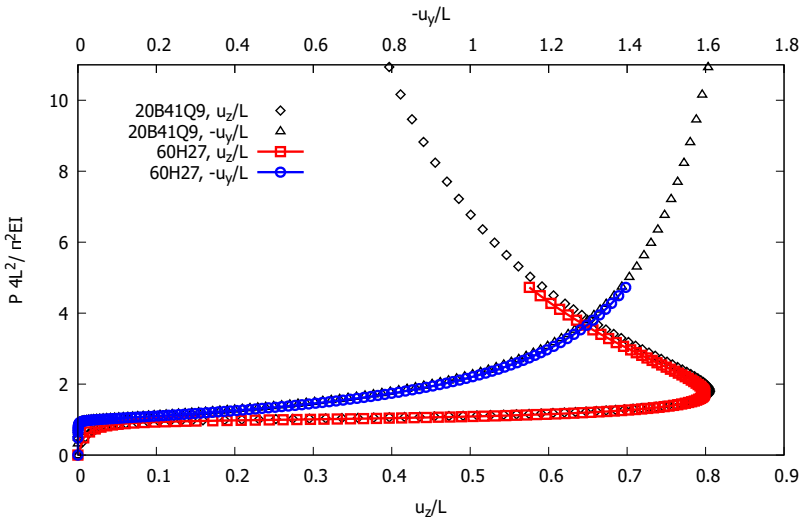

Figure 6.3.6: Cantiliver beam, $L/h = 100$, post-buckling equilibrium curves: 1D and 3D model results

6.3.3 Simply supported square beam: 3D model results

Again, large deflections of a square cross-section beam are analyzed: in this case, a simply supported square cross-section beam subjected to large deflection due to a vertical load applied at the mid-span of its axis, made of the same material of the previous case, in considered. This case has been proposed and carried out to analyze the influence of boundary condition application. The effects of length to cross-section side ratio is analyzed: given the lenght $L = 1$m of the beam, the same two cases are analyzed: $L/h = 10$ and $L/h = 100$. The discretization of the beam is carried out by considering 20B41Q9 1D beam elements for both cases, and the two convergent meshes, made of 60H27 for $L/h = 100$ case and 20H27 for $L/h = 10$ case.
Fig.6.3.8 shows the equilibrium curves of the beam: the solution obtained by the present implementation of 3D fully nonlinear elements is compared with the one obtained by 1D beam elements.

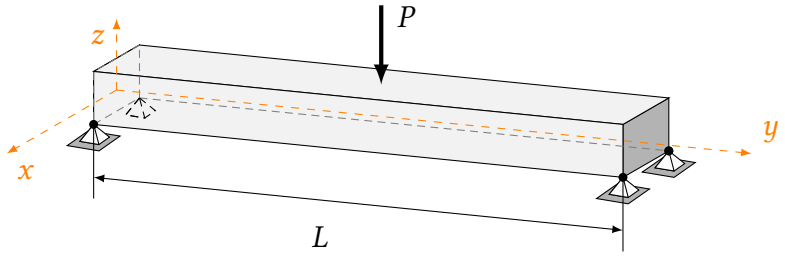

Figure 6.3.7: Simply supported beam, central shear load: geom. features and load condition

Fig.6.3.8(a) and fig.6.3.8(b) show the comparison between the equilibrium curve obtained adopting both 1D CUF-FEM elements and 3D FEM elements: results are matching, so numerical solution obtained by the present implementation of 3D FEM elements can be considered valid and accurate.

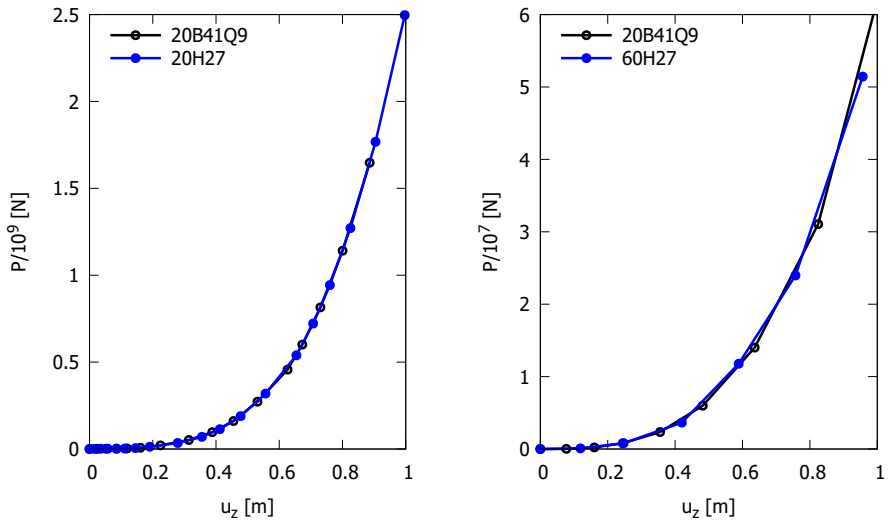

(a) $L/h = 10$ **(b)** $L/h = 100$

Figure 6.3.8: Simply supported beam equilibrium curves: 1D and 3D model results

Afterwards, post-buckling analysis of the simply-supported square-cross section beam is now carried out, considering the case of the beam $L/h = 100$, subjected now to an eccentric compression load P and a vertical load $d = 0.004\pi^2 EI/L^2$: solution is obtained in this case using using solid elements instead of 1D beam elements, employing the convergent mesh with 60H27 discretization.

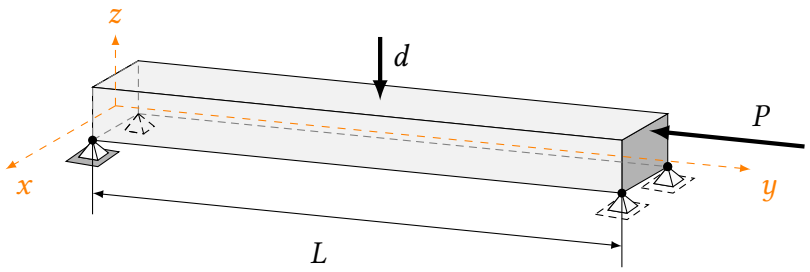

Figure 6.3.9: Simply supported beam, post-buckling analysis: geom. features and load conditions

Fig.6.3.10 shows the post-buckling equilibrium curves of the cantilever square-cross section beam, depending on the non-dimensional compression load P, scaled with respect of the critical Eulerian's instability load: the solution obtained by the present implementation of 3D fully nonlinear elements is compared with the one obtained by 1D beam elements. The post-buckling behavior of the beam can be correctly described adopting solid elements, as observed in the range of small/moderate displacement range and in the value of critical buckling load but the large displacement range of the actual solution is far from reference one: this can be justified by the limited model adopted.

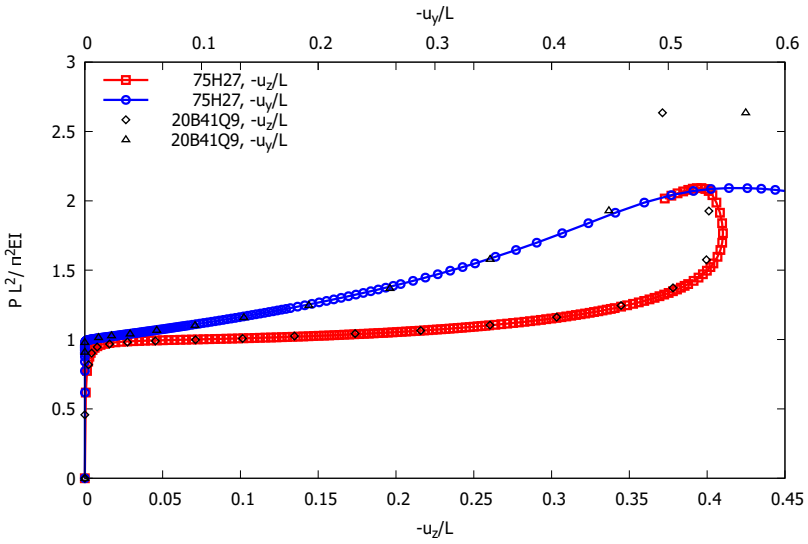

Figure 6.3.10: Simply supported beam, post-buckling equilibrium curves: 1D and 3D model results

6.3.4 Unsymmetric C-section beam: 3D model results

Large deflection analyses of 1D solid cross section is carried out in the case of a cantilever, unsymmetric C-section beam subjected to large deflection due to a vertical load: again, the same beam of the previous case is considered. The two beam discretization considered are the previously defined convergent meshes made of 20B4-12Q9 1D elements and another one made of 600 H27 solid elements.

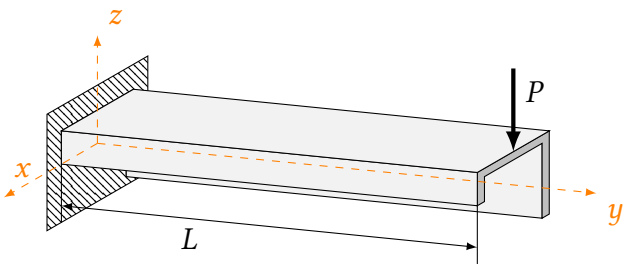

Figure 6.3.11: Unsymmetric C-section beam: geometrical features and load conditions

Fig.6.3.15 shows the equilibrium curve of the unsymmetric C-section cantilever beam in the range of small/moderate displacements, comparing solutions obtained by adopting different elements; the same comparison is made in fig.6.3.12 in the range of moderate/large displacement. As seen, solution are perfectly overlapping and actual numerical results obtained by 3D elements are validated. However, from a computational cost point of view, due to aspect ratio constraints on the definition of 3D mesh, the adoption of solid elements is again not convenient since the total number of degrees of freedom increases.

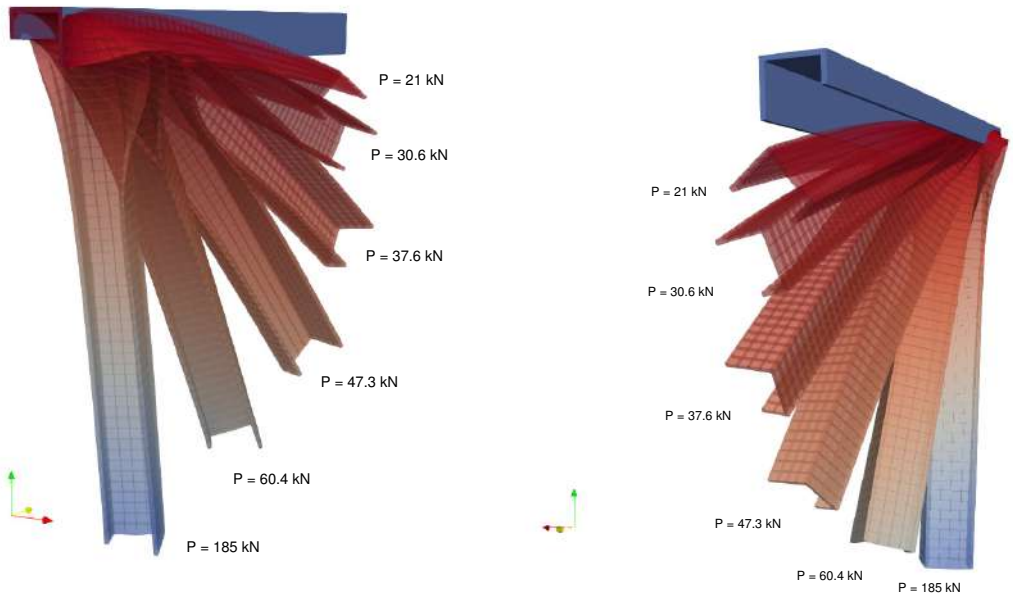

(a) Side view **(b)** Front view

Figure 6.3.12: Unsymmetric C-section beam: deformed configuration shapshots

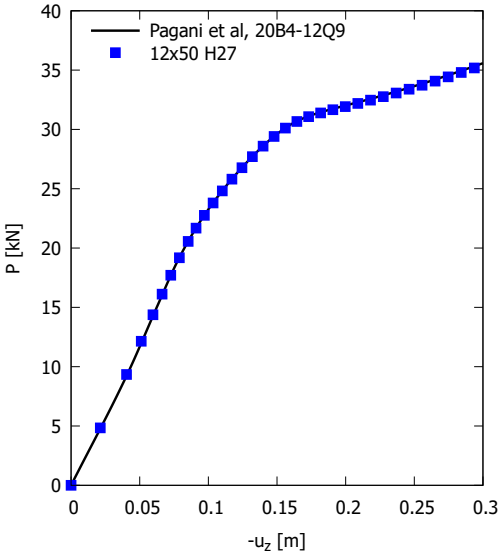

(a) u_z: small/moderate range

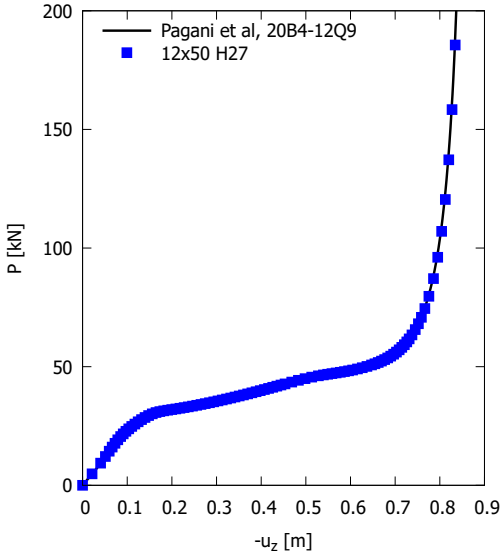

(b) u_z: moderate/large range

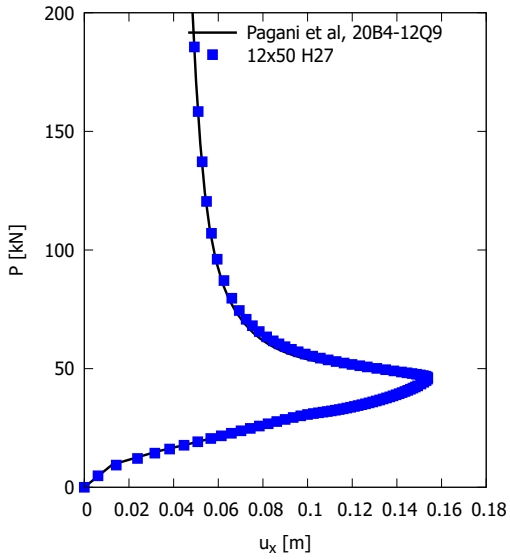

(c) u_x: moderate/large range

Figure 6.3.13: Unsymmetric C-section beam: equilibrium curves obtained with solid elements

6.3.5 L-shape angle-frame structure: 3D models results

Large deflections of an isotropic angle-frame structure are analyzed. This example is a popular benchmark problem in geometrically nonlinear analysis, proposed by Battini [14] and analyzed by Zouari *et al.*[15]: the frame is clamped at left end and subjected to an uniform distribution of horizontal forces at the top-right end. The mechanical properties are expressed in terms of Young's modulus and Poisson's ratio, respectively set to $E = 3 \cdot 10^{11}\ N/m^2$ and $\nu = 0.3$. The dimensions of the frame are $L = 0.1m$, $h = 0.01m$ and thickness $t = 0.01m$, as shown in fig.6.3.14(b). The structure has been discretized by adopting two different meshes: solutions are obtained employing 152 H8 linear in the first case, and 76 H27 parabolic in the second case, for geometrical and numerical reasons due to solid elements aspect ratio constraints.

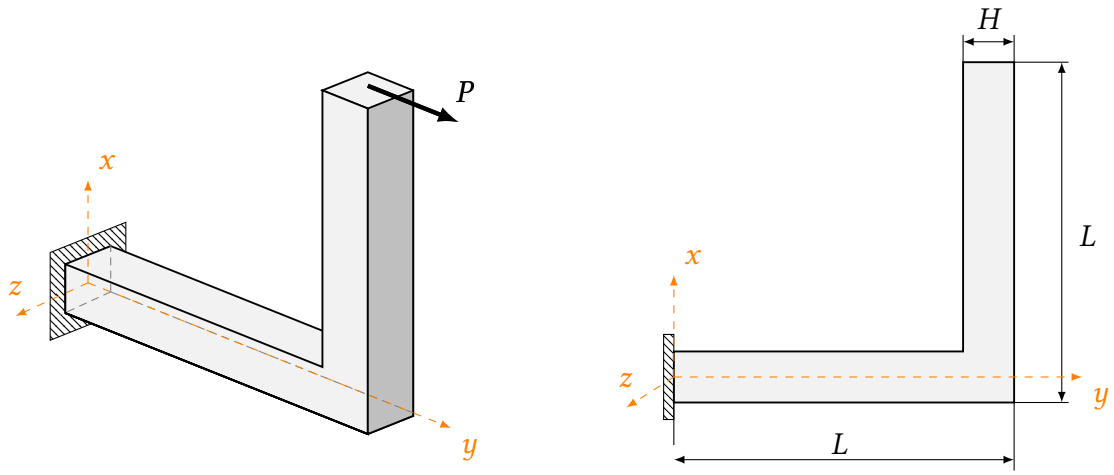

(a) Isometric view **(b)** Front view

Figure 6.3.14: L-shape angle-frame: geom. features and load condition

Fig.6.3.15 shows the equilibrium curve of the angle-frame in the range of moderate/large displacements, considering the horizontal displacement of the point A vs the horizontal pressure.
Fig.6.3.16 shows some snapshot of the deformed structure under the same load conditions, comparing the solution obtained with the different discretization adopted: as it is possible to see, for critical loads, the major effect of non-linearities are captured by parabolic elements, instead linear ones are not able to follow precisely the equilibrium path due to numerical limitations during the bending. This simple example shows immediately the limitations of a linear elements in the range of moderate/large displacements regime: locking correction of the solid elements by adopting more complex theories in the definition of the variational principle are intended to deal with this kind of problems, due to the fact that stiffness matrix is overestimated and the resulting displacement configuration results underestimated.

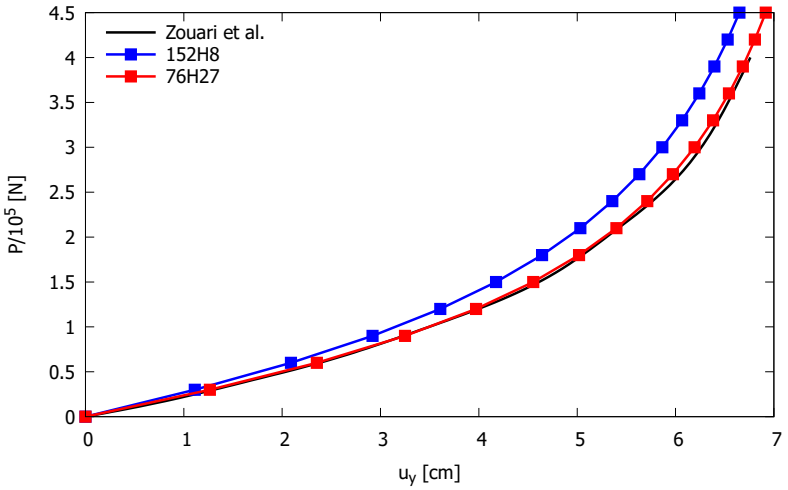

Figure 6.3.15: L-shape clamped angle-frame: equilibrium curves

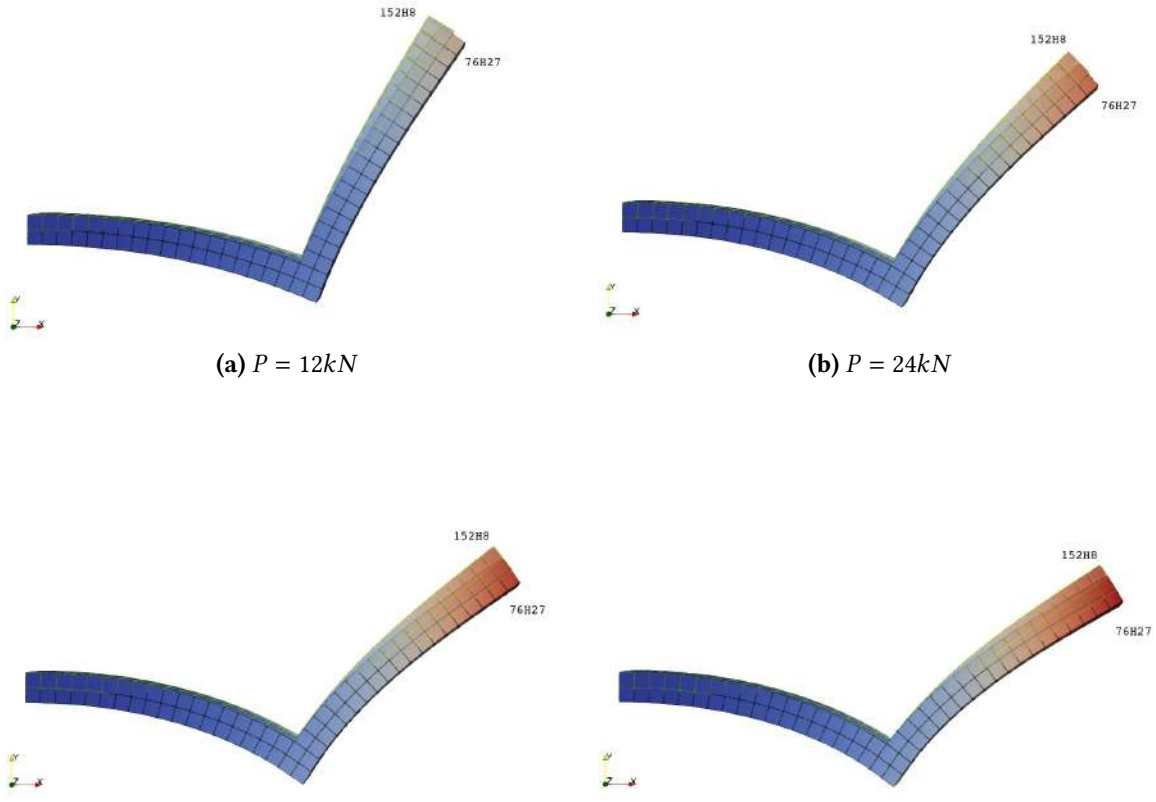

(a) $P = 12kN$ **(b)** $P = 24kN$

(c) $P = 33kN$ **(d)** $P = 45kN$

Figure 6.3.16: L-shape angle-frame: deformed configuration shapshots 76H27 vs 152H8

6.3.6 Symmetric thin shallow arch: 3D models results

Large deflections of a symmetric isotropic shallow arch are analyzed. This example is a popular benchmark problem for geometrically nonlinear analysis, proposed by Battini[14]: the frame is clamped at both ends and subjected to a concentrated vertical load $2P$ at the mid-span. Due to the symmetry of the problem, only half structure is analyzed. The mechanical properties are expressed in terms of Young's modulus and Poisson's ratio, respectively set to $E = 3 \cdot 10^{11}\ N/m^2$ and $\nu = 0.25$. The dimensions of the frame are $R_1 = 0.2m$, $d = 0.01m$ and thickness $t = 0.01m$, geometry is depicted in fig.6.3.17(b). The half-structure has been discretized by adopting 30H27 solid elements for geometrical and numerical reasons due to solid elements aspect ratio constraints.

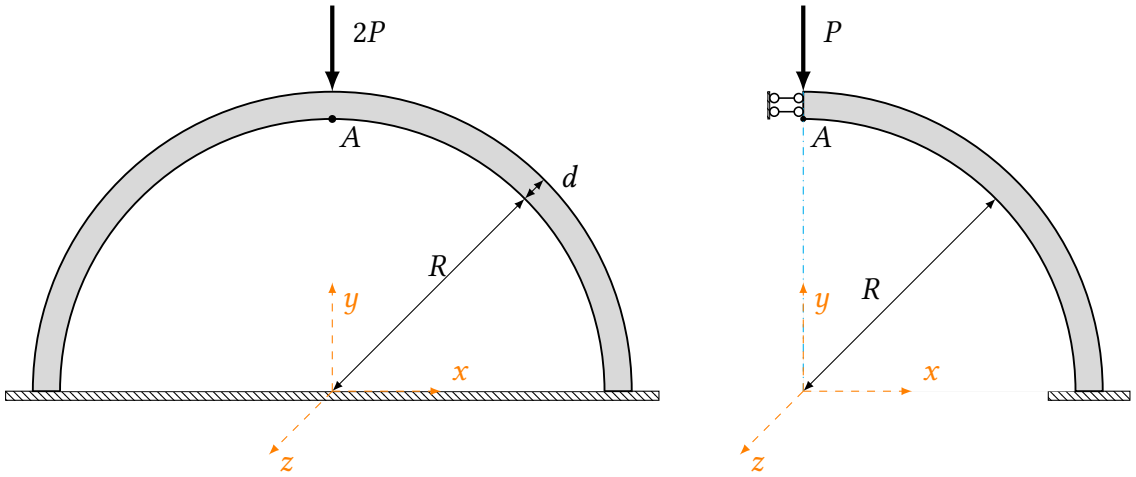

(a) Constraints and load conditions **(b)** Semi-half structure

Figure 6.3.17: Symmetric shallow arch: geometry and load conditions

Fig.6.3.18 shows the equilibrium curve of the symmetric shallow arch in the range of moderate/large displacements, considering the horizontal displacement of the point A vs the modulus of the vertical concentrated force.
Fig.6.3.19 shows some snapshot of the deformed structure under different load conditions. This interesting case proves the capabilities of the present implementation of linear-elastic solid elements dealing with curvilinear geometries: these kind of features can be useful in the analysis of curved structures, since one can avoid the definition of finite elements in curvilinear coordinates that requires much more mathematical and numerical efforts. Actually, the solution can be obtain by considering only an arc-lenght method for the solution of the nonlinear system of equation due to *snap-through* phenomenon, that one can observe from the actual numerical solution.

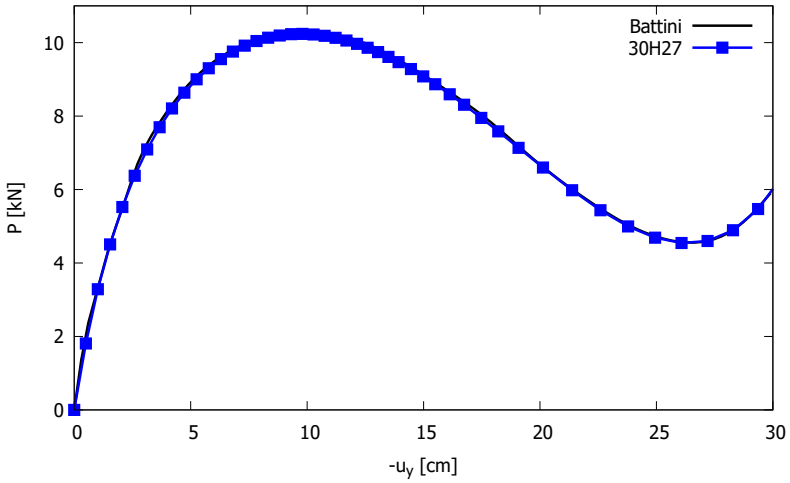

Figure 6.3.18: Symmetric shallow arch: equilibrium curve

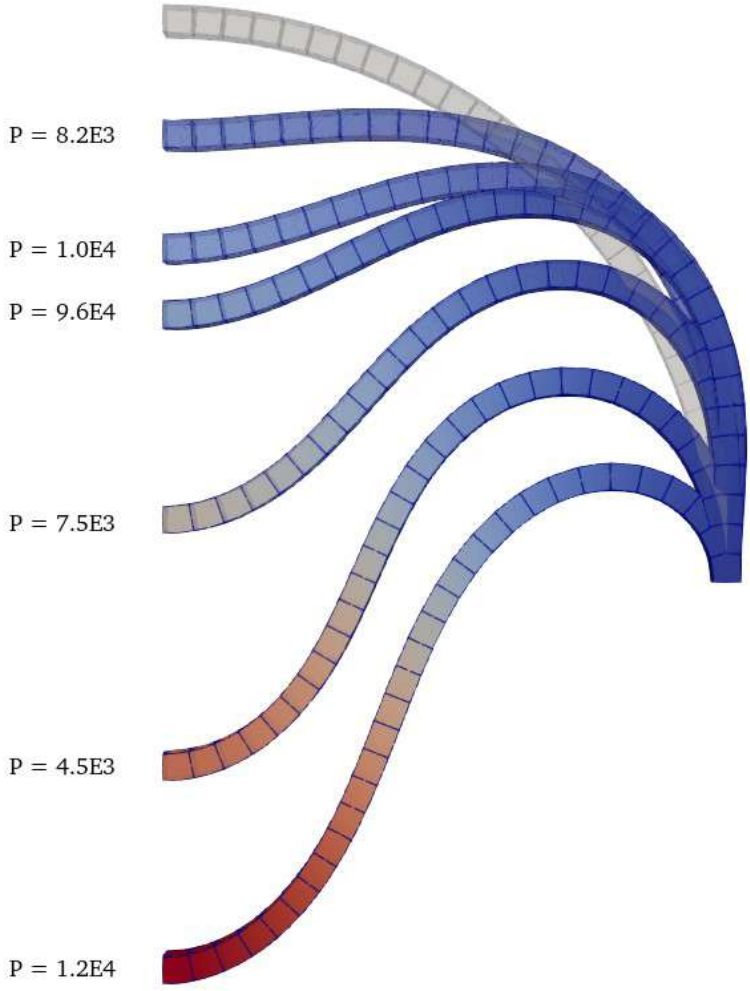

Figure 6.3.19: Symmetric shallow arch: deformed configuration shapshots

6.3.7 Cylindrical hinged panel: 3D models results

Large deflections of a symmetric isotropic cylindrical panel are analyzed. This example is a popular benchmark problem for geometrically nonlinear analysis, proposed by Sze *et al.*[12] and analyzed by Carrera *et al.*[11] and Payette *et al.*[18]: the panel is hinged at lateral straight edges and subjected to a concentrated vertical load P at the mid-span. Due to the symmetry of the problem, only a quarted of structure is analyzed. The mechanical properties are expressed in terms of Young's modulus and Poisson's ratio, respectively set to E=3.10275 GPa and $\nu = 0.3$. The dimensions of the panel are R=0.254 m, L=0.508 m but two different thickness values are considered: thin panel with h=12.7mm and thick panel with h=25.4 mm. Geometry is depicted in fig.6.3.17(b). The two structures has been discretized by adopting 200H27 solid elements in the case of thick plate, and 400H27 solid elements for geometrical and numerical reasons due to solid elements aspect ratio constraints.

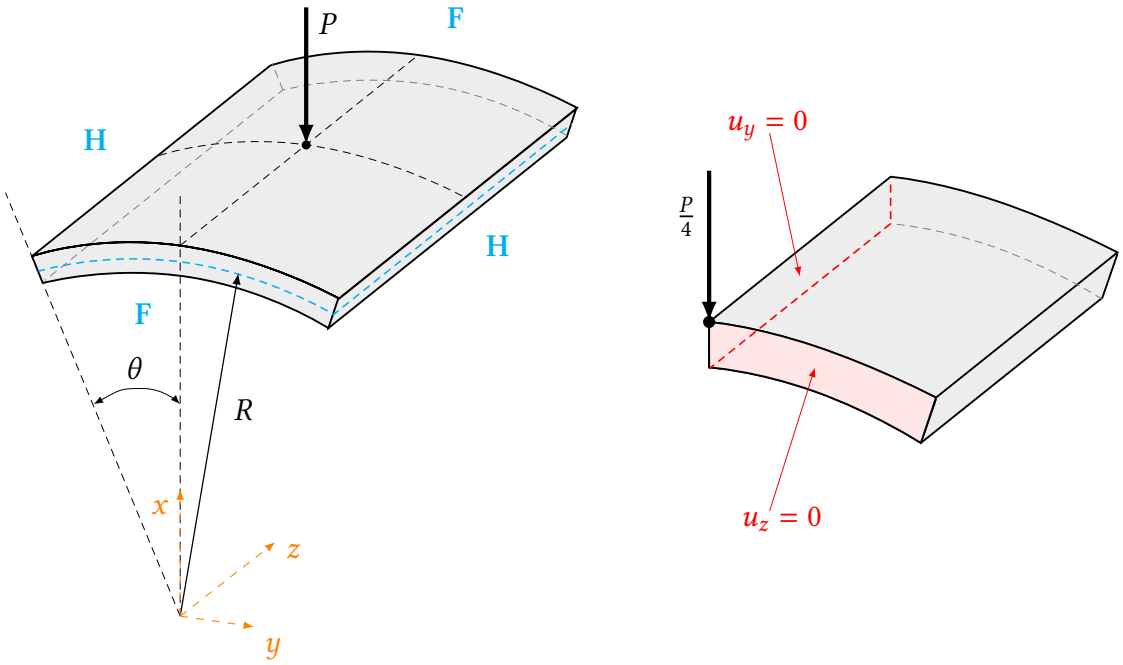

(a) Constraints and load conditions **(b)** Quarter of structure

Figure 6.3.20: Symmetric cylindrical panel: geometry and load conditions

Fig.6.3.21 shows the equilibrium curve of the hinged panel in the range of moderate/large displacements, considering the vertical displacement of the point A, u_{x_A}, with respect of the modulus of the vertical concentrated force.

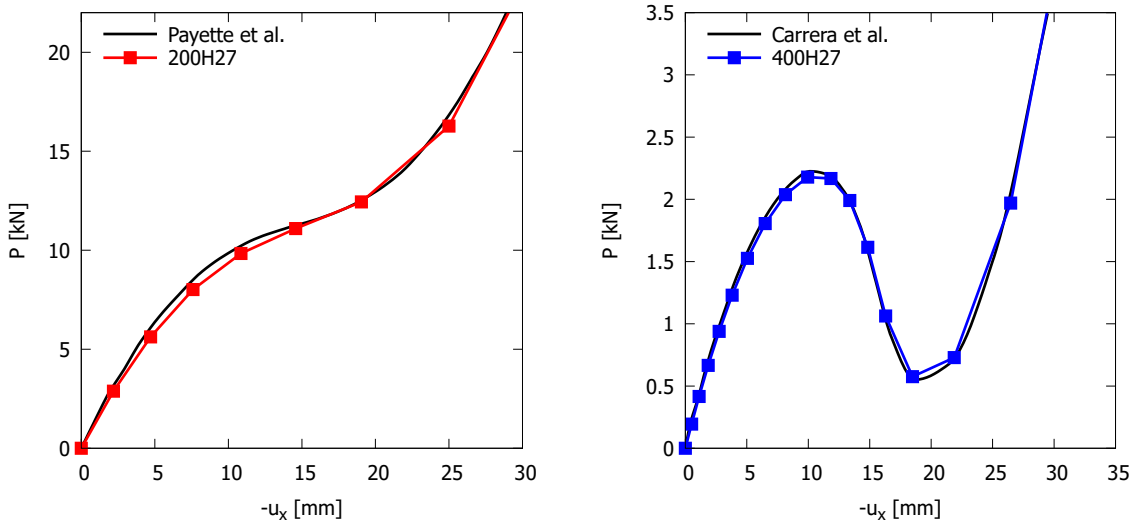

(a) $h = 25.4mm$ **(b)** $h = 12.7mm$

Figure 6.3.21: Cylindrical hinged plate: equilibrium curves

The whole equilibrium curves are correctly predicted, solution obtained with the present 3D model match the reference one: the present implementation of 3D solid elements is capable to predict the behaviour of the structure in all the regimes, small differences can be observed in the case of thick hinged panel.

6.3.8 Plate strip: 3D models results

Post-buckling analysis of an isotropic plate strip is now carried out. This example, proposed by Massin *et al.*[16] has also been studied by Arciniega *et al.*[17] and Payette *et al.*[18]: the frame is clamped at left end and subjected to an linear uniform compression load at the free end. The mechanical properties are expressed in terms of Young's modulus and Poisson's ratio, respectively set to $E = 2 \cdot 10^{11}\ N/m^2$ and $\nu = 0.3$. The dimensions of the frame are $L = 0.50m$, $h = 0.0045m$ and $w = 0.075m$, as shown in fig.6.3.22. The critical compression load applied at the free end is the Euler's buckling load, that can be computed analytically and equal to $P_{cr} = \pi^2 EI/(4L^2) = 1124.41N$ but, differently with respect of the reference case, it is applied on the top edge of the free cross-section, instead of its application at mid thickness span with a small inclination angle different from zero. The structure has been discretized by adopting 270 H27 parabolic, due geometrical and numerical reasons due to solid elements aspect ratio constraints.

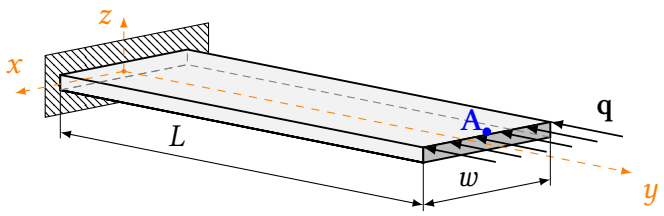

Figure 6.3.22: Plate strip post-buckling: geometrical features and load conditions

Fig.6.3.23(a) shows the equilibrium curves of the plate strip in the range of moderate/large displacements, considering both horizontal and vertical displacement of the point A vs the modulus of the vertical concentrated force, comparing reference solution from Arciniega *et al*[17] with the actual one obtained by solid elements-.
Fig.6.3.23(b) shows some snapshot of the deformed structure under different load conditions. This interesting case proves the capabilities of the present implementation of linear-elastic solid elements dealing with post-buckling analysis: the critical value of compression load that causes instability is evaluated correctly and the post-buckling behavior of the structure is followed.

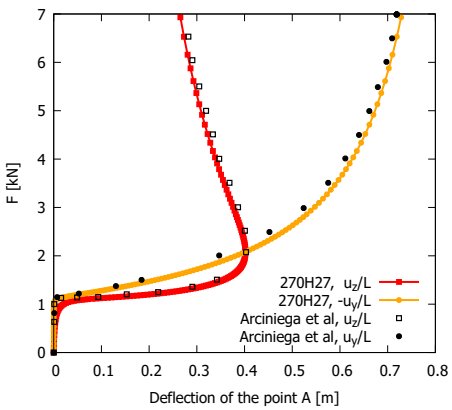

(a) Equilibrium curves

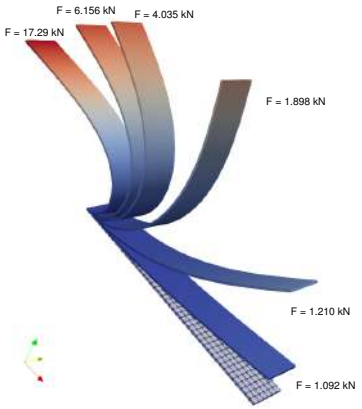

(b) Deformed configuration shapshots

Figure 6.3.23: Plate strip post-buckling: solid elements results

6.3.9 Square plates: comparison with 2D model results

Large deflection analyses of 2D plate are analyzed: consider again the same homogeneous isotropic square plate subjected to large deflection and the same boundary conditions already depicted in ch.6.2.1. For geometrical and numerical reason, 100H27 3D elements are employed for the discretization of the thick plate, instead for the thin plate 400 H27 elements are employed. In order to replicate the results, since for the 3D solid elements pressure boundary conditions is not implemented in the code, pressure is applied as an equivalent distribution of concentrated forces applied on top-surface nodes.

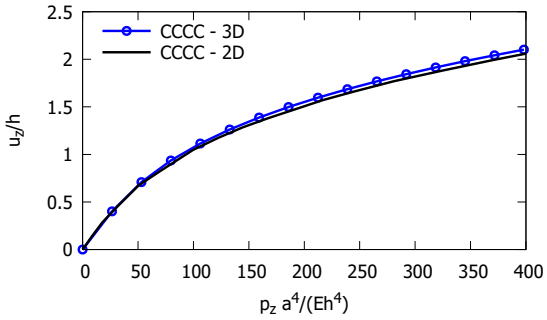

(a) $h/a = 0.1$: CCCC

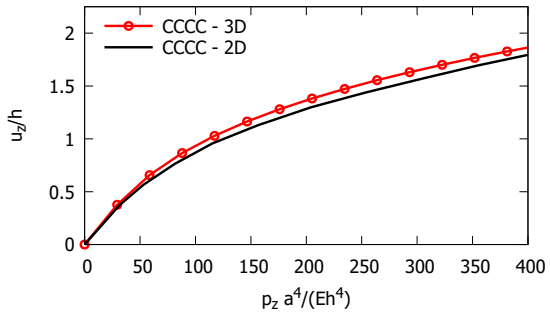

(b) $h/a = 0.02$: CCCC

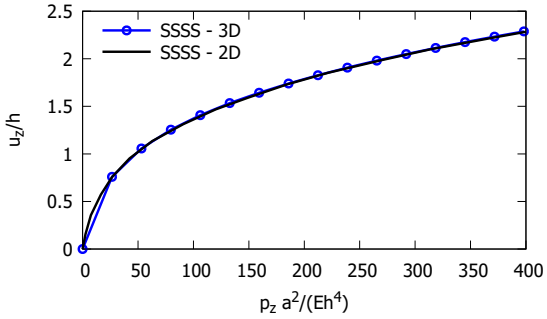

(c) $h/a = 0.1$: SSSS

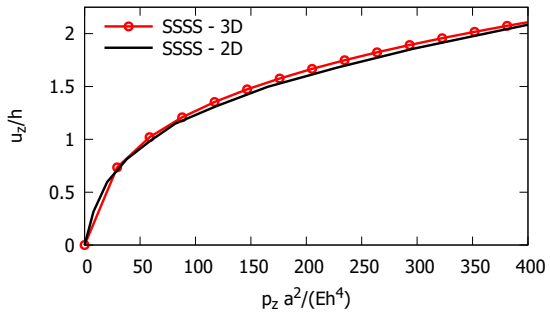

(d) $h/a = 0.02$: SSSS

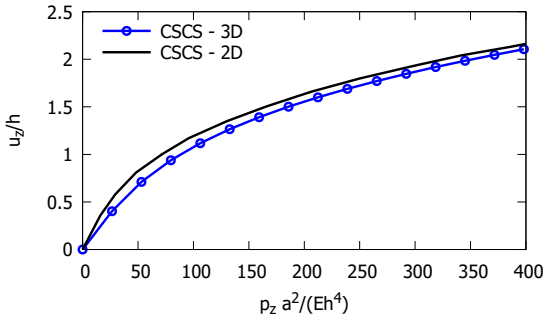

(e) $h/a = 0.1$: CSCS

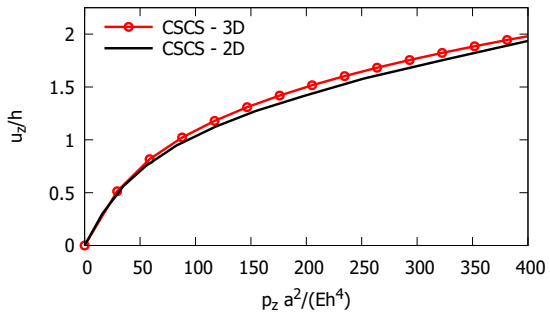

(f) $h/a = 0.02$: CSCS

Figure 6.3.24: Square plate, equilibrium curves: comparison between 2D and 3D model results

This popular study proves the capabilities of the present implementation of linear-elastic solid elements dealing with large deflection of plates but some inaccuracy can be observed depending on the thickness and the support conditions considered. Thus, investigations about boundary conditions influence on large deflections of squadre plates are now carried out: how derivatives at the boundaries influences solutions obtained by 3D models is now investigated, by considering different geometrical boundary conditions. The same square plate is now considered in two new configurations, characterized by different boundary conditions: clamped-free-clamped-free plate, simply supported-free and clamped plate supports conditions are analyzed, as depicted in fig.6.3.25, in other words now only two edges/faces of the plate are constrained. Load boundary conditions is the same of previous cases: pressure is applied on the top surface of the plate as an equivalent distribution of concentrated forces. The present implementation of solid elements can reproduce precisely the actual behavior of thin and thick structures:

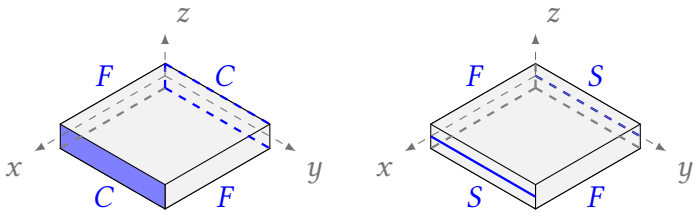

(a) CFCF **(b)** SFSF

Figure 6.3.25: Different edge support conditions: (a) CFCF, (b) SFSF

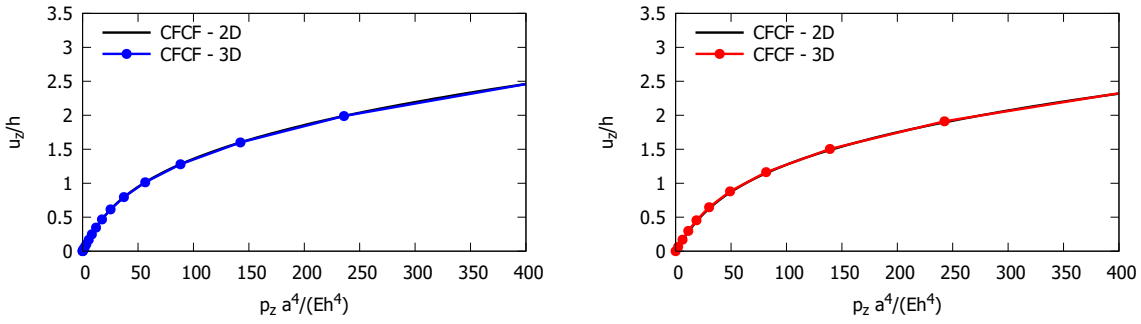

(a) $h/a = 0.1$: CFCF **(b)** $h/a = 0.02$: CFCF

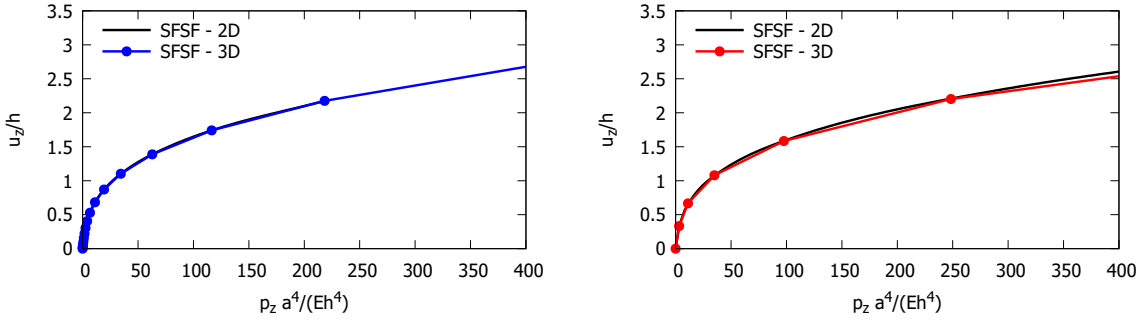

(c) $h/a = 0.1$: SFSF **(d)** $h/a = 0.02$: SFSF

Figure 6.3.26: Square plate, equilibrium curves: comparison between 2D and 3D model results

6.4 Hyperelastic 1D and 3D elements

6.4.1 Uniaxial tension problem: validation of the constitutive law

Large strains of an incompressible cubic block under uniaxial tension are now analyzed. This popular benchmark problem in hyperelasticity, analyzed by Pagani *et al.*[22] and Suchochi [19], is a special case for which analytical solution is known: in this study case, validation of the numerical solution obtained by the present implementation of hyperelastic finite elements is carried out, comparing results with analytic solutions. Geometry and boundary conditions are depicted in fig.6.4.1.

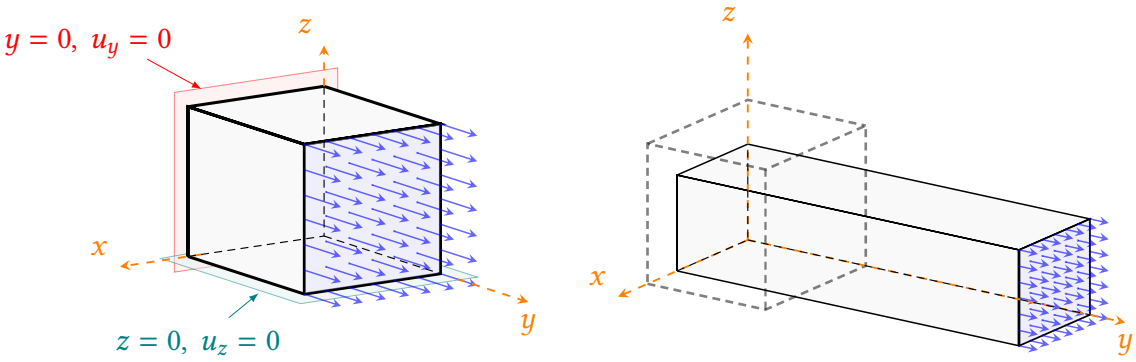

(a) Geometry and boundary conditions **(b)** Behavior of the cube

Figure 6.4.1: Uniaxial tension test: description of the problem

Considering first-invariant hyperelasticity model described before, explicit expression of deformation gradient in terms of eigenvalues is known, so analytic expression of PK1, PK2 and Cauchy's stress tensor are known. If λ_1 is the principal stretch along the y:

$$\lambda_{2,3} = \frac{1}{\sqrt{\lambda_1}} \quad \rightarrow \quad \bar{I}_1 = I_1 = \lambda_1^2 + \frac{2}{\lambda_1}$$

Given the expression of strain-energy function adopted, considering uniaxial tension, analytic expression of axial stress components are know, by definition:

$$P_{11} = \frac{\partial \Psi}{\partial \lambda_1} = \frac{\partial \Psi}{\partial I_1}\frac{\partial I_1}{\partial \lambda_1} = 2\frac{\partial \Psi}{\partial I_1}\left(\lambda_1 - \frac{1}{\lambda_1^2}\right)$$

$$S_{11} = \frac{1}{\partial \lambda_1}\frac{\partial \Psi}{\partial \lambda_1} = \frac{1}{\lambda_1}P_{11} \quad \rightarrow \quad \sigma_{11} = J^{-1}\lambda_1\frac{\partial \Psi}{\partial \lambda_1} = \lambda_1 P_{11}$$

Two different discretization are adopted in the following: in the case of 1D CUF-FEM elements, 1B2-1Q4 linear element is considered, instead in the case of 3D solid elements, the equivalent eight-node H8 finite elements is employed.
In this study case, four different strain-energy function are employed to show the capabilities of present formulation of hyperleastic CUF-FEM elements with respect of different strain energy function. Numerical constants and material parameter adopted in each strain energy function is listed in the table T.6.2. Again, analytic expression of strain energy functions adopted can be found in App.C.

Model	**Parameter**	
Neo-Hookean	$\mu = 0.27$	[MPa]
Gent	$\mu = 0.27$	[MPa]
	$J_m = 85.91$	-
Exp-Ln	$A = 0.195$	[MPa]
	$a = 0.018$	-
	$b = 0.22$	-
Fung-Demiray	$\beta = 0.2$	[MPa]
	$\alpha = 16$	-
Penalty par.	$D_1 = 33 \cdot 10^{-9}$	[MPa^{-1}]

Table 6.2: Material parameter adopted in each strain energy function considered

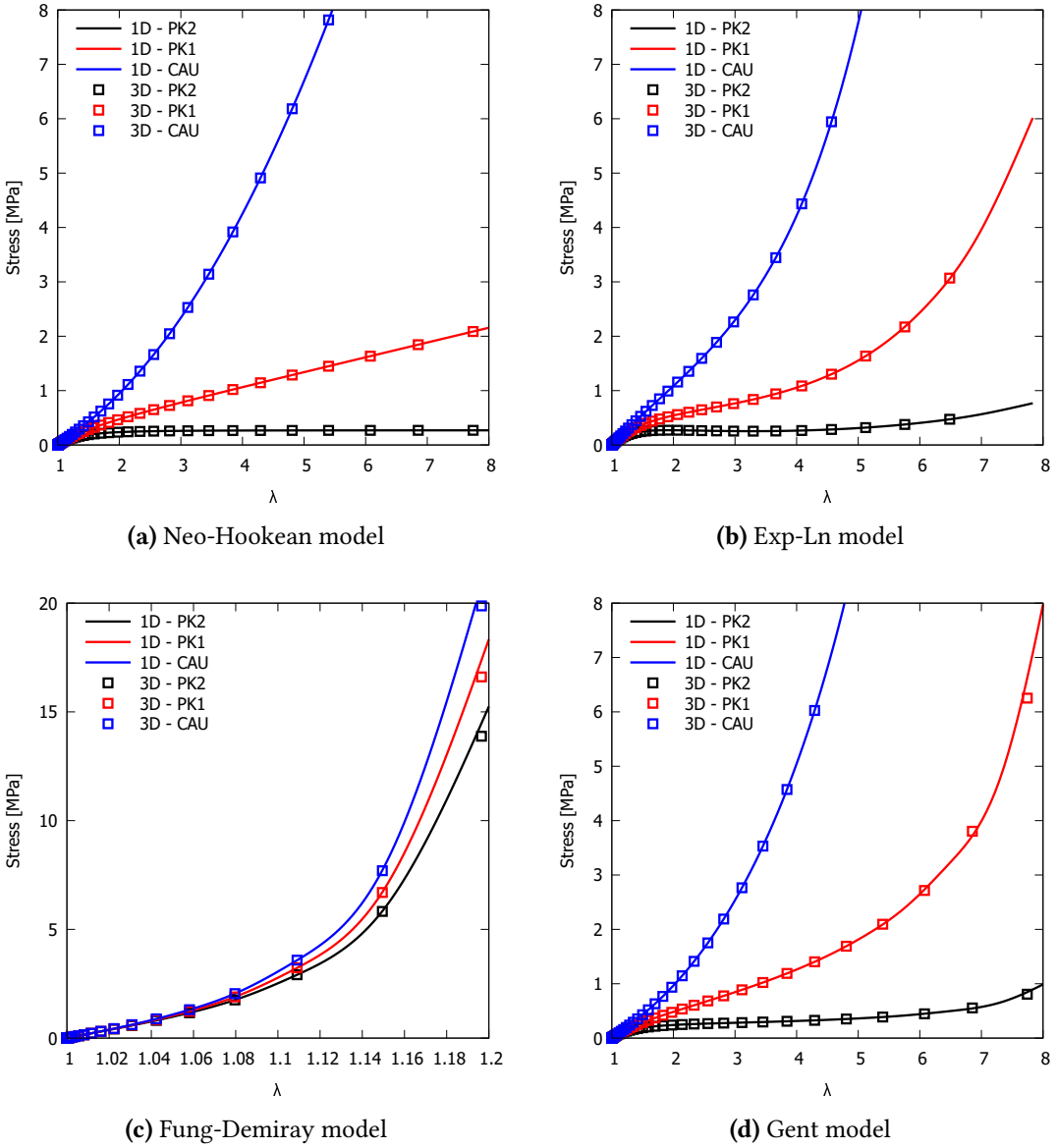

(a) Neo-Hookean model

(b) Exp-Ln model

(c) Fung-Demiray model

(d) Gent model

Figure 6.4.2: Uniaxial tension test: comparison between analytic, 1D and 3D CUF-FEM solutions

6.4.2 Neo-Hookean beam subjected to bending

Large displacement and large strains analysis of an hyperelastic cantilever beam subjected to shear load at the free end are now carried out. This study case has been analyzed by Maas *et at.*[26], and reference solutions are taken by Pagani *et al.*[22]. The cross-section of the cantilever beam is rectangular, whose side are respectively equal to t=100 mm and h=150 mm, and the length-to-thickness ratio has been set equal to 100, as shown in fig.6.4.3. The hyperleastic beam is modeled adopting a neo-Hooekan strain energy function with infinitesimal shear modulus μ = 50 MPa and bulk modulus $k = 2/3\mu$.

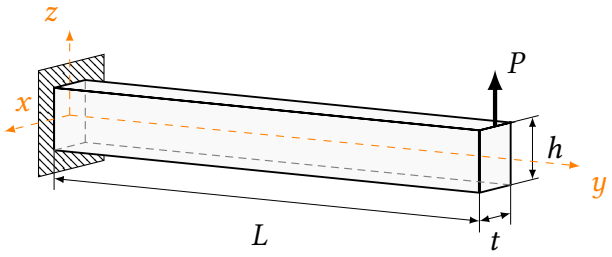

Figure 6.4.3: Hyperleastic neo-Hookean beam: geometrical features and load conditions

In the following, 20B4-1L16 are adopted in the discretization adopting 1D FEM-CUF elements; in the meanwhile, 120 H27 parabolic elements are adopted in the case of discretization by solid elements, obtained from 2 sub-division of the cross section along the z-axis of the thickness and 60 subdivision along the axis of the beam.
Fig.6.4.4 shows the equilibrium curve of the cantilever hyperelastic beam in the range of moderate/large displacements, considering the horizontal displacement of the point A vs the modulus of the vertical concentrated force, comparing the reference results with the one obtained adopting the H27 discretization described before. Results are matching.
Fig.6.4.5 and 6.4.6 show the through-the-thickness distribution of Piola-Kirchoff 2 normal and shear stress components, comparing results obtained by adopting 1D FEM-CUF elements with the one obtained by the present implementation of hyperelastic solid elements. In this case, the employment of parabolic solid elements is not sufficient for the description of the degenerate parabolic behavior captured only by adopting cubic expansion elements in the discretization of the cross section, like in 1D FEM-CUF elements, thus much more effort in mathematical 3D models are required.

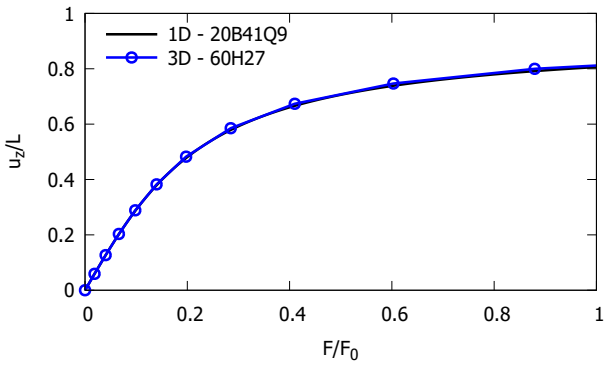

Figure 6.4.4: Hyperleastic neo-Hookean beam: equilibrium curve

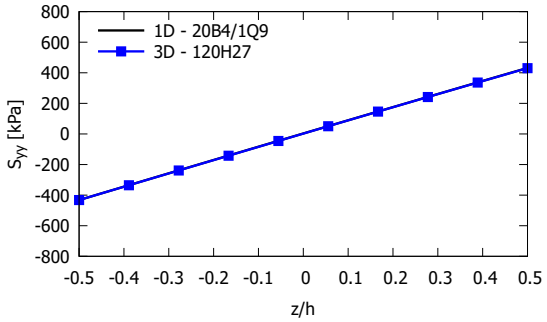

(a) $F/F_0 = 0.12$

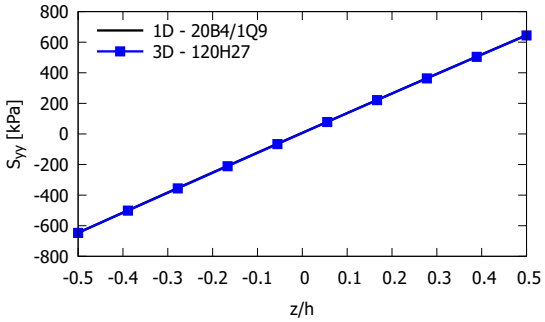

(b) $F/F_0 = 0.28$

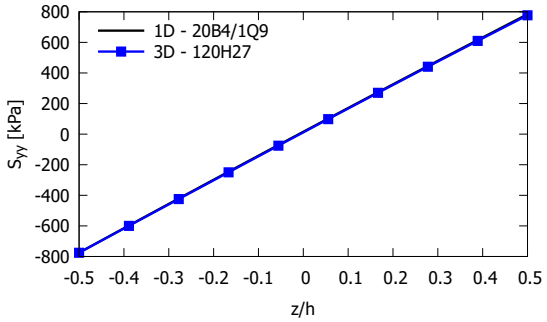

(c) $F/F_0 = 0.49$

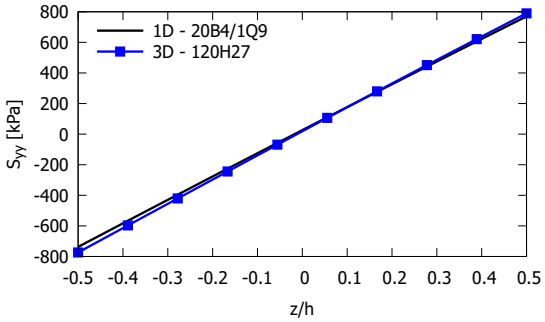

(d) $F/F_0 = 0.94$

Figure 6.4.5: Hyperleastic neo-Hookean beam: $PK2_{yy}$ through-the-thickness distribution

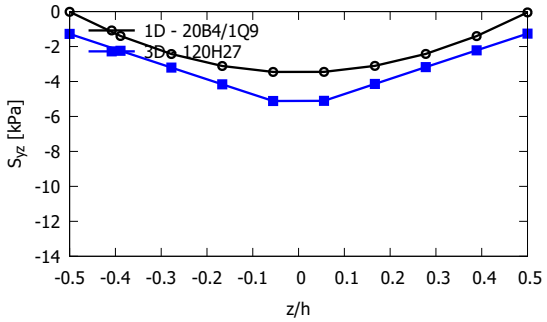

(a) $F/F_0 = 0.12$

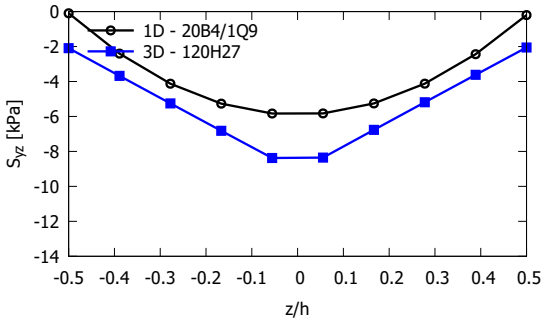

(b) $F/F_0 = 0.28$

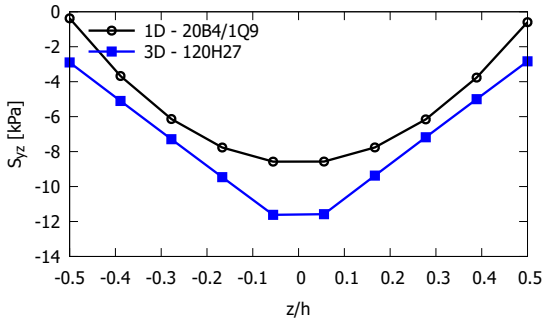

(c) $F/F_0 = 0.49$

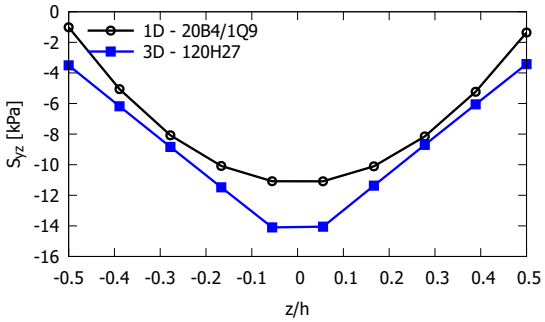

(d) $F/F_0 = 0.94$

Figure 6.4.6: Hyperleastic neo-Hookean beam: $PK2_{yz}$ through-the-thickness distribution

6.4.3 Nearly incompressible block under compression

Large displacement and large strains analysis of nearly incompressible block under uniform pressure is now carried out. This study case has been proposed by Reese *et al.*[25] and analyzed by many authors as in [22, 29, 28]. Geometrical features, boundary conditions and loads applied are depicted in fig.6.4.7. Thanks to symmetry, only one half of structure has been considered: symmetric Dirichlet boundary conditions have been applied on the lateral symmetric face, and a uniform vertical pressure is applied on the top free surface. Material is modeled adopting a neo-Hookean strain energy function, with bulk modulus k = 400′653.269 MPa and infinitesimal shear modulus fixed to μ = 80.194 MPa.

The block is a 2 *mm* x 2 *mm*, but in the case of symmetry geometry considered is an half block 1 *mm* x 2 *mm* and a fixed height of 1 *mm*. Analysis are carried out considering as reference solution Pagani *et al.*[22], adopting different discretization to compete with locking: in the following, each mesh will be named by the number of split of x,y and z base edges of the structures, that will identify the global number of parabolic elements adopted $N = N_x \cdot N_y \cdot N_z$, due to the cartesian structures of the discretization.

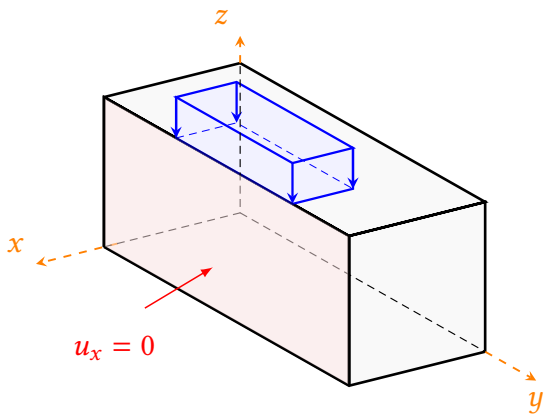

Figure 6.4.7: Geometry and boundary conditions for the uniaxial cube under uniform pressure

Solutions obtained by the present implementation of hyperleastic solid elements are affected by locking, as fig.6.4.8(a) and fig.6.4.8(b) show. In order to contrast locking phenomenon, one can consider different approach to hyperelasticity or more accurate evaluation of the hydrostatic pressure by computing it as a general variable of the problem and not as penalty parameter of the strain-energy function in first-invariant hyperelasticity formulation here adopted. In the case of 6x12x8 H27 mesh, the actual numerical results are able to follow the general path of the equilibrium curve, but much more meshing effort in the discretization of the structure are required.
In the following, for a more detailed analysis of locking phenomenon, only a quarter of structure is considered: the block is a 2 *mm* x 2 *mm*, in the case of symmetry, geometry considered is an quarter block 1 *mm* x 1 *mm* and a fixed height of 1 *mm*. Analysis are carried out considering different discretization to compete with locking: in the following, the nomenclature of the mesh follows the previous definition. By adopting only one quarter of structure, one can increase the global number of elements describing the structure, with a comparable computational cost.

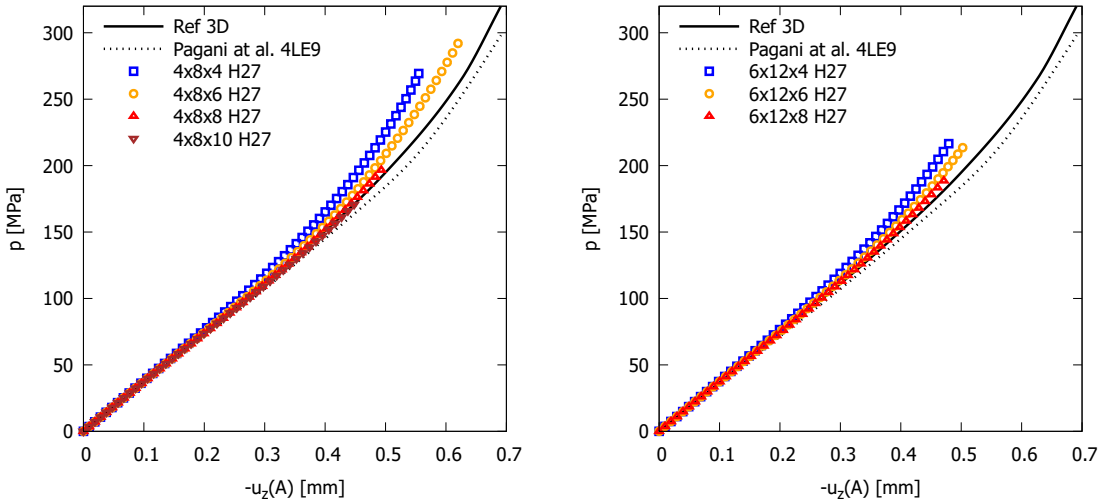

(a) 4x8 discretization of the base **(b)** 6x12 discretization of the base

Figure 6.4.8: Neo-Hookean block, half structure: equilibrium curves

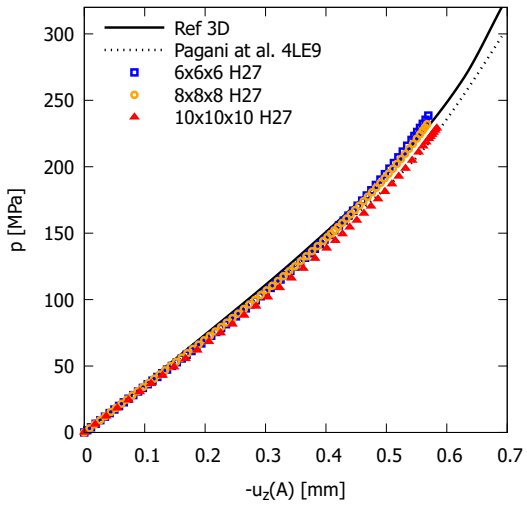

Figure 6.4.9: Neo-Hookean block, quarter of structure: equilibrium curve

In this study case, locking prevents the computation of the whole equilibrium curve: there are local effects that do not allow the complete description of the behavior of the structure. This can be justified by the fact that, in the present implementation, the *hydrostatic pressure* is a penalty variable and is not computed as an unknown of the problem. Enhanced volumetric locking prevent the computation of accurate solution: thus, much more research effort are required. Mixed formulation from a variational principle point of view and computation the hydrostatic pressure as a general variable of the problem can compete with volumetric locking.

6.4.4 Neo-Hookean hyperelastic cylinder

Large displacement and large strains analysis of neo-Hookean thick cylinder under vertical linear pressure is now carried out. This study case has been proposed and analyzed by different researchers adopting brick/shell finite elements, as done in [25, 29, 28]. Referring to the description of the problem in Pagani *et al.*[22], only a quarter of cylinder is analyzed by symmetries: the lower edge of the structures is hinged, uniform vertical pressure is applied on the top free edge and Dirichlet symmetry boundary conditions are considered at planes x=0 and y=0.
The length of the quarter of cylinder is $L = 15\ cm$, and the inner and outer radius are respectively $R_1 = 8\ cm$ and $R_2 = 10\ cm$, resulting in a global thickness of the cylinder of 2 cm. The hyperleastic cylinder is modeled adopting a neo-Hooekan strain energy function with bulk modulus $k = 280'000$ kN/cm^2 and infinitesimal shear modulus $\mu = 6000$ kN/cm^2.
This analysis are carried out considering first 1D CUF elements then 3D FEM elements, to validate the actual implementation of hyperelastic higher-order beam models and acutal implementation of solid elements: in the case of 1D CUF elements, one cubic element B4 has been adopted along the axis of the cylinder and cubic L16 elements are used in the discretization of the cross section; in the case of 3D elements, the cross section has been described splitting into 16 portion the whole cross section arch in the first case, in the second case by splitting into 2 portions along the radial direction and in 20 equal portions along the arch span. Different number of splits along the axis of the cylinder have been considered.

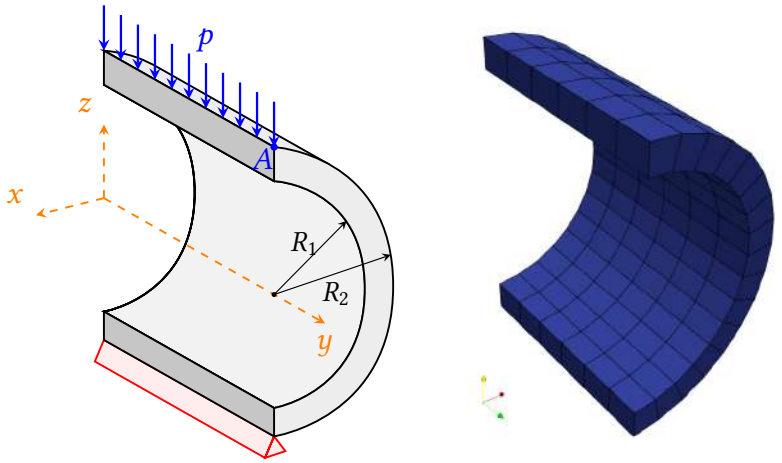

(a) Geometry and boundary conditions

(b) Discretization adopted: 16x6 H27

Figure 6.4.10: Neo-Hookean cylinder: quarter of structures features

Fig.6.4.11 shows the equilibrium curve obtained by each discretization adopted: locking prevent the evaluation of the real behavior adopting a limited number of elements.
Fig.6.4.12 shows some snapshots of deformed configuration for load value of linear pressure applied at the top free edge.
After the analysis, solutions obtained by the present implementation of hyperleastic solid elements, in the case of curvilinear structures, are affected by locking: thus, much more meshing effort in the discretization of the structure are required, adopting an higher number of elements satisfying aspect ratio constraints, in a resulting increasing computational

cost. In the case of 40x10 H27 mesh, the actual numerical results are able to follow the general path of the equilibrium curve.

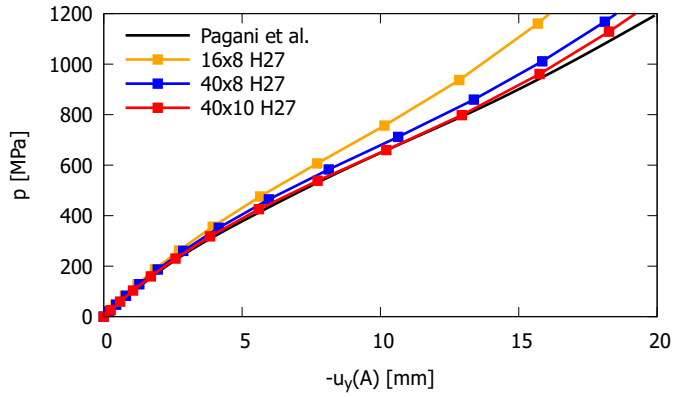

Figure 6.4.11: Neo-Hookean cylinder: equilibrium curve

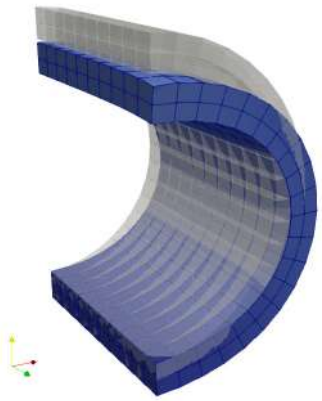

(a) $p = 230\ kN/cm^2$

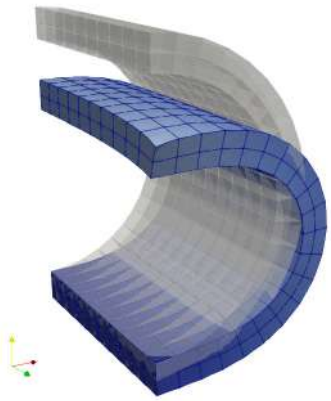

(b) $p = 426\ kN/cm^2$

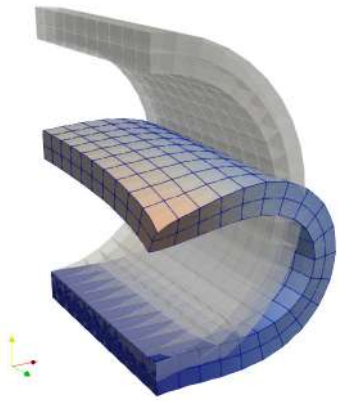

(c) $p = 660\ kN/cm^2$

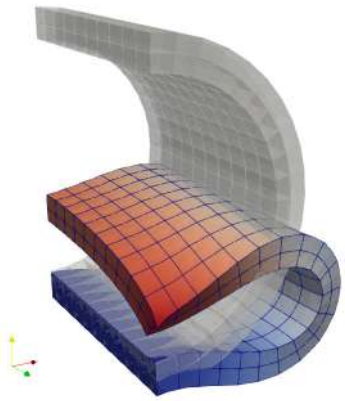

(d) $p = 961\ kN/cm^2$

Figure 6.4.12: Neo-Hookean cylinder: deformed configuration for different load conditions

Chapter 7

Conclusions

In the present thesis, geometrical nonlinear analyses based on linear elasticity and hyperelasticity have been presented. As already said, CUF allows the implementation of higher-order theories for beams, plates, shells and solid structure, where the full Green-Lagrange strain tensor is considered. Starting from the definition, beam (1D) models and plate (2D) models have been presented and adopted for the analysis of popular study cases, and finally isogeometric solid (3D) models have been built and adopted for research study cases.

Actual implementation of solid elements has been validated by studying popular problems in non-linear analysis described in literature and adopted for research study cases: large-deflection of beams and plates and post-buckling of simple structures, and large strains of hyperelastic soft structures have been analyzed. During the work, 3D models have been validated in very different cases, showing both the capabilities and the limitations arising from the adoption of classical FEM models instead of higher-order ones.

Starting from the linear-elastic constitutive law, only isotropic materials have been considered. Study cases with very simple Cartesian geometries and curvilinear symmetrical geometries have been analyzed: in all the cases, behavior of structures in the moderate/large displacement regime can be predicted, and these results validate the present implementation of geometrically non-linear solid finite elements. Specifically, in the case of large displacement regime, an accurate prediction of the stress state is obtained only by refined discretization of structures, due to mathematical limitation of the actual models.

The adoption of the solid elements in the case of hyperelastic materials has shown very important results in terms of large strains analysis of structures: the actual implementation of the MUL2 code is able to compete with different cases but convergent results are not easily obtained. An accurate description of displacements, strains and stresses have been reached but in all the cases locking phenomenon is observed: adopting refined discretization of geometries and by increasing the number of elements, solution can be obtained.

All the results, although the mathematical limitation already discussed, prove that implementation of parabolic solid elements used in this thesis is able to predict the actual behavior of materials and structures, also by considering different constitutive laws. Complex structures and innovative soft materials can be analyzed by this formulation of finite elements obtaining accurate results.

From a computational point of view, one important aspect have been remarked in this the-

sis: the adoption of 3D FEM elements require much more computational costs with respect of refined fully-nonlinear CUF elements: they are not convenient with respect of refined higher-order 1D or 2D models and show the classical known limitations in Finite Element Method, even if they are required in hyperelasticity to compete better with locking.

7.1 Future works

The present work is the first step in understanding complex structural problem also involving geometrical an material non-linearities. However, in this context, several aspects require further research efforts. Possible future works include fracture mechanics, nonlinear vibrations, fluid-structure interaction applications: several future developments can be considered starting from these encouraging results.
Regarding the structural models adopted for hyperelastic materials, the adoption of a mixed formulation (from a variational principle point of view) is the starting point for severe correction of the locking phenomenon. In addition, the computation of the hydrostatic pressure as a general variable of the problem is required for much more accurate large strains analysis of hyperleastic materials. Another goal that is intended to be achieved is the description of hyperelastic materials adopting more complex strain-energy function like models considering also second invariant of Cauchy-Green strain tensor, to overcoming the current limitations of the classic first-invariant formulation.
Finally, a major future development is the coupling between CUF-based finite elements with the in-house code of Fluid Dynamics research group of Polytechnic University of Bari for fluid-structure interaction problem: under the IB (Immersed Boundary) method, one of the most anticipated developments is the coupling of the two codes for the development of fluid-structure interaction solver for aerospace, mechanical engineering applications. The currently adopted structural solver based on isogeometric Kirchoff-Love shell models for hyperelastic material lead to limitations that can be exceeded by adopting higher-order CUF models described in this work or mixed solid elements.

Bibliography

[1] E. Carrera, M. Cinefra, M. Petrolo and E. Zappino, *Finite Element Analysis of Structures through Unified Formulation*, John Wiley & Sons, Chichester, UK, 2014.

[2] K.J. Bathe, *Finite Element Procedures*, Prentice Halle, Upper Saddle River, NJ, 1996.

[3] M.A. Crisfield, *Non-Linear Finite Element Analysis of Solid and Structures*, John Wiley & Sons, Chichester, England, 1991.

[4] J.N. Reddy, *An Introduction to Nonlinear Finite Element Analysis: With Applications to Heat Transfer, fluid Mechanics, and Solid Mechanics*, Oxford University Press, Oxford, UK, 2014.

[5] G.A. Holzapfel, *Nonlinear Solid Mechanics: A Continuum Approach for Engineering*, John Wiley & Sons, Chichester, England, 2000.

[6] A. Sollazzo, S. Marzano, *Elementi di meccanica dei continui e resistenza dei materiali*, Unione Tipografico-Editrice Torinese, 1998.

[7] L. Corradi Dell'Acqua, *Meccanica delle Strutture. Il comportamento dei mezzi continui*, Mc Graw-Hill Libri Italia S.r.l., 1992.

[8] M. A. Crisfield, *A fast incremental/iterative solution procedure that handles "snap-through"*, Comput. Struct., vol. 13, no. 1-3, pp. 55–62, 1981. DOI: 10.1016/0045-7949(81)90108-5.

[9] M. A. Crisfield, *An arc-length method including line searches and accelerations*, Int. J. Numer. Meth. Eng., vol. 19, no. 9, pp.1269–1289, 1983. DOI: 10.1002/nme.1620190902.

[10] A. Pagani, E. Carrera, *Unified formulation of geomtrically nonlinear refined beam theories*, Mechanics of Advanced Materials and Structures, 25:1, 15-31, DOI:10.1080/15376494.2016.1232458.

[11] E. Carrera, A. Pagani, R. Augello & B. Wu (2020), *Popular benchmarks of nonlinear shell analysis solved by 1D and 2D CUF-based finite elements*, Mechanics of Advanced Materials and Structures, 25:1, 15-31, DOI:10.1080/15376494.2020.1728450

[12] K.Y. Sze, X.H. Liu, S.H. Lo, *Popular benchmark problems for geometric nonlinear analysis of shells*, Finite Elements in Analysis and Design, 40 (2004), 1551-1569.

[13] B. Wu, A. Pagani, M. Filippi, W.Q. Chen, E. Carrera, *Large deflection and post-buckling analyses of isotropic rectangular plates by Carrera Unified Formulation*, International Journal of Non-Linear Mechanics, 166 (2019), 18-31.

[14] J-M. Battini, *A non-linear corotational 4-node plane elements*, Mechanics Research Communications 35 (2008), 408-413.

[15] W. Zouari, F. Hammadi, R. Ayad, *Quatrilateral membrane finite elements with rotational DOFs for the analysis of geometrically linear and nonlinear plane problems*, Computers and Structures 173 (2016), 139-149.

[16] P. Massin, M. Al Mikdad, *Nine node and seven node thick shell elements with large displacements and rotations*, Computers and Structures 80 (2002), 835-847.

[17] R.A. Arciniega, J.N. Reddy, *Tensor-based finite element formulation for geometrically nonlinear analysis of shell structures*, Comput. Methods Appl. Mech. Engrg. 196 (2007), 1048-1073.

[18] G.S. Payette, J.N. Reddy, *A seven-parameter spectral/hp finite element formulation for isotropic, laminated composite and functionally graded shell structures*, Comput. Methods Appl. Mech. Engrg. 278 (2014), 664-704.

[19] C. Suchocki, *Finite element implementation of slightly compressible and incompressible first invariant-based hyperelasticity: Theory, coding, exemplary problems*, Jtam., vol. 55, pp. 787, 2017. DOI: 10.15632/jtam-pl.55.3.787.

[20] C. Suchocki, *A finite element implementation of Knowles stored-energy function: Theory, coding and applications*, Arch. Mech. Eng., vol. 58, no. 3, pp. 319–346, 2011, DOI:10.2478/v10180-011-0021-7.

[21] P. Flory, *Thermodynamic relations for high elastic materials*, Trans. Faraday Soc., vol. 57, pp. 829–838, 1961. DOI: 10.1039/tf9615700829.

[22] A. Pagani, E. Carrera , *Unified one-dimensional finite element for the analysis of hyperelastic soft materials and structures*, Mechanics of Advanced Materials and Structures, 2021, DOI: 10.1080/15376494.2021.2013585.

[23] L. A. Lubbers, M. van Hecke, and C. Coulais, *A nonlinear beam model to describe the postbuckling of wide neo-hookean beams*, J. Mech. Phys. Solids, vol. 106, pp. 191–206, 2017, DOI: 10.1016/j.jmps.2017.06.001.

[24] T. Sussman, and K.-J. Bathe, *A finite element formulation for nonlinear incompressible elastic and inelastic analysis*, Comput.Struct., vol. 26, no. 1-2, pp. 357–409, 1987. DOI: 10.1016/0045-7949(87)90265-3.

[25] S. Reese, P. Wriggers, B. D. Reddy, *A new locking-free brick element formulation for continuous large deformation problems*, Computational Mechanics, New Trends and Applications, Proceedings of the Fourth World Congress on Computational Mechanics WCCM IV Buenos Aires, CIMNE (Centro Internacional de Métodes Numéericos in Enginerìa), Barcelona, 1998.

[26] S. A. Maas, B. J. Ellis, G. A. Ateshian, J. A. Weiss, *FEBio: Finite elements for biomechanics*, J. Biomech. Eng., vol. 134, no. 1, pp. 011005, 2012.

[27] Elguedj, Y. Bazilevs, V. M. Calo, T. J. R. Hughes, *$\bar{B}$ and $\bar{F}$ projection methods for nearly incompressible linear and nonlinear elasticity and plasticity using higher-order nurbs elements*, Comput. Methods Appl. Mech. Eng., vol. 197, no. 33-40, pp. 2732–2762, 2008.

[28] A. Masud, T. J. Truster, *A framework for residual-based stabilization of incompressible finite elasticity: Stabilized formulations and f methods for linear triangles and tetrahedra*, Comput. Methods Appl. Mech. Eng., vol. 267, pp. 359–399, 2013. DOI: 10.1016/j.cma.2013.08.010.

[29] N. Buchter, E. Ramm, and D. Roehl, *Three-dimensional extension of non-linear shell formulation based on the enhanced assumed strain concept*, Int. J. Numer. Meth. Eng., vol. 37, no.15, pp.2551–2568, 1994. DOI: 10.1002/nme.1620371504.

Appendix A

Explicit form of secant and tangent stiffness matrices

According to Carrera *et al.* [10] and [13], the fundamental nucleus of the stiffness matrix can be defined by using only two independent components without loss of generality. By exploting the summation over indeces τ, s, i, and j, used in the definition of real and virtual displacement field FEM-CUF discretization, derivation of all the nine components of each nucleus sub-matrices is straightforward. In the following, each volume integral over the whole domain will be expressed with the symbol $< (\cdot) >= \int_\Omega (\cdot) dV$, and, in order to write expressions in a more compact and general way, $\mathbf{u}_{,x}[r]$ represents the r-th component of the vector $\dfrac{\partial \mathbf{u}}{\partial x}$; e.g. $\mathbf{u}_{,x}[2] = u_{y,x}$.

A.1 Fundamental nuclei of 1D CUF elements

In the particular case of 1D beam CUF elements described in ch. 3.2.1, fundamental nuclei explicit expression of sub-matrices are carried out by adopting formal differential operator matrices eq.(3.2.3) and eq.(3.2.4) in eq.(4.1.5). Since the derivation is independent on the elasticity tensor $\mathbb{C}$, expressions of fundamental nuclei are now derived for an isotropic material, considering then the expression eq.(3.1.7).

The linear contribution fundamental nucleus is obtained by considering the volume integral of the following row-by-coloumn matrix product:

$$\mathbf{K}_{ll}^{\tau s i j} = \int_\Omega \mathbf{B_l^{sj}}^T \, \mathbb{C} \, \mathbf{B_l^{\tau i}} dV \tag{A.1.1}$$

The nine components of the 3×3 linear stiffness matrix fundamental nucleus of the are provided below in the form $\mathbf{K}_{ll}^{ij\tau s}[r, c]$, where r is the row number ($r = 1, 2, 3$) and c is the column number ($c = 1, 2, 3$).

$$\begin{aligned} \mathbf{K}_{ll}^{ij\tau s}[1,1] &= < C_{11} F_{\tau,x} F_{s,x} N_i N_j > + < C_{44} F_{\tau,z} F_{s,z} N_i N_j > \\ &+ < C_{66} F_\tau F_s N_{i,y} N_{j,y} > \end{aligned}$$

$$\mathbf{K}_{ll}^{ij\tau s}[1,2] = < C_{66} F_\tau F_{s,x} N_{i,y} N_j > + < C_{12} F_{\tau,x} F_s N_i N_{j,y} >$$

$$
\begin{aligned}
\mathbf{K}_{ll}^{ij\tau s}[1,3] &= < C_{13}\, F_{\tau,x}\, F_{s,z}\, N_i\, N_j > + < C_{44}\, F_{\tau,z}\, F_{s,x}\, N_i\, N_j > \\
\mathbf{K}_{ll}^{ij\tau s}[2,1] &= < C_{12}\, F_{\tau}\, F_{s,x}\, N_{i,y}\, N_j > + < C_{66}\, F_{\tau,x}\, F_{s}\, N_i\, N_{j,y} > \\
\mathbf{K}_{ll}^{ij\tau s}[2,2] &= < C_{66}\, F_{\tau,x}\, F_{s,x}\, N_i\, N_j > + < C_{55}\, F_{\tau,z}\, F_{s,z}\, N_i\, N_j > \\
&+ < C_{22}\, F_{\tau}\, F_{s}\, N_{i,y}\, N_{j,y} > \\
\mathbf{K}_{ll}^{ij\tau s}[2,3] &= < C_{23}\, F_{\tau}\, F_{s,z}\, N_{i,y}\, N_j > + < C_{55}\, F_{\tau,z}\, F_{s}\, N_i\, N_{j,y} > \\
\mathbf{K}_{ll}^{ij\tau s}[3,1] &= < C_{44}\, F_{\tau,x}\, F_{s,z}\, N_i\, N_j > + < C_{13}\, F_{\tau,z}\, F_{s,x}\, N_i\, N_j > \\
\mathbf{K}_{ll}^{ij\tau s}[3,2] &= < C_{55}\, F_{\tau}\, F_{s,z}\, N_{i,y}\, N_j > + < C_{23}\, F_{\tau,z}\, F_{s}\, N_i\, N_{j,y} > \\
\mathbf{K}_{ll}^{ij\tau s}[3,3] &= < C_{44}\, F_{\tau,x}\, F_{s,x}\, N_i\, N_j > + < C_{33}\, F_{\tau,z}\, F_{s,z}\, N_i\, N_j > \\
&+ < C_{55}\, F_{\tau}\, F_{s}\, N_{i,y}\, N_{j,y} >
\end{aligned}
$$

The first-order nonlinear contribution fundamental nucleus is obtained by considering the volume integral of the following row-by-coloumn matrix product:

$$
\mathbf{K}_{lnl}^{\tau sij} = \int_{\Omega} \mathbf{B}_{\mathbf{l}}^{\mathbf{sj}\,T}\, \mathbb{C}\, \mathbf{B}_{\mathbf{nl}}^{\tau\mathbf{i}} dV \tag{A.1.2}
$$

The nine components of the 3×3 nonlinear stiffness matrix fundamental nucleus of the are provided below in the form $\mathbf{K}_{nll}^{ij\tau s}[r,c]$, where r is the row number ($r = 1,2,3$) and c is the column number ($c = 1,2,3$):

For $c = 1$:

$$
\begin{aligned}
\mathbf{K}_{nll}^{ij\tau s}[r,c] &= < \mathbf{u}_{,x}[r]\, C_{11}\, F_{\tau,x}\, F_{s,x}\, N_i\, N_j > + < \mathbf{u}_{,x}[r]\, C_{44}\, F_{\tau,z}\, F_{s,z}\, N_i\, N_j > \\
&+ < \mathbf{u}_{,x}[r]\, C_{66}\, F_{\tau}\, F_{s}\, N_{i,y}\, N_{j,y} > + < \mathbf{u}_{,y}[r]\, C_{66}\, F_{\tau,x}\, F_{s}\, N_i\, N_{j,y} > \\
&+ < \mathbf{u}_{,x}[r]\, C_{12}\, F_{\tau}\, F_{s,x}\, N_{i,y}\, N_j > + < \mathbf{u}_{,z}[r]\, C_{44}\, F_{\tau,x}\, F_{s,z}\, N_i\, N_j > \\
&+ < \mathbf{u}_{,z}[r]\, C_{13}\, F_{\tau,z}\, F_{s,x}\, N_i\, N_j >
\end{aligned}
$$

For $c = 2$:

$$
\begin{aligned}
\mathbf{K}_{nll}^{ij\tau s}[r,c] &= < \mathbf{u}_{,x}[r]\, C_{12}\, F_{\tau,x}\, F_{s}\, N_i\, N_{j,y} > + < \mathbf{u}_{,x}[r]\, C_{66}\, F_{\tau}\, F_{s,x}\, N_{i,y}\, N_j > \\
&+ < \mathbf{u}_{,y}[r]\, C_{66}\, F_{\tau,x}\, F_{s,x}\, N_i\, N_j > + < \mathbf{u}_{,y}[r]\, C_{55}\, F_{\tau,z}\, F_{s,z}\, N_i\, N_j > \\
&+ < \mathbf{u}_{,y}[r]\, C_{22}\, F_{\tau}\, F_{s}\, N_{i,y}\, N_{j,y} > + < \mathbf{u}_{,z}[r]\, C_{23}\, F_{\tau,z}\, F_{s}\, N_i\, N_{j,y} > \\
&+ < \mathbf{u}_{,z}[r]\, C_{55}\, F_{\tau}\, F_{s,z}\, N_{i,y}\, N_j >
\end{aligned}
$$

For $c = 3$:

$$
\begin{aligned}
\mathbf{K}_{nll}^{ij\tau s}[r,c] &= < \mathbf{u}_{,x}[r]\, C_{13}\, F_{\tau,x}\, F_{s,z}\, N_i\, N_j > + < \mathbf{u}_{,x}[r]\, C_{44}\, F_{\tau,z}\, F_{s,x}\, N_i\, N_j > \\
&+ < \mathbf{u}_{,y}[r]\, C_{55}\, F_{\tau,z}\, F_{s}\, N_i\, N_{j,y} > + < \mathbf{u}_{,y}[r]\, C_{23}\, F_{\tau}\, F_{s,z}\, N_{i,y}\, N_j > \\
&+ < \mathbf{u}_{,z}[r]\, C_{44}\, F_{\tau,x}\, F_{s,x}\, N_i\, N_j > + < \mathbf{u}_{,z}[r]\, C_{33}\, F_{\tau,z}\, F_{s,z}\, N_i\, N_j > \\
&+ < \mathbf{u}_{,z}[r]\, C_{55}\, F_{\tau}\, F_{s}\, N_{i,y}\, N_{j,y} >
\end{aligned}
$$

The components of $\mathbf{K}_{lnl}^{ij\tau s}$ are not given here, but they can be easily obtained from $\mathbf{K}_{nll}^{ij\tau s}$. In fact, it is clear from Eq. (??) that $\left(\mathbf{K}_{lnl}^{ij\tau s}\right)^T = \frac{1}{2}\mathbf{K}_{nll}^{ij\tau s}$.

Finally, the generic component $[r, c]$ of the matrix $\mathbf{K}^{ij\tau s}_{nlnl}$ is summarized in the following:

$$
\begin{aligned}
2 \times \mathbf{K}^{ij\tau s}_{nlnl}[r,c] &= < \mathbf{u}_{,x}[r]\, \mathbf{u}_{,x}[c]\; C_{11}\, F_{\tau_{,x}}\, F_{s_{,x}}\, N_i\, N_j > + < \mathbf{u}_{,x}[r]\, \mathbf{u}_{,x}[c]\, C_{44}\, F_{\tau_{,z}}\, F_{s_{,z}}\, N_i\, N_j > \\
&+ < \mathbf{u}_{,x}[r]\, \mathbf{u}_{,x}[c]\, C_{66}\, F_{\tau}\, F_{s}\, N_{i_{,y}}\, N_{j_{,y}} > + < \mathbf{u}_{,y}[r]\, \mathbf{u}_{,y}[c]\; C_{66}\, F_{\tau_{,x}}\, F_{s_{,x}}\, N_i\, N_j > \\
&+ < \mathbf{u}_{,y}[r]\, \mathbf{u}_{,y}[c]\, C_{55}\, F_{\tau_{,z}}\, F_{s_{,z}}\, N_i\, N_j > + < \mathbf{u}_{,y}[r]\, \mathbf{u}_{,y}[c]\, C_{22}\, F_{\tau}\, F_{s}\, N_{i_{,y}}\, N_{j_{,y}} > \\
&+ < \mathbf{u}_{,z}[r]\, \mathbf{u}_{,z}[c]\; C_{44}\, F_{\tau_{,x}}\, F_{s_{,x}}\, N_i\, N_j > + < \mathbf{u}_{,z}[r]\, \mathbf{u}_{,z}[c]\, C_{33}\, F_{\tau_{,z}}\, F_{s_{,z}}\, N_i\, N_j > \\
&+ < \mathbf{u}_{,z}[r]\, \mathbf{u}_{,z}[c]\, C_{55}\, F_{\tau}\, F_{s}\, N_{i_{,y}}\, N_{j_{,y}} > + < \mathbf{u}_{,x}[r]\, \mathbf{u}_{,y}[c]\, C_{12}\, F_{\tau_{,x}}\, F_{s}\, N_i\, N_{j_{,y}} > \\
&+ < \mathbf{u}_{,x}[r]\, \mathbf{u}_{,y}[c]\, C_{66}\, F_{\tau}\, F_{s_{,x}}\, N_{i_{,y}}\, N_j > + < \mathbf{u}_{,y}[r]\, \mathbf{u}_{,x}[c]\, C_{12}\, F_{\tau}\, F_{s_{,x}}\, N_{i_{,y}}\, N_j > \\
&+ < \mathbf{u}_{,y}[r]\, \mathbf{u}_{,x}[c]\, C_{66}\, F_{\tau_{,x}}\, F_{s}\, N_i\, N_{j_{,y}} > + < \mathbf{u}_{,x}[r]\, \mathbf{u}_{,z}[c]\, C_{13}\, F_{\tau_{,x}}\, F_{s_{,z}}\, N_i\, N_j > \\
&+ < \mathbf{u}_{,x}[r]\, \mathbf{u}_{,z}[c]\, C_{44}\, F_{\tau_{,z}}\, F_{s_{,x}}\, N_i\, N_j > + < \mathbf{u}_{,z}[r]\, \mathbf{u}_{,x}[c]\, C_{13}\, F_{\tau_{,z}}\, F_{s_{,x}}\, N_i\, N_j > \\
&+ < \mathbf{u}_{,z}[r]\, \mathbf{u}_{,x}[c]\, C_{44}\, F_{\tau_{,x}}\, F_{s_{,z}}\, N_i\, N_j > + < \mathbf{u}_{,y}[r]\, \mathbf{u}_{,z}[c]\, C_{23}\, F_{\tau}\, F_{s_{,z}}\, N_{i_{,y}}\, N_j > \\
&+ < \mathbf{u}_{,y}[r]\, \mathbf{u}_{,z}[c]\, C_{55}\, F_{\tau_{,z}}\, F_{s}\, N_i\, N_{j_{,y}} > + < \mathbf{u}_{,z}[r]\, \mathbf{u}_{,y}[c]\, C_{55}\, F_{\tau}\, F_{s_{,z}}\, N_{i_{,y}}\, N_j > \\
&+ < \mathbf{u}_{,z}[r]\, \mathbf{u}_{,y}[c]\, C_{23}\, F_{\tau_{,z}}\, F_{s}\, N_i\, N_{j_{,y}} >
\end{aligned}
$$

By these expression, the fundamental nuclei of the sub-matrices of tangent matrix can be obtained immediately, remembering the relations between secant and tangent stiffnes matrix nuclei eq.(4.1.11).

A.2 Fundamental nuclei of 2D CUF elements

In the particular case of 2D beam CUF elements described in ch. 3.2.2, fundamental nuclei explicit expression of sub-matrices are carried out by adopting formal differential operator matrices eq.(3.2.3) and eq.(3.2.4) in eq.(4.1.5). Since the derivation is independent on the elasticity tensor $\mathbb{C}$, expressions of fundamental nuclei are now derived for an isotropic material, considering then the expression eq.(3.1.7).

The linear contribution fundamental nucleus is obtained by considering the volume integral of the following row-by-coloumn matrix product:

$$\mathbf{K}_{ll}^{\tau sij} = \int_{\Omega} \mathbf{B_l^{sj}}^T \, \mathbb{C} \, \mathbf{B_l^{\tau i}} dV \tag{A.2.1}$$

The nine components of the 3×3 linear stiffness matrix fundamental nucleus of the are provided below in the form $\mathbf{K}_{ll}^{ij\tau s}[r, c]$, where r is the row number ($r = 1, 2, 3$) and c is the column number ($c = 1, 2, 3$).

$$\begin{aligned}
\mathbf{K}_0^{ij\tau s}[1,1] &= < C_{11} F_\tau F_s N_{i,x} N_{j,x} > + < C_{44} F_{\tau,z} F_{s,z} N_i N_j > \\
&+ < C_{66} F_\tau F_s N_{i,y} N_{j,y} > + < C_{16} F_\tau F_s N_{i,y} N_{j,x} > \\
&+ < C_{16} F_\tau F_s N_{i,x} N_{j,y} >,
\end{aligned}$$

$$\begin{aligned}
\mathbf{K}_0^{ij\tau s}[1,2] &= < C_{66} F_\tau F_s N_{i,y} N_{j,x} > + < C_{12} F_\tau F_s N_{i,x} N_{j,y} > \\
&+ < C_{45} F_{\tau,z} F_{s,z} N_i N_j > + < C_{16} F_\tau F_s N_{i,x} N_{j,x} > \\
&+ < C_{26} F_\tau F_s N_{i,y} N_{j,y} >,
\end{aligned}$$

$$\begin{aligned}
\mathbf{K}_0^{ij\tau s}[1,3] &= < C_{13} F_\tau F_{s,z} N_{i,x} N_j > + < C_{44} F_{\tau,z} F_s N_i N_{j,x} > \\
&+ < C_{45} F_{\tau,z} F_s N_i N_{j,y} > + < C_{36} F_\tau F_{s,z} N_{i,y} N_j >,
\end{aligned}$$

$$\begin{aligned}
\mathbf{K}_0^{ij\tau s}[2,1] &= < C_{12} F_\tau F_s N_{i,y} N_{j,x} > + < C_{66} F_\tau F_s N_{i,x} N_{j,y} > \\
&+ < C_{45} F_{\tau,z} F_{s,z} N_i N_j > + < C_{16} F_\tau F_s N_{i,x} N_{j,x} > \\
&+ < C_{26} F_\tau F_s N_{i,y} N_{j,y} >,
\end{aligned}$$

$$\begin{aligned}
\mathbf{K}_0^{ij\tau s}[2,2] &= < C_{66} F_\tau F_s N_{i,x} N_{j,x} > + < C_{55} F_{\tau,z} F_{s,z} N_i N_j > \\
&+ < C_{22} F_\tau F_s N_{i,y} N_{j,y} > + < C_{26} F_\tau F_s N_{i,x} N_{j,y} > \\
&+ < C_{26} F_\tau F_s N_{i,y} N_{j,x} >,
\end{aligned}$$

$$\begin{aligned}
\mathbf{K}_0^{ij\tau s}[2,3] &= < C_{23} F_\tau F_{s,z} N_{i,y} N_j > + < C_{55} F_{\tau,z} F_s N_i N_{j,y} > \\
&+ < C_{45} F_{\tau,z} F_s N_i N_{j,x} > + < C_{36} F_\tau F_{s,z} N_{i,x} N_j >,
\end{aligned}$$

$$\begin{aligned}
\mathbf{K}_0^{ij\tau s}[3,1] &= < C_{44} F_\tau F_{s,z} N_{i,x} N_j > + < C_{13} F_{\tau,z} F_s N_i N_{j,x} > \\
&+ < C_{45} F_\tau F_{s,z} N_{i,y} N_j > + < C_{36} F_{\tau,z} F_s N_i N_{j,y} >,
\end{aligned}$$

$$\begin{aligned}
\mathbf{K}_0^{ij\tau s}[3,2] &= < C_{55} F_\tau F_{s,z} N_{i,y} N_j > + < C_{23} F_{\tau,z} F_s N_i N_{j,y} > \\
&+ < C_{45} F_\tau F_{s,z} N_{i,x} N_j > + < C_{36} F_{\tau,z} F_s N_i N_{j,x} >,
\end{aligned}$$

$$\begin{aligned}
\mathbf{K}_0^{ij\tau s}[3,3] &= < C_{44}\, F_\tau\, F_s\, N_{i,x}\, N_{j,x} > + < C_{33}\, F_{\tau,z}\, F_{s,z}\, N_i\, N_j > \\
&+ < C_{55}\, F_\tau\, F_s\, N_{i,y}\, N_{j,y} > + < C_{45}\, F_\tau\, F_s\, N_{i,y}\, N_{j,x} > \\
&+ < C_{45}\, F_\tau\, F_s\, N_{i,x}\, N_{j,y} > .
\end{aligned}$$

The nine components of the FN of the first-order nonlinear stiffness matrix $\mathbf{K}_{nll}^{ij\tau s}(r,c)$ can be derived in a similar way as

For $c = 1$:

$$\begin{aligned}
\mathbf{K}_{nll}^{ij\tau s}[r,1] &= < \mathbf{u}_{,x}[r]\, C_{11}\, F_\tau\, F_s\, N_{i,x}\, N_{j,x} > + < \mathbf{u}_{,x}[r]\, C_{44}\, F_{\tau,z}\, F_{s,z}\, N_i\, N_j > \\
&+ < \mathbf{u}_{,x}[r]\, C_{66}\, F_\tau\, F_s\, N_{i,y}\, N_{j,y} > + < \mathbf{u}_{,x}[r]\, C_{16}\, F_\tau\, F_s\, N_{i,y}\, N_{j,x} > \\
&+ < \mathbf{u}_{,x}[r]\, C_{16}\, F_\tau\, F_s\, N_{i,x}\, N_{j,y} > + < \mathbf{u}_{,y}[r]\, C_{66}\, F_\tau\, F_s\, N_{i,x}\, N_{j,y} > \\
&+ < \mathbf{u}_{,y}[r]\, C_{12}\, F_\tau\, F_s\, N_{i,y}\, N_{j,x} > + < \mathbf{u}_{,y}[r]\, C_{45}\, F_{\tau,z}\, F_{s,z}\, N_i\, N_j > \\
&+ < \mathbf{u}_{,y}[r]\, C_{16}\, F_\tau\, F_s\, N_{i,x}\, N_{j,x} > + < \mathbf{u}_{,y}[r]\, C_{26}\, F_\tau\, F_s\, N_{i,y}\, N_{j,y} > \\
&+ < \mathbf{u}_{,z}[r]\, C_{44}\, F_\tau\, F_{s,z}\, N_{i,x}\, N_j > + < \mathbf{u}_{,z}[r]\, C_{13}\, F_{\tau,z}\, F_s\, N_i\, N_{j,x} > \\
&+ < \mathbf{u}_{,z}[r]\, C_{45}\, F_\tau\, F_{s,z}\, N_{i,y}\, N_j > + < \mathbf{u}_{,z}[r]\, C_{36}\, F_{\tau,z}\, F_s\, N_i\, N_{j,y} >,
\end{aligned}$$

For $c = 2$:

$$\begin{aligned}
\mathbf{K}_{nll}^{ij\tau s}[r,2] &= < \mathbf{u}_{,x}[r]\, C_{12}\, F_\tau\, F_s\, N_{i,x}\, N_{j,y} > + < \mathbf{u}_{,x}[r]\, C_{66}\, F_\tau\, F_s\, N_{i,y}\, N_{j,x} > \\
&+ < \mathbf{u}_{,x}[r]\, C_{45}\, F_{\tau,z}\, F_{s,z}\, N_i\, N_j > + < \mathbf{u}_{,x}[r]\, C_{16}\, F_\tau\, F_s\, N_{i,x}\, N_{j,x} > \\
&+ < \mathbf{u}_{,x}[r]\, C_{26}\, F_\tau\, F_s\, N_{i,y}\, N_{j,y} > + < \mathbf{u}_{,y}[r]\, C_{66}\, F_\tau\, F_s\, N_{i,x}\, N_{j,x} > \\
&+ < \mathbf{u}_{,y}[r]\, C_{55}\, F_{\tau,z}\, F_{s,z}\, N_i\, N_j > + < \mathbf{u}_{,y}[r]\, C_{22}\, F_\tau\, F_s\, N_{i,y}\, N_{j,y} > \\
&+ < \mathbf{u}_{,y}[r]\, C_{26}\, F_\tau\, F_s\, N_{i,y}\, N_{j,x} > + < \mathbf{u}_{,y}[r]\, C_{26}\, F_\tau\, F_s\, N_{i,x}\, N_{j,y} > \\
&+ < \mathbf{u}_{,z}[r]\, C_{23}\, F_{\tau,z}\, F_s\, N_i\, N_{j,y} > + < \mathbf{u}_{,z}[r]\, C_{55}\, F_\tau\, F_{s,z}\, N_{i,y}\, N_j > \\
&+ < \mathbf{u}_{,z}[r]\, C_{45}\, F_\tau\, F_{s,z}\, N_{i,x}\, N_j > + < \mathbf{u}_{,z}[r]\, C_{36}\, F_{\tau,z}\, F_s\, N_i\, N_{j,x} >,
\end{aligned}$$

For $c = 3$:

$$\begin{aligned}
\mathbf{K}_{nll}^{ij\tau s}[r,3] &= < \mathbf{u}_{,x}[r]\, C_{13}\, F_\tau\, F_{s,z}\, N_{i,x}\, N_j > + < \mathbf{u}_{,x}[r]\, C_{44}\, F_{\tau,z}\, F_s\, N_i\, N_{j,x} > \\
&+ < \mathbf{u}_{,x}[r]\, C_{45}\, F_{\tau,z}\, F_s\, N_i\, N_{j,y} > + < \mathbf{u}_{,x}[r]\, C_{36}\, F_\tau\, F_{s,z}\, N_{i,y}\, N_j > \\
&+ < \mathbf{u}_{,y}[r]\, C_{55}\, F_{\tau,z}\, F_s\, N_i\, N_{j,y} > + < \mathbf{u}_{,y}[r]\, C_{23}\, F_\tau\, F_{s,z}\, N_{i,y}\, N_j > \\
&+ < \mathbf{u}_{,y}[r]\, C_{45}\, F_{\tau,z}\, F_s\, N_i\, N_{j,x} > + < \mathbf{u}_{,y}[r]\, C_{36}\, F_\tau\, F_{s,z}\, N_{i,x}\, N_j > \\
&+ < \mathbf{u}_{,z}[r]\, C_{44}\, F_\tau\, F_s\, N_{i,x}\, N_{j,x} > + < \mathbf{u}_{,z}[r]\, C_{33}\, F_{\tau,z}\, F_{s,z}\, N_i\, N_j > \\
&+ < \mathbf{u}_{,z}[r]\, C_{55}\, F_\tau\, F_s\, N_{i,y}\, N_{j,y} > + < \mathbf{u}_{,z}[r]\, C_{45}\, F_\tau\, F_s\, N_{i,x}\, N_{j,y} > \\
&+ < \mathbf{u}_{,z}[r]\, C_{45}\, F_\tau\, F_s\, N_{i,y}\, N_{j,x} > .
\end{aligned}$$

The nine components of $\mathbf{K}_{lnl}^{ij\tau s}$ can be easily obtained from Eq. (**??**) as $\left(\mathbf{K}_{lnl}^{ij\tau s}\right)^{\mathrm{T}} = \mathbf{K}_{nll}^{jis\tau}/2$.

Finally, the nine components of the matrix $\mathbf{K}^{ij\tau s}_{nlnl}[r,c]$ are provided in the following:

$$
\begin{aligned}
2\times\mathbf{K}^{ij\tau s}_{nlnl}[r,c] &= <\mathbf{u}_{,x}[r]\,\mathbf{u}_{,x}[c]\;C_{11}\,F_\tau\,F_s\,N_{i,x}\,N_{j,x}> + <\mathbf{u}_{,x}[r]\,\mathbf{u}_{,x}[c]\,C_{44}\,F_{\tau,z}\,F_{s,z}\,N_i\,N_j> \\
&+ <\mathbf{u}_{,x}[r]\,\mathbf{u}_{,x}[c]\,C_{66}\,F_\tau\,F_s\,N_{i,y}\,N_{j,y}> + <\mathbf{u}_{,x}[r]\,\mathbf{u}_{,x}[c]\,C_{16}\,F_\tau\,F_s\,N_{i,x}\,N_{j,y}> \\
&+ <\mathbf{u}_{,x}[r]\,\mathbf{u}_{,x}[c]\,C_{16}\,F_\tau\,F_s\,N_{i,y}\,N_{j,x}> + <\mathbf{u}_{,y}[r]\,\mathbf{u}_{,y}[c]\;C_{66}\,F_\tau\,F_s\,N_{i,x}\,N_{j,x}> \\
&+ <\mathbf{u}_{,y}[r]\,\mathbf{u}_{,y}[c]\,C_{55}\,F_{\tau,z}\,F_{s,z}\,N_i\,N_j> + <\mathbf{u}_{,y}[r]\,\mathbf{u}_{,y}[c]\,C_{22}\,F_\tau\,F_s\,N_{i,y}\,N_{j,y}> \\
&+ <\mathbf{u}_{,y}[r]\,\mathbf{u}_{,y}[c]\,C_{26}\,F_\tau\,F_s\,N_{i,x}\,N_{j,y}> + <\mathbf{u}_{,y}[r]\,\mathbf{u}_{,y}[c]\,C_{26}\,F_\tau\,F_s\,N_{i,y}\,N_{j,x}> \\
&+ <\mathbf{u}_{,z}[r]\,\mathbf{u}_{,z}[c]\;C_{44}\,F_\tau\,F_s\,N_{i,x}\,N_{j,x}> + <\mathbf{u}_{,z}[r]\,\mathbf{u}_{,z}[c]\,C_{33}\,F_{\tau,z}\,F_{s,z}\,N_i\,N_j> \\
&+ <\mathbf{u}_{,z}[r]\,\mathbf{u}_{,z}[c]\,C_{55}\,F_\tau\,F_s\,N_{i,y}\,N_{j,y}> + <\mathbf{u}_{,z}[r]\,\mathbf{u}_{,z}[c]\,C_{45}\,F_\tau\,F_s\,N_{i,x}\,N_{j,y}> \\
&+ <\mathbf{u}_{,z}[r]\,\mathbf{u}_{,z}[c]\,C_{45}\,F_\tau\,F_s\,N_{i,y}\,N_{j,x}> + <\mathbf{u}_{,x}[r]\,\mathbf{u}_{,y}[c]\,C_{12}\,F_\tau\,F_s\,N_{i,x}\,N_{j,y}> \\
&+ <\mathbf{u}_{,x}[r]\,\mathbf{u}_{,y}[c]\,C_{66}\,F_\tau\,F_s\,N_{i,y}\,N_{j,x}> + <\mathbf{u}_{,x}[r]\,\mathbf{u}_{,y}[c]\,C_{45}\,F_{\tau,z}\,F_{s,z}\,N_i\,N_j> \\
&+ <\mathbf{u}_{,x}[r]\,\mathbf{u}_{,y}[c]\,C_{16}\,F_\tau\,F_s\,N_{i,x}\,N_{j,x}> + <\mathbf{u}_{,x}[r]\,\mathbf{u}_{,y}[c]\,C_{26}\,F_\tau\,F_s\,N_{i,y}\,N_{j,y}> \\
&+ <\mathbf{u}_{,y}[r]\,\mathbf{u}_{,x}[c]\,C_{12}\,F_\tau\,F_s\,N_{i,y}\,N_{j,x}> + <\mathbf{u}_{,y}[r]\,\mathbf{u}_{,x}[c]\,C_{66}\,F_\tau\,F_s\,N_{i,x}\,N_{j,y}> \\
&+ <\mathbf{u}_{,y}[r]\,\mathbf{u}_{,x}[c]\,C_{45}\,F_{\tau,z}\,F_{s,z}\,N_i\,N_j> + <\mathbf{u}_{,y}[r]\,\mathbf{u}_{,x}[c]\,C_{16}\,F_\tau\,F_s\,N_{i,x}\,N_{j,x}> \\
&+ <\mathbf{u}_{,y}[r]\,\mathbf{u}_{,x}[c]\,C_{26}\,F_\tau\,F_s\,N_{i,y}\,N_{j,y}> + <\mathbf{u}_{,x}[r]\,\mathbf{u}_{,z}[c]\,C_{13}\,F_\tau\,F_{s,z}\,N_{i,x}\,N_j> \\
&+ <\mathbf{u}_{,x}[r]\,\mathbf{u}_{,z}[c]\,C_{44}\,F_{\tau,z}\,F_s\,N_i\,N_{j,x}> + <\mathbf{u}_{,x}[r]\,\mathbf{u}_{,z}[c]\,C_{45}\,F_{\tau,z}\,F_s\,N_i\,N_{j,y}> \\
&+ <\mathbf{u}_{,x}[r]\,\mathbf{u}_{,z}[c]\,C_{36}\,F_\tau\,F_{s,z}\,N_{i,y}\,N_j> + <\mathbf{u}_{,z}[r]\,\mathbf{u}_{,x}[c]\,C_{13}\,F_{\tau,z}\,F_s\,N_i\,N_{j,x}> \\
&+ <\mathbf{u}_{,z}[r]\,\mathbf{u}_{,x}[c]\,C_{44}\,F_\tau\,F_{s,z}\,N_{i,x}\,N_j> + <\mathbf{u}_{,z}[r]\,\mathbf{u}_{,x}[c]\,C_{45}\,F_\tau\,F_{s,z}\,N_{i,y}\,N_j> \\
&+ <\mathbf{u}_{,z}[r]\,\mathbf{u}_{,x}[c]\,C_{36}\,F_{\tau,z}\,F_s\,N_i\,N_{j,y}> + <\mathbf{u}_{,y}[r]\,\mathbf{u}_{,z}[c]\,C_{23}\,F_\tau\,F_{s,z}\,N_{i,y}\,N_j> \\
&+ <\mathbf{u}_{,y}[r]\,\mathbf{u}_{,z}[c]\,C_{55}\,F_{\tau,z}\,F_s\,N_i\,N_{j,y}> + <\mathbf{u}_{,y}[r]\,\mathbf{u}_{,z}[c]\,C_{45}\,F_{\tau,z}\,F_s\,N_i\,N_{j,x}> \\
&+ <\mathbf{u}_{,y}[r]\,\mathbf{u}_{,z}[c]\,C_{36}\,F_\tau\,F_{s,z}\,N_{i,x}\,N_j> + <\mathbf{u}_{,z}[r]\,\mathbf{u}_{,y}[c]\,C_{55}\,F_\tau\,F_{s,z}\,N_{i,y}\,N_j> \\
&+ <\mathbf{u}_{,z}[r]\,\mathbf{u}_{,y}[c]\,C_{23}\,F_{\tau,z}\,F_s\,N_i\,N_{j,y}> + <\mathbf{u}_{,z}[r]\,\mathbf{u}_{,y}[c]\,C_{45}\,F_\tau\,F_{s,z}\,N_{i,x}\,N_j> \\
&+ <\mathbf{u}_{,z}[r]\,\mathbf{u}_{,y}[c]\,C_{36}\,F_{\tau,z}\,F_s\,N_i\,N_{j,x}>
\end{aligned}
$$

A.3 Fundamental nuclei of 3D elements

In the particular case of 1D beam CUF elements described in ch. 3.2.1, fundamental nuclei explicit expression of sub-matrices are carried out by adopting formal differential operator matrices eq.(3.2.3) and eq.(3.2.4) in eq.(4.1.5). Since the derivation is independent on the elasticity tensor $\mathbb{C}$, expressions of fundamental nuclei are now derived for a general material without particular hypotesis on the elasticity tensor, considering then the expression eq.(3.1.6).

$$
\begin{aligned}
\mathbf{K}_{ll}^{ij\tau s}[1,1] &= < C_{11}N_{i_x}N_{j_x} > + < C_{14}N_{i_z}N_{j_x} > + < C_{66}N_{i_y}N_{j_y} > + \\
&+ < C_{46}N_{i_z}N_{j_y} > + < C_{16}N_{i_y}N_{j_x} > + < C_{16}N_{i_x}N_{j_y} > + \\
&+ < C_{14}N_{i_x}N_{j_z} > + < C_{46}N_{i_y}N_{j_z} > + < C_{44}N_{i_z}N_{j_z} > \\
\mathbf{K}_{ll}^{ij\tau s}[1,2] &= < C_{16}N_{i_x}N_{j_x} > + < C_{12}N_{i_y}N_{j_x} > + < C_{15}N_{i_z}N_{j_x} > + \\
&+ < C_{66}N_{i_x}N_{j_y} > + < C_{26}N_{i_y}N_{j_y} > + < C_{56}N_{i_z}N_{j_y} > + \\
&+ < C_{46}N_{i_x}N_{j_z} > + < C_{24}N_{i_y}N_{j_z} > + < C_{45}N_{i_z}N_{j_z} > \\
\mathbf{K}_{ll}^{ij\tau s}[1,3] &= < C_{14}N_{i_x}N_{j_x} > + < C_{15}N_{i_y}N_{j_x} > + < C_{13}N_{i_z}N_{j_x} > + \\
&+ < C_{46}N_{i_x}N_{j_y} > + < C_{56}N_{i_y}N_{j_y} > + < C_{36}N_{i_z}N_{j_y} > + \\
&+ < C_{44}N_{i_x}N_{j_z} > + < C_{45}N_{i_y}N_{j_z} > + < C_{34}N_{i_z}N_{j_z} > \\
\mathbf{K}_{ll}^{ij\tau s}[2,1] &= < C_{16}N_{i_x}N_{j_x} > + < C_{66}N_{i_y}N_{j_x} > + < C_{46}N_{i_z}N_{j_x} > + \\
&+ < C_{12}N_{i_x}N_{j_y} > + < C_{26}N_{i_y}N_{j_y} > + < C_{24}N_{i_z}N_{j_y} > + \\
&+ < C_{15}N_{i_x}N_{j_z} > + < C_{56}N_{i_y}N_{j_z} > + < C_{45}N_{i_z}N_{j_z} > \\
\mathbf{K}_{ll}^{ij\tau s}[2,2] &= < C_{66}N_{i_x}N_{j_x} > + < C_{56}N_{i_z}N_{j_x} > + < C_{22}N_{i_y}N_{j_y} > + \\
&+ < C_{25}N_{i_z}N_{j_y} > + < C_{26}N_{i_y}N_{j_x} > + < C_{26}N_{i_x}N_{j_y} > + \\
&+ < C_{56}N_{i_x}N_{j_z} > + < C_{25}N_{i_y}N_{j_z} > + < C_{55}N_{i_z}N_{j_z} > \\
\mathbf{K}_{ll}^{ij\tau s}[2,3] &= < C_{46}N_{i_x}N_{j_x} > + < C_{56}N_{i_y}N_{j_x} > + < C_{36}N_{i_z}N_{j_x} > + \\
&+ < C_{24}N_{i_x}N_{j_y} > + < C_{25}N_{i_y}N_{j_y} > + < C_{23}N_{i_z}N_{j_y} > + \\
&+ < C_{45}N_{i_x}N_{j_z} > + < C_{55}N_{i_y}N_{j_z} > + < C_{35}N_{i_z}N_{j_z} > \\
\mathbf{K}_{ll}^{ij\tau s}[3,1] &= < C_{14}N_{i_x}N_{j_x} > + < C_{46}N_{i_y}N_{j_x} > + < C_{44}N_{i_z}N_{j_x} > + \\
&+ < C_{15}N_{i_x}N_{j_y} > + < C_{56}N_{i_y}N_{j_y} > + < C_{45}N_{i_z}N_{j_y} > + \\
&+ < C_{13}N_{i_x}N_{j_z} > + < C_{36}N_{i_y}N_{j_z} > + < C_{34}N_{i_z}N_{j_z} > \\
\mathbf{K}_{ll}^{ij\tau s}[3,2] &= < C_{46}N_{i_x}N_{j_x} > + < C_{24}N_{i_y}N_{j_x} > + < C_{45}N_{i_z}N_{j_x} > + \\
&+ < C_{56}N_{i_x}N_{j_y} > + < C_{25}N_{i_y}N_{j_y} > + < C_{55}N_{i_z}N_{j_y} > + \\
&+ < C_{36}N_{i_x}N_{j_z} > + < C_{23}N_{i_y}N_{j_z} > + < C_{35}N_{i_z}N_{j_z} >
\end{aligned}
$$

$$\begin{aligned}\mathbf{K}_{ll}^{ij\tau s}[3,3] &= < C_{44}N_{i_x}N_{j_x} > + < C_{34}N_{i_z}N_{j_x} > + < C_{55}N_{i_y}N_{j_y} > + \\ &+ < C_{35}N_{i_z}N_{j_y} > + < C_{45}N_{i_y}N_{j_x} > + < C_{45}N_{i_x}N_{j_y} > + \\ &+ < C_{34}N_{i_x}N_{j_z} > + < C_{35}N_{i_y}N_{j_z} > + < C_{33}N_{i_z}N_{j_z} >\end{aligned}$$

The first-order nonlinear contribution fundamental nucleus is obtained by considering the volume integral of the following row-by-coloumn matrix product:

$$\mathbf{K}_{nll}^{\tau sij} = \int_{\Omega} \mathbf{B}_{\mathbf{nl}}^{\mathbf{sj}\,T} \, \mathbb{C} \, \mathbf{B}_{\mathbf{l}}^{\tau \mathbf{i}} dV \tag{A.3.1}$$

The nine components of the 3×3 nonlinear stiffness matrix fundamental nucleus of the are provided below in the form $\mathbf{K}_{nll}^{ij\tau s}[r,c]$, where r is the row number ($r = 1, 2, 3$) and c is the column number ($c = 1, 2, 3$): For $c = 1$:

$$\begin{aligned}\mathbf{K}_{nll}^{ij\tau s}[r,c] &= < \mathbf{u}_{,x}[r]C_{11}N_{i_,x}N_{j,x} > + < \mathbf{u}_{,x}[r]C_{16}N_{i_,y}N_{j,x} > + < \mathbf{u}_{,x}[r]C_{14}N_{i,z}N_{j,x} > + \\ &+ < \mathbf{u}_{,x}[r]C_{16}N_{i,x}N_{j,y} > + < \mathbf{u}_{,x}[r]C_{66}N_{i_,y}N_{j,y} > + < \mathbf{u}_{,x}[r]C_{46}N_{i,z}N_{j,y} > + \\ &+ < \mathbf{u}_{,x}[r]C_{14}N_{i,x}N_{j,z} > + < \mathbf{u}_{,x}[r]C_{46}N_{i_,y}N_{j,z} > + < \mathbf{u}_{,x}[r]C_{44}N_{i,z}N_{j,z} > + \\ &+ < \mathbf{u}_{,y}[r]C_{16}N_{i,x}N_{j,x} > + < \mathbf{u}_{,y}[r]C_{66}N_{i_,y}N_{j,x} > + < \mathbf{u}_{,y}[r]C_{46}N_{i,z}N_{j,x} > + \\ &+ < \mathbf{u}_{,y}[r]C_{12}N_{i,x}N_{j,y} > + < \mathbf{u}_{,y}[r]C_{26}N_{i_,y}N_{j,y} > + < \mathbf{u}_{,y}[r]C_{24}N_{i,z}N_{j,y} > + \\ &+ < \mathbf{u}_{,y}[r]C_{15}N_{i,x}N_{j,z} > + < \mathbf{u}_{,y}[r]C_{56}N_{i_,y}N_{j,z} > + < \mathbf{u}_{,y}[r]C_{45}N_{i,z}N_{j,z} > + \\ &+ < \mathbf{u}_{,z}[r]C_{14}N_{i,x}N_{j,x} > + < \mathbf{u}_{,z}[r]C_{46}N_{i_,y}N_{j,x} > + < \mathbf{u}_{,z}[r]C_{44}N_{i,z}N_{j,x} > + \\ &+ < \mathbf{u}_{,z}[r]C_{15}N_{i,x}N_{j,y} > + < \mathbf{u}_{,z}[r]C_{56}N_{i_,y}N_{j,y} > + < \mathbf{u}_{,z}[r]C_{45}N_{i,z}N_{j,y} > + \\ &+ < \mathbf{u}_{,z}[r]C_{13}N_{i,x}N_{j,z} > + < \mathbf{u}_{,z}[r]C_{36}N_{i_,y}N_{j,z} > + < \mathbf{u}_{,z}[r]C_{34}N_{i,z}N_{j,z} >\end{aligned}$$

For $c = 2$:

$$\begin{aligned}\mathbf{K}_{nll}^{ij\tau s}[r,c] &= < \mathbf{u}_{,x}[r]C_{16}N_{i_,x}N_{j,x} > + < \mathbf{u}_{,x}[r]C_{12}N_{i_,y}N_{j,x} > + < \mathbf{u}_{,x}[r]C_{15}N_{i,z}N_{j,x} > \\ &+ < \mathbf{u}_{,x}[r]C_{66}N_{i,x}N_{j,y} > + < \mathbf{u}_{,x}[r]C_{26}N_{i_,y}N_{j,y} > + < \mathbf{u}_{,x}[r]C_{56}N_{i,z}N_{j,y} > + \\ &+ < \mathbf{u}_{,x}[r]C_{46}N_{i,x}N_{j,z} > + < \mathbf{u}_{,x}[r]C_{24}N_{i_,y}N_{j,z} > + < \mathbf{u}_{,x}[r]C_{45}N_{i,z}N_{j,z} > + \\ &+ < \mathbf{u}_{,y}[r]C_{66}N_{i,x}N_{j,x} > + < \mathbf{u}_{,y}[r]C_{26}N_{i_,y}N_{j,x} > + < \mathbf{u}_{,y}[r]C_{56}N_{i,z}N_{j,x} > + \\ &+ < \mathbf{u}_{,y}[r]C_{26}N_{i,x}N_{j,y} > + < \mathbf{u}_{,y}[r]C_{22}N_{i_,y}N_{j,y} > + < \mathbf{u}_{,y}[r]C_{25}N_{i,z}N_{j,y} > + \\ &+ < \mathbf{u}_{,y}[r]C_{56}N_{i,x}N_{j,z} > + < \mathbf{u}_{,y}[r]C_{25}N_{i_,y}N_{j,z} > + < \mathbf{u}_{,y}[r]C_{55}N_{i,z}N_{j,z} > + \\ &+ < \mathbf{u}_{,z}[r]C_{46}N_{i,x}N_{j,x} > + < \mathbf{u}_{,z}[r]C_{24}N_{i_,y}N_{j,x} > + < \mathbf{u}_{,z}[r]C_{45}N_{i,z}N_{j,x} > + \\ &+ < \mathbf{u}_{,z}[r]C_{56}N_{i,x}N_{j,y} > + < \mathbf{u}_{,z}[r]C_{25}N_{i_,y}N_{j,y} > + < \mathbf{u}_{,z}[r]C_{55}N_{i,z}N_{j,y} > + \\ &+ < \mathbf{u}_{,z}[r]C_{36}N_{i,x}N_{j,z} > + < \mathbf{u}_{,z}[r]C_{23}N_{i_,y}N_{j,z} > + < \mathbf{u}_{,z}[r]C_{35}N_{i,z}N_{j,z} >\end{aligned}$$

For $c = 3$:

$$\begin{aligned}
\mathbf{K}_{nll}^{ij\tau s}[r,c] &= < \mathbf{u}_{,x}[r]C_{14}N_{i,x}N_{j,x} > + < \mathbf{u}_{,x}[r]C_{15}N_{i,y}N_{j,x} > + < \mathbf{u}_{,x}[r]C_{13}N_{i,z}N_{j,x} > + \\
&+ < \mathbf{u}_{,x}[r]C_{46}N_{i,x}N_{j,y} > + < \mathbf{u}_{,x}[r]C_{56}N_{i,y}N_{j,y} > + < \mathbf{u}_{,x}[r]C_{36}N_{i,z}N_{j,y} > + \\
&+ < \mathbf{u}_{,x}[r]C_{44}N_{i,x}N_{j,z} > + < \mathbf{u}_{,x}[r]C_{45}N_{i,y}N_{j,z} > + < \mathbf{u}_{,x}[r]C_{34}N_{i,z}N_{j,z} > + \\
&+ < \mathbf{u}_{,y}[r]C_{46}N_{i,x}N_{j,x} > + < \mathbf{u}_{,y}[r]C_{56}N_{i,y}N_{j,x} > + < \mathbf{u}_{,y}[r]C_{36}N_{i,z}N_{j,x} > + \\
&+ < \mathbf{u}_{,y}[r]C_{24}N_{i,x}N_{j,y} > + < \mathbf{u}_{,y}[r]C_{25}N_{i,y}N_{j,y} > + < \mathbf{u}_{,y}[r]C_{23}N_{i,z}N_{j,y} > + \\
&+ < \mathbf{u}_{,y}[r]C_{45}N_{i,x}N_{j,z} > + < \mathbf{u}_{,y}[r]C_{55}N_{i,y}N_{j,z} > + < \mathbf{u}_{,y}[r]C_{35}N_{i,z}N_{j,z} > + \\
&+ < \mathbf{u}_{,z}[r]C_{44}N_{i,x}N_{j,x} > + < \mathbf{u}_{,z}[r]C_{45}N_{i,y}N_{j,x} > + < \mathbf{u}_{,z}[r]C_{34}N_{i,z}N_{j,x} > + \\
&+ < \mathbf{u}_{,z}[r]C_{45}N_{i,x}N_{j,y} > + < \mathbf{u}_{,z}[r]C_{55}N_{i,y}N_{j,y} > + < \mathbf{u}_{,z}[r]C_{35}N_{i,z}N_{j,y} > + \\
&+ < \mathbf{u}_{,z}[r]C_{34}N_{i,x}N_{j,z} > + < \mathbf{u}_{,z}[r]C_{35}N_{i,y}N_{j,z} > + < \mathbf{u}_{,z}[r]C_{33}N_{i,z}N_{j,z} >
\end{aligned}$$

The components of $\mathbf{K}_{lnl}^{ij\tau s}$ are not given since they are straightforword, since $\left(\mathbf{K}_{lnl}^{ij\tau s}\right)^T = \frac{1}{2}\mathbf{K}_{nll}^{ij\tau s}$.
The second-order nonlinear contribution fundamental nucleus is obtained by considering the volume integral of the following row-by-coloumn matrix product:

$$\mathbf{K}_{nll}^{\tau sij} = \int_{\Omega} \mathbf{B}_{\mathbf{nl}}^{\mathbf{sj}\,T} \,\mathbb{C}\, \mathbf{B}_{\mathbf{nl}}^{\tau \mathbf{i}} dV \tag{A.3.2}$$

The nine components of the 3×3 nonlinear stiffness matrix fundamental nucleus of the are provided below in the form $\mathbf{K}_{nll}^{ij\tau s}[r,c]$, where r is the row number ($r = 1, 2, 3$) and c is the column number ($c = 1, 2, 3$).
The outer-diagonal component are given by the general expression:

$$\begin{aligned}
2 \times \mathbf{K}_{nlnl}^{ij\tau s}[r,c] &= < \mathbf{u}_{,x}[c]\mathbf{u}_{,x}[r]C_{11}N_{i,x}N_{j,x} > + < \mathbf{u}_{,x}[c]\mathbf{u}_{,x}[r]C_{16}N_{i,y}N_{j,x} > + \\
&+ < \mathbf{u}_{,x}[c]\mathbf{u}_{,x}[r]C_{14}N_{i,z}N_{j,x} > + < \mathbf{u}_{,x}[c]\mathbf{u}_{,x}[r]C_{16}N_{i,x}N_{j,y} > + \\
&+ < \mathbf{u}_{,x}[c]\mathbf{u}_{,x}[r]C_{66}N_{i,y}N_{j,y} > + < \mathbf{u}_{,x}[c]\mathbf{u}_{,x}[r]C_{46}N_{i,z}N_{j,y} > + \\
&+ < \mathbf{u}_{,x}[c]\mathbf{u}_{,x}[r]C_{14}N_{i,x}N_{j,z} > + < \mathbf{u}_{,x}[c]\mathbf{u}_{,x}[r]C_{46}N_{i,y}N_{j,z} > + \\
&+ < \mathbf{u}_{,x}[c]\mathbf{u}_{,x}[r]C_{44}N_{i,z}N_{j,z} > + < \mathbf{u}_{,y}[c]\mathbf{u}_{,x}[r]C_{16}N_{i,x}N_{j,x} > + \\
&+ < \mathbf{u}_{,y}[c]\mathbf{u}_{,x}[r]C_{12}N_{i,y}N_{j,x} > + < \mathbf{u}_{,y}[c]\mathbf{u}_{,x}[r]C_{15}N_{i,z}N_{j,x} > + \\
&+ < \mathbf{u}_{,y}[c]\mathbf{u}_{,x}[r]C_{66}N_{i,x}N_{j,y} > + < \mathbf{u}_{,y}[c]\mathbf{u}_{,x}[r]C_{26}N_{i,y}N_{j,y} > + \\
&+ < \mathbf{u}_{,y}[c]\mathbf{u}_{,x}[r]C_{56}N_{i,z}N_{j,y} > + < \mathbf{u}_{,y}[c]\mathbf{u}_{,x}[r]C_{46}N_{i,x}N_{j,z} > + \\
&+ < \mathbf{u}_{,y}[c]\mathbf{u}_{,x}[r]C_{24}N_{i,y}N_{j,z} > + < \mathbf{u}_{,y}[c]\mathbf{u}_{,x}[r]C_{45}N_{i,z}N_{j,z} > + \\
&+ < \mathbf{u}_{,z}[c]\mathbf{u}_{,x}[r]C_{14}N_{i,x}N_{j,x} > + < \mathbf{u}_{,z}[c]\mathbf{u}_{,x}[r]C_{15}N_{i,y}N_{j,x} > + \\
&+ < \mathbf{u}_{,z}[c]\mathbf{u}_{,x}[r]C_{13}N_{i,z}N_{j,x} > + < \mathbf{u}_{,z}[c]\mathbf{u}_{,x}[r]C_{46}N_{i,x}N_{j,y} > + \\
&+ < \mathbf{u}_{,z}[c]\mathbf{u}_{,x}[r]C_{56}N_{i,y}N_{j,y} > + < \mathbf{u}_{,z}[c]\mathbf{u}_{,x}[r]C_{36}N_{i,z}N_{j,y} > + \\
&+ < \mathbf{u}_{,z}[c]\mathbf{u}_{,x}[r]C_{44}N_{i,x}N_{j,z} > + < \mathbf{u}_{,z}[c]\mathbf{u}_{,x}[r]C_{45}N_{i,y}N_{j,z} > + \\
&+ < \mathbf{u}_{,z}[c]\mathbf{u}_{,x}[r]C_{34}N_{i,z}N_{j,z} > + < \mathbf{u}_{,x}[c]\mathbf{u}_{,y}[r]C_{16}N_{i,x}N_{j,x} > +
\end{aligned}$$

$$
\begin{aligned}
&+ < \mathbf{u}_{,x}[c]\mathbf{u}_{,y}[r]C_{66}N_{i,y}N_{j,x} > + < \mathbf{u}_{,x}[c]\mathbf{u}_{,y}[r]C_{46}N_{i,z}N_{j,x} > + \\
&+ < \mathbf{u}_{,x}[c]\mathbf{u}_{,y}[r]C_{12}N_{i,x}N_{j,y} > + < \mathbf{u}_{,x}[c]\mathbf{u}_{,y}[r]C_{26}N_{i,y}N_{j,y} > + \\
&+ < \mathbf{u}_{,x}[c]\mathbf{u}_{,y}[r]C_{24}N_{i,z}N_{j,y} > + < \mathbf{u}_{,x}[c]\mathbf{u}_{,y}[r]C_{15}N_{i,x}N_{j,z} > + \\
&+ < \mathbf{u}_{,x}[c]\mathbf{u}_{,y}[r]C_{56}N_{i,y}N_{j,z} > + < \mathbf{u}_{,x}[c]\mathbf{u}_{,y}[r]C_{45}N_{i,z}N_{j,z} > + \\
&+ < \mathbf{u}_{,y}[c]\mathbf{u}_{,y}[r]C_{66}N_{i,x}N_{j,x} > + < \mathbf{u}_{,y}[c]\mathbf{u}_{,y}[r]C_{26}N_{i,y}N_{j,x} > + \\
&+ < \mathbf{u}_{,y}[c]\mathbf{u}_{,y}[r]C_{56}N_{i,z}N_{j,x} > + < \mathbf{u}_{,y}[c]\mathbf{u}_{,y}[r]C_{26}N_{i,x}N_{j,y} > + \\
&+ < \mathbf{u}_{,y}[c]\mathbf{u}_{,y}[r]C_{22}N_{i,y}N_{j,y} > + < \mathbf{u}_{,y}[c]\mathbf{u}_{,y}[r]C_{25}N_{i,z}N_{j,y} > + \\
&+ < \mathbf{u}_{,y}[c]\mathbf{u}_{,y}[r]C_{56}N_{i,x}N_{j,z} > + < \mathbf{u}_{,y}[c]\mathbf{u}_{,y}[r]C_{25}N_{i,y}N_{j,z} > + \\
&+ < \mathbf{u}_{,y}[c]\mathbf{u}_{,y}[r]C_{55}N_{i,z}N_{j,z} > + < \mathbf{u}_{,z}[c]\mathbf{u}_{,y}[r]C_{46}N_{i,x}N_{j,x} > + \\
&+ < \mathbf{u}_{,z}[c]\mathbf{u}_{,y}[r]C_{56}N_{i,y}N_{j,x} > + < \mathbf{u}_{,z}[c]\mathbf{u}_{,y}[r]C_{36}N_{i,z}N_{j,x} > + \\
&+ < \mathbf{u}_{,z}[c]\mathbf{u}_{,y}[r]C_{24}N_{i,x}N_{j,y} > + < \mathbf{u}_{,z}[c]\mathbf{u}_{,y}[r]C_{25}N_{i,y}N_{j,y} > + \\
&+ < \mathbf{u}_{,z}[c]\mathbf{u}_{,y}[r]C_{23}N_{i,z}N_{j,y} > + < \mathbf{u}_{,z}[c]\mathbf{u}_{,y}[r]C_{45}N_{i,x}N_{j,z} > + \\
&+ < \mathbf{u}_{,z}[c]\mathbf{u}_{,y}[r]C_{55}N_{i,y}N_{j,z} > + < \mathbf{u}_{,z}[c]\mathbf{u}_{,y}[r]C_{35}N_{i,z}N_{j,z} > + \\
&+ < \mathbf{u}_{,x}[c]\mathbf{u}_{,z}[r]C_{14}N_{i,x}N_{j,x} > + < \mathbf{u}_{,x}[c]\mathbf{u}_{,z}[r]C_{46}N_{i,y}N_{j,x} > + \\
&+ < \mathbf{u}_{,x}[c]\mathbf{u}_{,z}[r]C_{44}N_{i,z}N_{j,x} > + < \mathbf{u}_{,x}[c]\mathbf{u}_{,z}[r]C_{15}N_{i,x}N_{j,y} > + \\
&+ < \mathbf{u}_{,x}[c]\mathbf{u}_{,z}[r]C_{56}N_{i,y}N_{j,y} > + < \mathbf{u}_{,x}[c]\mathbf{u}_{,z}[r]C_{45}N_{i,z}N_{j,y} > + \\
&+ < \mathbf{u}_{,x}[c]\mathbf{u}_{,z}[r]C_{13}N_{i,x}N_{j,z} > + < \mathbf{u}_{,x}[c]\mathbf{u}_{,z}[r]C_{36}N_{i,y}N_{j,z} > + \\
&+ < \mathbf{u}_{,x}[c]\mathbf{u}_{,z}[r]C_{34}N_{i,z}N_{j,z} > + < \mathbf{u}_{,y}[c]\mathbf{u}_{,z}[r]C_{46}N_{i,x}N_{j,x} > + \\
&+ < \mathbf{u}_{,y}[c]\mathbf{u}_{,z}[r]C_{24}N_{i,y}N_{j,x} > + < \mathbf{u}_{,y}[c]\mathbf{u}_{,z}[r]C_{45}N_{i,z}N_{j,x} > + \\
&+ < \mathbf{u}_{,y}[c]\mathbf{u}_{,z}[r]C_{56}N_{i,x}N_{j,y} > + < \mathbf{u}_{,y}[c]\mathbf{u}_{,z}[r]C_{25}N_{i,y}N_{j,y} > + \\
&+ < \mathbf{u}_{,y}[c]\mathbf{u}_{,z}[r]C_{55}N_{i,z}N_{j,y} > + < \mathbf{u}_{,y}[c]\mathbf{u}_{,z}[r]C_{36}N_{i,x}N_{j,z} > + \\
&+ < \mathbf{u}_{,y}[c]\mathbf{u}_{,z}[r]C_{23}N_{i,y}N_{j,z} > + < \mathbf{u}_{,y}[c]\mathbf{u}_{,z}[r]C_{35}N_{i,z}N_{j,z} > + \\
&+ < \mathbf{u}_{,z}[c]\mathbf{u}_{,z}[r]C_{44}N_{i,x}N_{j,x} > + < \mathbf{u}_{,z}[c]\mathbf{u}_{,z}[r]C_{45}N_{i,y}N_{j,x} > + \\
&+ < \mathbf{u}_{,z}[c]\mathbf{u}_{,z}[r]C_{34}N_{i,z}N_{j,x} > + < \mathbf{u}_{,z}[c]\mathbf{u}_{,z}[r]C_{45}N_{i,x}N_{j,y} > + \\
&+ < \mathbf{u}_{,z}[c]\mathbf{u}_{,z}[r]C_{55}N_{i,y}N_{j,y} > + < \mathbf{u}_{,z}[c]\mathbf{u}_{,z}[r]C_{35}N_{i,z}N_{j,y} > + \\
&+ < \mathbf{u}_{,z}[c]\mathbf{u}_{,z}[r]C_{34}N_{i,x}N_{j,z} > + < \mathbf{u}_{,z}[c]\mathbf{u}_{,z}[r]C_{35}N_{i,y}N_{j,z} > + \\
&+ < \mathbf{u}_{,z}[c]\mathbf{u}_{,z}[r]C_{33}N_{i,z}N_{j,z} >
\end{aligned}
$$

Instead, the diagonal component are given by the general expression:

$$
\begin{aligned}
2 \times \mathbf{K}^{ij\tau s}_{nlnl}[r,r] &= < \mathbf{u}_{,x}[r]\mathbf{u}_{,x}[r]C_{11}N_{i,x}N_{j,x} > + < \mathbf{u}_{,x}[r]\mathbf{u}_{,x}[r]C_{16}N_{i,y}N_{j,x} > + \\
&+ < \mathbf{u}_{,x}[r]\mathbf{u}_{,x}[r]C_{14}N_{i,z}N_{j,x} > + < \mathbf{u}_{,x}[r]\mathbf{u}_{,x}[r]C_{16}N_{i,x}N_{j,y} > + \\
&+ < \mathbf{u}_{,x}[r]\mathbf{u}_{,x}[r]C_{66}N_{i,y}N_{j,y} > + < \mathbf{u}_{,x}[r]\mathbf{u}_{,x}[r]C_{46}N_{i,z}N_{j,y} > + \\
&+ < \mathbf{u}_{,x}[r]\mathbf{u}_{,x}[r]C_{14}N_{i,x}N_{j,z} > + < \mathbf{u}_{,x}[r]\mathbf{u}_{,x}[r]C_{46}N_{i,y}N_{j,z} > + \\
&+ < \mathbf{u}_{,x}[r]\mathbf{u}_{,x}[r]C_{44}N_{i,z}N_{j,z} > + < 2\mathbf{u}_{,x}[r]\mathbf{u}_{,y}[r]C_{16}N_{i,x}N_{j,x} > + \\
&+ < \mathbf{u}_{,x}[r]\mathbf{u}_{,y}[r]C_{12}N_{i,y}N_{j,x} > + < \mathbf{u}_{,x}[r]\mathbf{u}_{,y}[r]C_{66}N_{i,y}N_{j,x} > +
\end{aligned}
$$

$$
\begin{aligned}
&+ < \mathbf{u}_{,x}[r]\mathbf{u}_{,y}[r]C_{15}N_{i,z}N_{j,x} > + < \mathbf{u}_{,x}[r]\mathbf{u}_{,y}[r]C_{46}N_{i,z}N_{j,x} > +\\
&+ < \mathbf{u}_{,x}[r]\mathbf{u}_{,y}[r]C_{12}N_{i,x}N_{j,y} > + < \mathbf{u}_{,x}[r]\mathbf{u}_{,y}[r]C_{66}N_{i,x}N_{j,y} > +\\
&+ < 2\mathbf{u}_{,x}[r]\mathbf{u}_{,y}[r]C_{26}N_{i,y}N_{j,y} > + < \mathbf{u}_{,x}[r]\mathbf{u}_{,y}[r]C_{24}N_{i,z}N_{j,y} > +\\
&+ < \mathbf{u}_{,x}[r]\mathbf{u}_{,y}[r]C_{56}N_{i,z}N_{j,y} > + < \mathbf{u}_{,x}[r]\mathbf{u}_{,y}[r]C_{15}N_{i,x}N_{j,z} > +\\
&+ < \mathbf{u}_{,x}[r]\mathbf{u}_{,y}[r]C_{46}N_{i,x}N_{j,z} > + < \mathbf{u}_{,x}[r]\mathbf{u}_{,y}[r]C_{24}N_{i,y}N_{j,z} > +\\
&+ < \mathbf{u}_{,x}[r]\mathbf{u}_{,y}[r]C_{56}N_{i,y}N_{j,z} > + < 2\mathbf{u}_{,x}[r]\mathbf{u}_{,y}[r]C_{45}N_{i,z}N_{j,z} > +\\
&+ < \mathbf{u}_{,y}[r]\mathbf{u}_{,y}[r]C_{66}N_{i,x}N_{j,x} > + < \mathbf{u}_{,y}[r]\mathbf{u}_{,y}[r]C_{26}N_{i,y}N_{j,x} > +\\
&+ < \mathbf{u}_{,y}[r]\mathbf{u}_{,y}[r]C_{56}N_{i,z}N_{j,x} > + < \mathbf{u}_{,y}[r]\mathbf{u}_{,y}[r]C_{26}N_{i,x}N_{j,y} > +\\
&+ < \mathbf{u}_{,y}[r]\mathbf{u}_{,y}[r]C_{22}N_{i,y}N_{j,y} > + < \mathbf{u}_{,y}[r]\mathbf{u}_{,y}[r]C_{25}N_{i,z}N_{j,y} > +\\
&+ < \mathbf{u}_{,y}[r]\mathbf{u}_{,y}[r]C_{56}N_{i,x}N_{j,z} > + < \mathbf{u}_{,y}[r]\mathbf{u}_{,y}[r]C_{25}N_{i,y}N_{j,z} > +\\
&+ < \mathbf{u}_{,y}[r]\mathbf{u}_{,y}[r]C_{55}N_{i,z}N_{j,z} > + < 2\mathbf{u}_{,x}[r]\mathbf{u}_{,z}[r]C_{14}N_{i,x}N_{j,x} > +\\
&+ < \mathbf{u}_{,x}[r]\mathbf{u}_{,z}[r]C_{15}N_{i,y}N_{j,x} > + < \mathbf{u}_{,x}[r]\mathbf{u}_{,z}[r]C_{46}N_{i,y}N_{j,x} > +\\
&+ < \mathbf{u}_{,x}[r]\mathbf{u}_{,z}[r]C_{13}N_{i,z}N_{j,x} > + < \mathbf{u}_{,x}[r]\mathbf{u}_{,z}[r]C_{44}N_{i,z}N_{j,x} > +\\
&+ < \mathbf{u}_{,x}[r]\mathbf{u}_{,z}[r]C_{15}N_{i,x}N_{j,y} > + < \mathbf{u}_{,x}[r]\mathbf{u}_{,z}[r]C_{46}N_{i,x}N_{j,y} > +\\
&+ < 2\mathbf{u}_{,x}[r]\mathbf{u}_{,z}[r]C_{56}N_{i,y}N_{j,y} > + < \mathbf{u}_{,x}[r]\mathbf{u}_{,z}[r]C_{36}N_{i,z}N_{j,y} > +\\
&+ < \mathbf{u}_{,x}[r]\mathbf{u}_{,z}[r]C_{45}N_{i,z}N_{j,y} > + < \mathbf{u}_{,x}[r]\mathbf{u}_{,z}[r]C_{13}N_{i,x}N_{j,z} > +\\
&+ < \mathbf{u}_{,x}[r]\mathbf{u}_{,z}[r]C_{44}N_{i,x}N_{j,z} > + < \mathbf{u}_{,x}[r]\mathbf{u}_{,z}[r]C_{36}N_{i,y}N_{j,z} > +\\
&+ < \mathbf{u}_{,x}[r]\mathbf{u}_{,z}[r]C_{45}N_{i,y}N_{j,z} > + < 2\mathbf{u}_{,x}[r]\mathbf{u}_{,z}[r]C_{34}N_{i,z}N_{j,z} > +\\
&+ < 2\mathbf{u}_{,y}[r]\mathbf{u}_{,z}[r]C_{46}N_{i,x}N_{j,x} > + < \mathbf{u}_{,y}[r]\mathbf{u}_{,z}[r]C_{24}N_{i,y}N_{j,x} > +\\
&+ < \mathbf{u}_{,y}[r]\mathbf{u}_{,z}[r]C_{56}N_{i,y}N_{j,x} > + < \mathbf{u}_{,y}[r]\mathbf{u}_{,z}[r]C_{36}N_{i,z}N_{j,x} > +\\
&+ < \mathbf{u}_{,y}[r]\mathbf{u}_{,z}[r]C_{45}N_{i,z}N_{j,x} > + < \mathbf{u}_{,y}[r]\mathbf{u}_{,z}[r]C_{24}N_{i,x}N_{j,y} > +\\
&+ < \mathbf{u}_{,y}[r]\mathbf{u}_{,z}[r]C_{56}N_{i,x}N_{j,y} > + < 2\mathbf{u}_{,y}[r]\mathbf{u}_{,z}[r]C_{25}N_{i,y}N_{j,y} > +\\
&+ < \mathbf{u}_{,y}[r]\mathbf{u}_{,z}[r]C_{23}N_{i,z}N_{j,y} > + < \mathbf{u}_{,y}[r]\mathbf{u}_{,z}[r]C_{55}N_{i,z}N_{j,y} > +\\
&+ < \mathbf{u}_{,y}[r]\mathbf{u}_{,z}[r]C_{36}N_{i,x}N_{j,z} > + < \mathbf{u}_{,y}[r]\mathbf{u}_{,z}[r]C_{45}N_{i,x}N_{j,z} > +\\
&+ < \mathbf{u}_{,y}[r]\mathbf{u}_{,z}[r]C_{23}N_{i,y}N_{j,z} > + < \mathbf{u}_{,y}[r]\mathbf{u}_{,z}[r]C_{55}N_{i,y}N_{j,z} > +\\
&+ < 2\mathbf{u}_{,y}[r]\mathbf{u}_{,z}[r]C_{35}N_{i,z}N_{j,z} > + < \mathbf{u}_{,z}[r]\mathbf{u}_{,z}[r]C_{44}N_{i,x}N_{j,x} > +\\
&+ < \mathbf{u}_{,z}[r]\mathbf{u}_{,z}[r]C_{45}N_{i,y}N_{j,x} > + < \mathbf{u}_{,z}[r]\mathbf{u}_{,z}[r]C_{34}N_{i,z}N_{j,x} > +\\
&+ < \mathbf{u}_{,z}[r]\mathbf{u}_{,z}[r]C_{45}N_{i,x}N_{j,y} > + < \mathbf{u}_{,z}[r]\mathbf{u}_{,z}[r]C_{55}N_{i,y}N_{j,y} > +\\
&+ < \mathbf{u}_{,z}[r]\mathbf{u}_{,z}[r]C_{35}N_{i,z}N_{j,y} > + < \mathbf{u}_{,z}[r]\mathbf{u}_{,z}[r]C_{34}N_{i,x}N_{j,z} > +\\
&+ < \mathbf{u}_{,z}[r]\mathbf{u}_{,z}[r]C_{35}N_{i,y}N_{j,z} > + < \mathbf{u}_{,z}[r]\mathbf{u}_{,z}[r]C_{33}N_{i,z}N_{j,z} >
\end{aligned}
$$

By these expression, the fundamental nuclei of the sub-matrices of tangent matrix can be obtained immediately, remembering the relations between secant and tangent stiffnes matrix nuclei eq.(4.1.11).

Appendix B

Numerical integration by Gauss-Legendre quadrature

In the evaluation of the fundamental nuclei of nonlinear stiffness matrices, integral have to be computed. Under the isoparametric formulation adopted in the present thesis of the 3D solid finite elements, integration by Gauss-Legendre quadrature technique is performed.

In general, integrals of shape functions, derivative of shape functions and displacement derivatives over the domain has to be computed over the physical considered domain. In the specific case of the present formulation, isoparametric formulation is adopted: the same formulation is used either for the displacement field expression either for geometrical quantities. One of the most powerful aspect of the adoption of the Gauss-Legendre quadrature is the computation of integrals independently on the geometry by a finite sum.

Gauss-Legendre quadrature is performed in the *natural* reference frame of the element: the physical reference frame, by the Jacobian, can be manipulated starting from *natural* reference frame of coordinates $\xi,\ \eta,\ \nu$, as already shown in the description of Q4 2D and H8 3D finite element.

In the most general case, each natural variable is defined over the real interval $[-1, 1]$, and the generic volume integral in the natural reference frame is obtained by:

$$\int_{\Omega_N} f(\xi,\eta,\nu)d\xi d\eta d\nu = \int_{-1}^{1}\int_{-1}^{1}\int_{-1}^{1} f(\xi,\eta,\nu)d\xi d\eta d\nu \approx \sum_{l=1}^{NGP}\sum_{m=1}^{NGP}\sum_{k=1}^{NGP} f(\xi_l,\eta_m,\nu_k)w_l w_m w_k \tag{B.0.1}$$

The computation of the whole integral requires only the computation of the function in specified points in the natural reference frame, the so-called *Gauss points*, which coordinates are known, multiplied by the *quadrature weight*, standardized value since they are defined in the natural reference frame. The isoparametric formulation allow rapidly the transformation of integrals from the physical to natural reference frame thanks to the Jacobian.
Starting from the fundamental theorem of change of variables in integral computation, an

integral in the physical reference frame can be written as:

$$\int_{\Omega} f(x,y,z)dxdydz = \int_{\Omega_N} f(\xi,\eta,\nu)|\mathbf{J}(\xi,\eta,\nu)|d\xi d\eta d\nu \tag{B.0.2}$$

Applying the above definition of Gauss-Legendre quadrature, the integral will be:

$$\int_{\Omega} f(x,y,z)dxdydz = \sum_{l=1}^{NGP}\sum_{m=1}^{NGP}\sum_{k=1}^{NGP} f(\xi_l,\eta_m,\nu_k)|\mathbf{J}(\xi_l,\eta_m,\nu_m)|w_l w_m w_k \tag{B.0.3}$$

The accuracy of the estimated integrals is strictly dependent on the number of Gauss points used. Gauss-Legendre quadrature is also adopted to prevent shear locking phenomena during the computation of the stiffness matrices: by reducing the number of Gauss-points, the overestimation due to locking of the stiffness matrix can be mitigate by an underestimation of integrals by reducing the number of Gauss-points, that has to be correctly located to computed correct quantities.

Appendix C

Strain-energy functions adopted

According to first-invariant hypereleasticity, the general expression of the strain-energy function is given by the volumetric part and the isochoric part depending only on the first invariant of the volumetric right Cauchy-Green strain tensor, namely:

$$\Psi(\mathbf{C}) = \Psi_{vol}(J) + \Psi_{iso}(\bar{\mathbf{C}}) = \Psi_{vol}(I_3) + \bar{\Psi}(\bar{I}_1) \tag{C.0.1}$$

In the actual implementation of hyperelastic finite elements, the volumetric strain energy function acts like a penalization constraint on incompressibility, so:

$$\Psi_{vol}(J) = \frac{1}{D_1}(J-1)^2 = \frac{k}{2}(J-1)^2 \tag{C.0.2}$$

where the incompressibility parameter $D_1 = 2/k$ is defined from the bulk modulus k. Instead, in the case of isochoric part, there are in literature different models adopted depending on the specific application. In the present work, the following models are adopted:

- *Neo-Hookean* model: defined starting from the infinitesimal shear modulus μ

$$\bar{\Psi}(\bar{I}_1) = \frac{\mu}{2}(\bar{I}_1 - 3) \tag{C.0.3}$$

- *Gent* model: two model parameter base of J_m, the limit value of $(\bar{I}_1 - 3)$

$$\bar{\Psi}(\bar{I}_1) = -\frac{\mu J_m}{2}\log\left(1 - \frac{\bar{I}_1 - 3}{J_m}\right) \tag{C.0.4}$$

- *Exp-Ln* model: derived by Khajesaeid *et al.*[CITA], where a, b are tuning parameter

$$\bar{\Psi}(\bar{I}_1) = \frac{\mu}{2}\left[\frac{1}{a}exp(a(\bar{I}_1 - 3)) + b(\bar{I}_1 - 2)(1 - \log(\bar{I}_1 - 2)) - \frac{1}{a} - b\right] \tag{C.0.5}$$

- *Fung-Demiray* model: typically used for biological applications, where $\beta = \mu$ and α is a stiffening parameter

$$\bar{\Psi}(\bar{I}_1) = \frac{\beta}{2\alpha}[\exp(\alpha(\bar{I}_1 - 3)) - 1] \tag{C.0.6}$$